

**A Systematic Evaluation of Initiation Criteria for River Ice Breakup**

**Using Field Data**

by

**Yanqi Ye**

A thesis submitted in partial fulfillment of the requirements for the degree of

Master of Science

in

Water Resources Engineering

Department of Civil and Environmental Engineering

University of Alberta

© Yanqi Ye, 2020

## Abstract

River ice breakup has great implications to the environment, ecology and economy. A mechanical breakup tends to occur if fast-rising river flow instigates ice movements. The breaking front, the interface between moving and stationary ice, can sometimes travel hundreds of kilometres, resulting in extensive ice runs. A breaking front may also stop, resulting in formation of ice jams and the associated flood risk is high. There are still many unknowns about the mechanism of the onset, sustaining, and stop of ice cover breakup. The hydraulic storage released from the broken ice is postulated to lead to the formation of a non-attenuating, i.e. self-sustaining wave (SSW), offering an explanation to the long distance ice breaking, but the postulation is mainly based on numerical studies in hypothetical rectangular channels. This study focused on the mechanical breakup process of the river ice, serving to improve the breakup forecasting capability. Six empirical and semi-empirical/physics-based breakup criteria were incorporated into the University of Alberta's *RiverID* model and systemically and quantitatively evaluated using three years of breakup data collected on the Athabasca River and the Peace River. The existence and characteristics of the self-sustaining wave (SSW) under natural channel conditions were also explored.

This study showed that the empirical breakup criteria based on water level or discharge can often be calibrated to reproduce the documented breaking front propagation. However, the calibrated parameters appeared to be site and situation specific. On the other hand, the physics-based boundary constraint criterion, which is based on the requirement of broken ice sheet to move around geometric constraints in the river, showed better potential to be transferable from year to year and river to river. It did not provide as good agreement to field observations as compared to some of the empirical criteria, emphasizing the importance of adequately accounting for the real

channel morphological characteristics when implementing such criterion. The other physics-based criteria based on side resistance and flexural strength of the ice cover did not work well for any of the modeled events. The side resistance is highly dynamic in field condition and hard to quantify. The flexural and buckling criterion reduces to water surface slope criterion is too simplified to use when breakup is initiated by an ice jam release wave. Unlike previous findings about SSW in idealized channel conditions, this study showed that the SSWs in natural channels do not always develop a sharp wave front and long, flat crest under the natural channel conditions. The ice breaking distance and speed, which are affected by the varying resistance along a river, can greatly impact the characteristics of an SSW.

## **Preface**

This thesis is original work by Yanqi Ye with the assistance of Dr. She. Part of the thesis has been published as a conference paper at the 20<sup>th</sup> Workshop on the Hydraulics of Ice Covered Rivers by Canadian Geophysical Union Hydrology Section (CGU HS) Committee on River Ice Processes and the Environment (CRIPE). This thesis is expected to be adapted for journal paper publication in 2020.

## **Acknowledgments**

First, I would like to express my heartfelt appreciation to my supervisor Dr. Yuntong She. This study would not have been possible without her persistent help. Knowledgeable, wise and kind, she is the best supervisor that I could ever ask for. I always feel grateful for having her guiding me through this journey.

This research would not have been achievable without the data provided by Alberta Environment and Parks (AEP), BC Hydro and Water Survey of Canada (WSC). Their help is deeply appreciated. I also wish to express my sincere gratitude to Jennifer Nafziger and Martin Jasek for sharing me with valuable information and data.

The funding provided by Natural Sciences and Engineering Research Council of Canada (NSERC) is truly appreciated. And I would like to say thank you to Drs. Loewen, Liu and Deng for being a part of the final oral examination committee.

I would like to acknowledge the love and support received from my family. Thanks for being always by my side. And a huge thank you to all of my friends for helping me in various ways. This was not possible without you.

## Table of Contents

Abstract.....	ii
Preface.....	iv
Acknowledgments.....	v
Table of Contents.....	vi
List of Figures.....	x
Chapter 1 Introduction.....	1
1.1 Mechanical Breakup Process.....	2
1.2 Ice jam release wave (jave) induced breakup.....	3
1.3 Previous Research.....	5
1.3.1 Empirical breakup criteria.....	5
1.3.2 Semi-empirical/physics-based breakup criteria.....	7
1.3.3 Self-sustaining wave (SSW).....	10
1.4 Study Objectives.....	11
Chapter 2 Methodology.....	13
2.1 Model Description.....	13
2.2 Incorporating Breakup Criteria into River1D.....	17
2.2.1 Water level criterion.....	17
2.2.2 Discharge criteria.....	18

2.2.3 Side resistance criterion .....	19
2.2.4 Boundary constraint criterion .....	20
2.2.5 Flexural and buckling criterion .....	21
2.3 Validation of Proposed Modeling Method .....	22
2.3.1 Case description .....	22
2.3.2 Transition zone.....	23
2.3.3 Results and discussions.....	24
Chapter 3 2007 Breakup Event on the Athabasca River.....	29
3.1 Study Reach .....	29
3.2 2007 Ice Jam Release Event Description.....	32
3.3 Model Configuration.....	34
3.3.1 Geometric model.....	34
3.3.2 Initial condition .....	36
3.3.3 Other considerations .....	37
3.4 Results and Discussions .....	38
3.4.1 Breakup criteria assessment.....	38
3.4.2 Stage hydrographs.....	48
3.4.3 Self-sustaining wave (SSW) .....	50
Chapter 4 2014 and 2018 Breakup Events on the Peace River.....	54

4.1 Study Reach .....	54
4.2 Geometric Model .....	56
4.3 Open Water Calibrations.....	60
4.4 Breakup events modeling.....	66
4.4.1 Event descriptions .....	67
4.4.2 Model configuration.....	72
4.5 Results and Discussions.....	79
4.5.1 Breakup criteria assessment.....	79
4.5.2 Stage hydrographs.....	95
4.5.3 Self-sustaining wave (SSW) .....	98
Chapter 5 Conclusions and Recommendations.....	107
References.....	111

## List of Tables

Table 2-1. Summary of modeling runs by <i>CRISSPID</i> and <i>RiverID</i> .....	25
Table 3-1. Channel characteristics of five river sites (adapted from Beltaos, 1997a).....	46
Table 4-1. A comparison of key locations along the Peace River .....	58
Table 4-2. List of all gauge stations and the corresponding data availability for each year’s event .....	59
Table 4-3. Peace River tributaries considered in this study (adapted from Hicks, 1996).....	59
Table 4-4. Initial and boundary conditions of all flood events .....	60
Table 4-5. Overview of validation results at Town of Peace River and Fort Vermillion.....	66
Table 4-6. Documented ice front location of breakup between Sunny Valley and Fort Vermillion in 2014 (source: BC Hydro).....	69
Table 4-7. Sheet breaking front locations observed over a 214 km reach of the Peace River in 2018 (adapted from Jasek 2019a) .....	72

## List of Figures

Figure 1-1. Illustrations of two types of breaking fronts: a) rubble breaking font; b) sheet breaking front (Jasek 2003). .....	4
Figure 2-1. Definition diagram of ice movement near the breaking front (adapted from She and Hicks 2006a). .....	15
Figure 2-2. Minimum required wave amplitude and water slope to initiate ice rupture for ice cover of various thickness ( $h$ ) for $E = 7$ GPa and $\sigma = 0.7$ MPa (Nzokou et al. 2009). .....	22
Figure 2-3. Comparison of discharge domain snapshots of the breakup and no breakup cases (Run 1 in table). .....	25
Figure 3-1. Map of Athabasca River basin and river reaches in the vicinity of Fort McMurray (Adapted from Friesenhan et al. 2008). .....	31
Figure 3-2. Monitoring stations in the vicinity of Fort McMurray in 2007 (She et al. 2009). .....	33
Figure 3-3. Measurements of the top of the ice jam prior to release on April 19, 2007 and locations of breaking front tracking (adapted form She et al. 2009). .....	34
Figure 3-4. Bed profile of the interest area on the Athabasca River with available surveyed cross sections and key locations. ....	35
Figure 3-5. The computed profile of the 2007 Athabasca River water intake ice jam. ....	36
Figure 3-6. Cross section geometry downstream (285 km) and upstream (294.9 km) of the Clearwater River confluence (293.0 km). .....	38
Figure 3-7. Comparison of observed and modeled breaking front location in 2007 on the Athabasca River (water level criterion). .....	39

Figure 3-8. Comparison of observed and modeled breaking front location in 2007 on the Athabasca River (discharge criterion). .....	41
Figure 3-9. Comparison of observed and modeled breaking front location in 2007 on the Athabasca River (discharge rate criterion). .....	42
Figure 3-10. Comparison of observed and modeled breaking front location in 2007 on the Athabasca River (side resistance criterion).....	43
Figure 3-11. Comparison of m values computed using different spatial interval.....	44
Figure 3-12. Comparison of observed and modeled breaking front location in 2007 on the Athabasca River (boundary constraint criterion).....	46
Figure 3-13. Comparison of observed and modeled breaking front location (flexural and buckling or water surface slope criterion). .....	48
Figure 3-14. Stage hydrographs by model compared with record at various stations on the Athabasca River (discharge criterion with $Q_{br} = 4000 \text{ m}^3/\text{s}$ ). .....	50
Figure 3-15. Comparison of water depth between cases with and without ice breakup at various times after the ice jam release on the Athabasca River. ....	53
Figure 4-1. Map of the Peace River basin with pertinent locations (Jasek 2017b). .....	55
Figure 4-2. Bed profile of the Peace River with surveyed cross sections and key locations.....	58
Figure 4-3. Comparisons of measured and computed discharge and water level hydrographs of the 1987 open water event. ....	61
Figure 4-4. Comparisons of measured and computed discharge and water level hydrographs of the 2009 open water event. ....	63

Figure 4-5. Comparisons of measured and computed discharge and water level hydrographs of the 2011 open water event. ....	64
Figure 4-6. Comparisons of measured and computed discharge and water level hydrographs of the 2019 open water event. ....	65
Figure 4-7. Water surface elevation at Sunny Valley indicating the ice jam movement (Data obtained from AEP). ....	68
Figure 4-8. Water surface elevation at Carcajou indicating the breaking front movement (Data before 16:45 April 26 <sup>th</sup> from AEP and afterwards digitized from Jasek 2017b). ....	69
Figure 4-9. Documented ice front location of breakup between Sunny Valley and Fort Vermillion (Data provided by BC Hydro). ....	70
Figure 4-10. Discharge hydrograph of the South Gauge at Town of Peace River during the 2014 jam release (Digitized from Jasek 2017b). ....	73
Figure 4-11. Initial condition of the 2014 partial ice jam release event. ....	75
Figure 4-12. Initial condition of the 2014 complete ice jam release event. ....	75
Figure 4-13. Comparisons of the computed and measured water levels at Sunny Valley during the 2014 jam release events. ....	76
Figure 4-14. Discharge hydrograph of WSC gauge at Town of Peace River during the 2018 jam release (digitized from Jasek 2019a). ....	77
Figure 4-15. Initial condition of the 2018 ice jam release event. ....	78
Figure 4-16. Comparison of the computed and measured water levels at Sunny Valley during the 2018 jam release event. ....	78

Figure 4-17. Comparison of observed and modeled breaking front location in 2014 and 2018 on the Peace River (water level criterion).....	81
Figure 4-18. Comparison of observed and modeled breaking front location in 2014 and 2018 on the Peace River (discharge criterion).....	84
Figure 4-19. Comparison of observed and modeled breaking front location in 2014 and 2018 on the Peace River (discharge rate criterion).....	86
Figure 4-20. Comparison of observed and modeled breaking front location in 2014 and 2018 on the Peace River (side resistance criterion).....	88
Figure 4-21. Comparison of observed and modeled breaking front location in 2014 and 2018 on the Peace River (boundary constraint criterion). ....	91
Figure 4-22. Comparison of observed and modeled breaking front location in 2014 and 2018 on the Peace River (flexural and buckling or water surface slope criterion criterion). ....	94
Figure 4-23. Comparison of modeled and measured water level hydrographs at various stations on the Peace River during the 2014 breakup event.....	96
Figure 4-24. Comparison of modeled and measured water level hydrographs at various stations on the Peace River during the 2018 breakup event.....	97
Figure 4-25. Comparison of discharge in the study reach between breakup and no-breakup cases at various times after the 2014 complete ice jam release on the Peace River (discharge criterion). .....	100
Figure 4-26. Comparison of discharge in the study reach between breakup and no-breakup cases at various times after the 2018 ice jam release on the Peace River (discharge criterion).....	101

Figure 4-27. Comparison of discharge in the study reach between the breakup and no-breakup cases at various times after the ice jam release in 2018 on the Peace River (boundary constraint c).

..... 104

Figure 4-28. The variation of sustaining wave discharge and breakup initiating discharge. Both excess ratios were normalized with base discharge and subtracted by 1 to show the storage release amount. The data of the 2014 complete release and 2018 event of the Peace River are added (adapted from Beltaos 2017a)..... 106

## Chapter 1 Introduction

River ice is an essential component of the global cryosphere, affecting the northern areas every winter season. It can have both beneficial and adverse impact on environment, ecology, and economy. For example, ice roads and ice bridges are important to the transportation of Canada's north, while many northern riverside communities face risks of flooding caused by river ice. River ice breakup is a brief but critical period, during which many processes change dynamically as the relatively intact ice cover disintegrates and the river transitions to open water. Breakup is often associated with ice jams as large amount of broken ice from the disintegrated ice cover accumulates and blocks the channel. This obstructs the river flow and leads to fast-rising water levels. Ice jam related flood is often more severe and challenging to predict than rainfall flood. Ice jams can lead to changes in river morphology, since bed and bank scouring is often associated with the thick ice accumulation and sediment transport significantly increases when the accumulation releases (Beltaos and Burrell 1999; 2000). It is also known that breakup can change a number of water-quality parameters, including water temperature, nutrients, and the movement of sediment-related contaminants and toxins (e.g. Prowse 2003; Nafziger et al. 2016; Beltaos 2016).

The manner of breakup depends on the relative importance of the meteorological (mainly warm temperature and increased solar radiation) and hydrological (e.g. increased discharge due to snowmelt or rain) factors. If the river discharge remains relatively steady during days of mild weather, a thermal breakup would occur. The ice cover deteriorates and melts in place, with little or no ice movement. On the other hand, if a large snowmelt runoff wave or a rain on snow event occurs before any significant thermal deterioration, a mechanical breakup tends to happen when ice cover is lifted, fractured, dislodged, and set in motion by the increased flow. A mechanical breakup is often associated with ice runs and ice jams, which can pose great flood risk to adjacent

communities. Therefore, mechanical breakup is the focus of this thesis, with particular interest in predicting the onset of ice cover breakup.

### **1.1 Mechanical Breakup Process**

A mechanical breakup generally develops in stages (Nafziger et al. 2016). It begins just like a thermal breakup when snow on the ice cover melts and sections of ice cover also melt to form open leads in the otherwise intact ice cover. Overflow spilling onto the ice downstream of the open leads is an indication of fast-rising water levels, which differs from a thermal breakup. Hinge cracks are often seen on the ice cover along the two banks as the rising water levels lift the ice cover and detach the middle portion from the shore-fast ice. Generally, there will be two cracks splitting the ice cover into a central part and two side strips. But a single mid-channel crack is also normal in narrower streams with thick ice cover. The middle strip of the ice cover is now free to float and will float to a higher position as water level increases. It is no longer supported laterally by the river banks or the side ice strips. The action of flow drag and downstream component of the weight of the ice sheet produces forces, which in a meandering river leads to bending moments and tensile stresses in the horizontal plane. As a result, transverse cracks form across the channel, which further fractures the ice cover into separate fragments. At this point, these floating ice sheets cannot move much due to the constraint of river bends (Beltaos 1990a). However, minor shifting, short starts and stops generate localized fluctuations in water levels which further break the ice sheets into smaller pieces. As these sheet ice continues to shift and push, their size reduces and eventually they are small enough to overcome the geometric constraints and begin to move with the flow. This is considered the onset of breakup. Ice jam may form if the broken ice accumulates against intact segments of the ice cover or at geometric constrictions such as tight river bends, islands and bridges.

## 1.2 Ice jam release wave (jave) induced breakup

Ice cover breakup may be initiated by snowmelt runoff, mid-winter thaw, hydro-peaking operation, or a wave caused by upstream ice jam release (Beltaos 2017a). When an ice jam suddenly releases, the water and ice come out from storage quickly, leading to a water wave and a run of broken ice rubble progressing down the river channel. Ice jam release waves, or “javes” for short, are highly dynamic. Water level rise of a couple of meters and wave celerity of over 5 m/s are not uncommon (see Beltaos 2008). The front of the wave travels ahead of the ice run and often has the capability of dislodging lengthy intact ice cover downstream. In relatively flat rivers and river deltas like the lower Peace or the lower Mackenzie River (Beltaos and Carter 2009; Beltaos, 2013a), javes may be the only driver for ice breakup.

Jasek (2003) classified the progression of jave-induced breakup into two types: rubble breaking front or sheet breaking front where “breaking front” refers to the transition point between moving and stationary ice (Figure 1-1). A rubble breaking front typically happens when the intact ice cover downstream is confined, for example in a river with steep banks or when a river enters a lake and the water level is controlled by the lake level. The ice run from the released jam ploughs through the intact ice cover especially when the ice is relatively weak, breaking it into small pieces and consuming them. There is a sharp transition between the moving rubble ice and the intact ice cover (Figure 1-1a). On the other hand, a sheet breaking front tends to happen in river reaches where the water level has increased significantly before the breaking front arrived, allowing a large amount of open water spaces for larger ice sheet to move around. As can be seen in Figure 1-1b, the broken ice sheets are too large to be tipped over and included into the ice rubble. Instead, they are pushed ahead or ride up onto the ice rubbles. There is a section between the rubble ice from the released ice jam and the downstream intact ice cover, in which the ice sheets move, closing the open water

spaces and creating ridges as they push against each other. This section is called a transition zone (She and Hicks 2006b). In this manner, the ice sheets crack into smaller and smaller pieces. Sheet breaking fronts have been more commonly observed in the field as compared to rubble breaking front (e.g. Jasek 2003, 2019a,b; She et al. 2009). A similar characterization was also suggested by Ferrick and Mulherin (1989), where they described rubble fronts and sheet fronts as ‘strength-dominated’ breakup and ‘support-dominated’ breakup, respectively.

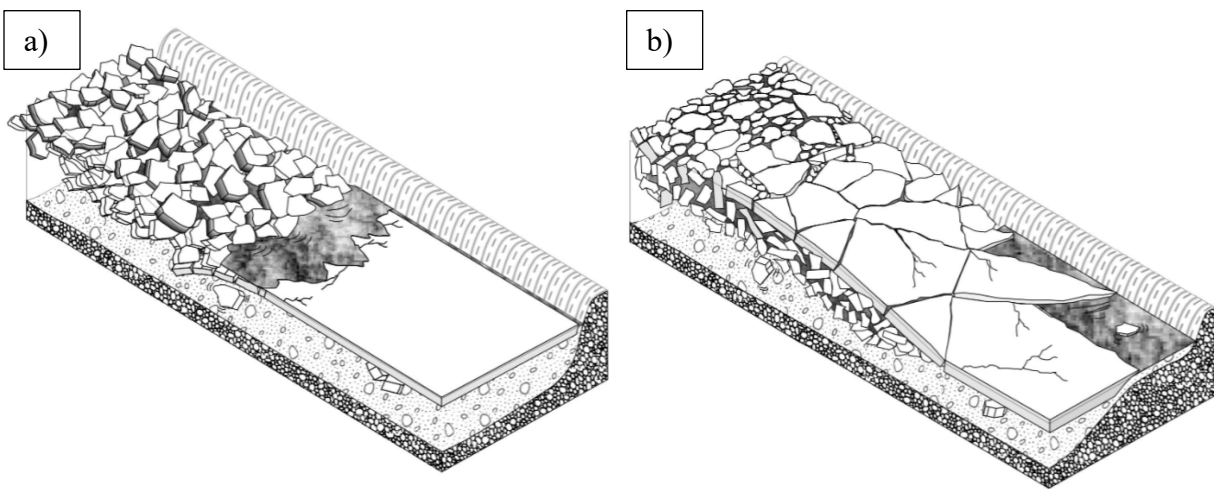


Figure 1-1. Illustrations of two types of breaking fronts: a) rubble breaking front; b) sheet breaking front (Jasek 2003).

It has been observed that sheet breaking fronts travel over long distance at relatively high speed. For example, Gerard et al. (1984) reported an ice breaking event progressed at an average celerity of 5.2 m/s on the Yukon River in 1983. Jasek (2019a,b) also documented a series of high-speed ice breaking events on the Peace River in 2014 and 2018. The rate of ice breaking within a part of the reach peaked at an astonishing number of 7.1 m/s. It is understood that the jave from the released jam would attenuate and eventually to the point that it can no longer break the stationary ice cover, but sheet breaking fronts appear to be sustained by the water being released from storage

as the ice cover breaks up (Beltaos 2018a). The long-distance progression of sheet breaking fronts potentially can lead to the formation of substantial ice accumulations (i.e. ice jams) when the breaking front is arrested, posing significant flood risk to riverside communities. Understanding the mechanisms initiating a breakup event and sustaining a sheet breaking front is not only essential to the prediction of ice jam occurrence and associated flood, but also has great implication to many other ice breakup related problems.

### 1.3 Previous Research

The study of river ice breakup has been an area of interest for many years. A number of studies into the criteria of breakup initiation, jave-induced breakup, wave sustained by storage release and its characteristics have been conducted. These previous studies are reviewed in this section.

#### 1.3.1 Empirical breakup criteria

Examples of empirical breakup criteria include different combinations of water level, discharge, ice thickness, shear stress, ice strength, freeze-up conditions, and indices of thermal effects (e.g. see Shulyakovskii 1966; Beltaos 1990a, 2003). The ice cover is considered broken up when a single-variable threshold is met. Based on the premise that ice cover must lift above the water level at freeze-up to get moving, the following type of equation using stage rise as a threshold has been widely used as a practical breakup criterion (Beltaos 1990a, 1995b).

$$H_B - H_F > K\eta - F(\sum_5) \quad [1-1]$$

where  $H_B$  and  $H_F$  are the water surface elevations at the onset of breakup and freeze-up, respectively;  $\eta$  is the ice cover thickness just prior to breakup;  $K$  is a dimensionless site-specific coefficient. Beltaos (1990a) showed that  $K$  value falls within a limited range of 2 to 3 using field data collected from six river sites;  $\sum_5$  is the accumulated degree-day of thawing with a base

temperature of  $-5^{\circ}\text{C}$ ; and  $F$  is a site-specific function with  $F(0) = 0$ . The first term on the right-hand side of the equation represents the amount of water level increase required to detach an ice cover; and the second term describes how deteriorated the ice cover is prior to breakup. Beltaos (2008) proposed that this empirical criterion can be practical for those rivers with little or no channel geometry data but detailed hydrometric records.

Empirical criteria are often employed when modeling ice cover breakup. For example, Jasek et al. (2005) used the unsteady one-dimensional (1D) river ice model CRISSP (Comprehensive River Ice Simulation System Program) to study wave-induced ice breakup in prismatic rectangular channels. Waves with different forms, both mild and steep, were introduced one at a time from the upstream end and the ice cover in the channel was considered broken up when the discharge exceeds a specified threshold discharge (so called breakup initiating discharge) at any point along the channel. Beltaos (2017a) used the University of Alberta's *River1D* model to simulate wave-induced breakup in a prismatic channel. The open-channel module of *River1D* was used and ice was simulated by increasing the bed roughness from 0.03 to 0.05. A shear stress threshold was used to initiate breakup, and the bed roughness was reduced back to 0.03 when the criterion is satisfied. Rate of change of water level or discharge has also been used as breakup criteria in which the rate of change of water level or discharge needs to exceed a threshold value for a specific time duration (CRISSP1D Programmer's Manual Version 1.0).

These empirical criteria are simple to apply and often use easily obtained data. However, the empirical criteria do not explicitly account for the physical processes involved during ice breakup, thus tend to be highly site and situation specific. Additionally, many hydrological and meteorological parameters involved in the complex process are left out of the empirical equations

so are assumed to be constant. As a result, the empirical criteria may become unreliable if changes occurred in these parameters.

### 1.3.2 Semi-empirical/physics-based breakup criteria

Semi-empirical/physics-based breakup criteria have been developed to account for the actual mechanism of river ice breakup and have a basis on physical reasoning. For example, Ferrick and Mulherin (1989) used side resistance as a breakup threshold. Shear stress develops at the sides of the ice cover (at the hinge cracks between the ice sheet and the shore-fast ice strips) due to the flow drag acting on the bottom of the ice and the downslope component of the weight of the ice cover. The side resistance  $\tau_s$  at the hinge cracks of an ice cover can be calculated as:

$$\tau_s = \frac{\bar{\omega}_i W_i}{2\eta} \quad [1-2]$$

where  $\bar{\omega}_i$  is the tractive stress which includes the flow shear stress and the weight of the ice cover per unit area;  $W_i$  is the width of ice by the time the ice is about to move (distance between hinge cracks). Beltaos (1997a) calculated values of side resistance ranged from 0.2 to 7 kPa for five river sites. The rationale behind this criterion is that fast flow tends to break up ice more easily as the flow shear stress is greater. Although thermal effects are not explicitly accounted for in this criterion, Beltaos (1997a) argued that the thermal inputs will abate the ice strength thus causing the value of  $\tau_s$  to decline. In extreme cases  $\tau_s$  can become 0 when the remaining ice strips attached to riverbanks are too weak to hold the middle ice sheet.

Another semi-empirical criterion relates the tractive force exerted on the ice cover to the geometric characteristics of the channel, as well as the strength and competence of the ice cover. The physical basis lies in this criterion is originated from calculating the water surface width needed for a

separate ice sheet to move past a river bend. The criterion is called boundary constraint criterion and can be expressed as:

$$\frac{8(W-W_i)\bar{\omega}_i m^2}{(m-0.5)\eta_0} > \Phi_{B0} F(\Sigma_5) = \Phi_{B0} f_{ic} \quad [1-3]$$

where  $W$  is the water surface width when breakup occurs;  $m$  is the radius of channel curvature divided by  $W_i$ , this term represents the river planform effects, and its value is typically larger when the reach is relatively straight and with islands present;  $\eta_0$  is the maximum thickness of winter ice cover;  $\Phi_{B0}$  is a reference value of a composite parameter which has the unit of stress when there is negligible ice decay; and  $f_{ic}$  describes the ice competence as a ratio relative to the non-decayed value, and can be expressed as a function of the degree-days of thawing  $\Sigma_5$  (base of  $-5^\circ\text{C}$ ).  $f_{ic}$  ranges between 0 and 1, but Beltaos (2003) stated that its value has to remain above 0.3 because otherwise equation [1-3] will no longer be applicable for mechanical breakup.

Beltaos (1996a, 2008) applied the boundary constraint criterion to several river sites. The left-hand side of the equation was calculated using field data and then plotted against the degree-days of thawing  $\Sigma_5$  which accounts for the thermal inputs. Despite the scatter, the values of  $\Phi_{B0}$  decrease with the increase of  $\Sigma_5$ . Typical values of  $\Phi_{B0}$  of the tested 6 river sites had been shown to be in the range of  $\sim 70 - 120$  kPa (e.g. Beltaos 2013b). Mao et al. (2009) applied the boundary constraint criterion to predict the mechanical breakup on the Hequ reach of the Yellow River in China using data collected from 1985 to 1994. The authors rearranged equation [1-3] to calculate the critical discharge required to initiate a mechanical breakup. When compared with the measured discharge at the onset of breakup, the mean relative error of the calculated critical discharge was 11.29%. Beltaos (2013b) applied this criterion to explore the ice cover breakup induced by javes and showed that the increased water surface slope and shear stress during the passage of a jave are

essential for triggering mechanical breakup. Additionally, it is worth mentioning that this criterion can be simplified to a similar form to the water level criterion by assuming trapezoidal channel (Beltaos 1990a).

Numerical studies have also been carried out to assess the ice-fracturing capability of different forms of water waves in river channels. Daly (1993) studied wave-ice interactions with linear analysis method. Five bands of wave celerity were defined after the non-dimensional wave celerity was plotted against the non-dimensional wave number. Two ranges, quasi-open-channel range and ice-influenced range, were identified based on if the wave propagation is affected by ice. Based on this analysis, Daly (1995) found that transverse cracks can be potentially produced by small waves at a certain wavelength of  $2\pi l$  (where  $l$  is the characteristic length of the ice cover); however, field data was not adequate to prove this finding. Xia and Shen (2002) applied a non-linear analysis to further investigate this topic. It was found that waves that can fracture an ice cover typically have amplitude in the range of 0.2 to 0.8 m and corresponding wavelengths varying from 50 to a few hundred meters. Nzokou et al. (2009) built a computational fluid dynamics (CFD) model to simulate the flexure and breakup of an ice sheet. By solving for the deflection of a freely floating ice sheet, practical breakup criteria were obtained which determines the critical wave amplitude or water surface slope for fracturing an ice cover of certain thickness and strength for waves with wavelength from 10 to 1000 m. The required wave amplitude to break an ice cover increases with the increase of wavelength of the incoming wave, while the required water surface slope appeared to be plateaued for longer wavelengths.

Although these semi-empirical/physics-based criteria do not entirely describe the many complex interacting factors at play during breakup initiation, they have the potential to be transferable from site to site. Transferability is essential for enhancing our forecasting capability. However, no

physics-based breakup criterion has been implemented in any of the existing river ice process models.

### **1.3.3 Self-sustaining wave (SSW)**

An important aspect of ice breakup is the associated storage release. It has been postulated that the storage release leads to the formation of a non-attenuating, i.e. self-sustaining wave (SSW), which maintains ice breaking over long distance. Ferrick and Mulherin (1989) conducted a series of numerical simulations of ice breakup on the Connecticut River. Simplified geometry with river widths ranging from 100 to 200 m and an average bed slope of 0.00037 was used. Ice breakup was simulated using the side resistance criterion. When comparing to the parallel non-breakup case, they found that the ice breakup case produced less reduced or even amplified waves. Also, these waves tend to travel at a higher speed than those in the non-breakup case.

Using CRISSPID model and a discharge threshold criterion, Jasek et al. (2005) conducted a series of numerical simulations with combinations of different breakup initiating discharge, incoming waveform, bed slope and roughness. As ice is being broken up quickly, the wave was greatly amplified and then slightly abated with its discharge later reached a self-sustaining value. The results revealed some features of SSW which has a typical shape of a steep front and a flat crest. It was shown that SSW formed in prismatic rectangular channel can cause an increase of up to ~60% of the peak discharge of the incoming wave. The magnitude of SSW increases with the increase of bed slope and breakup initiating discharge. When compared with non-breakup cases, the celerity of the incoming wave as it travels downstream is also relatively high with the generation of SSW, breaking the downstream ice cover very quickly. This is consistent with field observations.

Beltaos (2017a) compared the storage release in an ice-covered rectangular channel from thermal deterioration and mechanical breaking up. It was found that the latter case generated far greater flow enhancement than thermal deterioration and under certain conditions produced SSW. A theoretical framework was established and applied to an event of rapid ice breaking over hundreds of kilometres observed on the Peace River during 2014 breakup. The SSW theory only partially explained the highly dynamic breakup event in an average sense, likely due to the natural river conditions were not accounted for.

#### **1.4 Study Objectives**

Mechanical breakup is associated with high flood risks as well as disruption/change of many hydrological, biological, and ecological processes. The mechanism of how a mechanical breakup is initiated and sustained is not yet well understood. Our current ability to model mechanical breakup is very limited. Existing river ice models either require the user to specify the time and location for ice cover breakup or they employ empirical criteria to simulate breakup. Therefore, the objectives of this study are to systematically evaluate existing criteria for simulating the initiation of ice cover breakup and the existence and characteristics of the self-sustaining wave, with the goal to enhance our breakup forecasting capability.

To achieve these objectives, six empirical and semi-empirical/physics-based breakup criteria were incorporated into the University of Alberta's *RiverID* model to test them quantitatively using data collected in the field. Three documented breakup events, the 2007 breakup of the Athabasca River (She et al. 2009), the 2014 and 2018 breakup of the Peace River (Jasek 2017b, 2019a), were used to facilitate this systematic test. Common to all these breakup events are that ice cover breaking was induced by javes and breakup progressed in the manner of a sheet breaking front. The breakup criteria were evaluated in terms of their ability to capture the observed breaking front propagation

and their transferability among different sites or situations. The features of the self-sustaining wave were also examined. This research is expected to improve breakup modeling capability, which is essential for environmental impact assessment under climatic and hydrologic changes. It also has implications to the prediction of when and where an ice jam may form as a result of the arrest of a breaking front, and thus can potentially enhance our capability of predicting ice jam caused flood.

Chapter 2 presents the methodology used in this study including model description, implementation of various breakup criteria in *River1D*, and a numerical case study for validating the proposed modeling method. Chapter 3 elaborates on the 2007 breakup event on the Athabasca River, along with the reach description and how the numerical simulation was set up for this event. The modeling results as compared to field observations are also detailed in this chapter. Chapter 4 focuses on the Peace River, where the 2014 and 2018 breakup events are depicted. It contains a brief introduction to the study reach, model setup, and results comparison. Finally, Chapter 5 summarizes the main conclusions of the study.

## Chapter 2 Methodology

### 2.1 Model Description

The University of Alberta's public domain software *RiverID* was used to facilitate the comparison of different breakup criteria in this study. *RiverID* was originally developed as an open water hydrodynamic model which solves the Saint-Venant equations using the characteristic-dissipative-Galerkin (CDG) finite element method (FEM) (Hicks and Steffler, 1990, 1992, 1995). This method has been shown to be more stable and accurate than many other finite element and finite difference numerical schemes particularly when modeling highly dynamic events (Hicks and Steffler, 1992). This advantage makes it particularly suitable for this study, in which dynamic javes are simulated. The capability of simulating various thermal and dynamic ice processes have been built into *RiverID* over the years and validated with a number of field events (Andrishak and Hicks, 2008; She et al., 2009a,b; Blackburn and She, 2019).

The version of *RiverID* model with natural channel geometry for open water and under-ice flow was used in this study. With the presence of an ice cover, the mass and momentum conservation equations can be written as:

$$\frac{\partial(s(A_w+A_0))}{\partial t} + \frac{\partial Q_w}{\partial x} = - \frac{\partial(s_i B_{ws} t_i)}{\partial t} \quad [2-1]$$

$$\frac{\partial(sQ_w)}{\partial t} + \frac{\partial(\beta Q_w^2/A_w)}{\partial x} + gA_w \frac{\partial y_{max}}{\partial x} + gA_w \frac{\partial z_b}{\partial x} + gA_w \frac{\partial s_i t_i}{\partial x} + gA_w S_f = 0 \quad [2-2]$$

where,  $A_w$  and  $Q_w$  are the cross-sectional area and discharge of flow under the ice cover, respectively;  $s_i$  is the specific gravity of the ice;  $t_i$  is the thickness of the ice;  $y_{max}$  is the maximum depth of the natural channel cross-section;  $B_{ws}$  is the width of the channel at the water surface;  $s$  is sinuosity, which is defined as the ratio of the main channel length to the valley length;  $\beta$  is the

momentum correction coefficient taken as 1.06 for natural channels based on Fread (1998); and  $S_f$  is the longitudinal boundary friction slope. The friction slope term is a function of shear stress:

$$gA_w S_f = \frac{\tau_b P_b + \tau_i P_i}{\rho_w} \quad [2-3]$$

where,  $\rho_w$  is the density of water;  $P_b$  and  $P_i$  are the wetted perimeter of the river bed and the ice, respectively;  $\tau_b$  and  $\tau_i$  are the shear stresses on the water due to the friction of the bed and the underside of the ice and are calculated using Manning's equation:

$$\tau_b = \frac{n_b^2 |U_w| U_w}{R_b^{1/3}} \rho_w g \quad [2-4]$$

$$\tau_i = \frac{n_i^2 |U_w - U_i| (U_w - U_i)}{R_i^{1/3}} \rho_w g \quad [2-5]$$

where  $n_b$  and  $n_i$  are the Manning's coefficient for the river bed and the underside of the ice;  $R_b$  and  $R_i$  are the hydraulic radius of the flow area affected by bed and by ice, respectively;  $U_w$  and  $U_i$  are the velocity of the water and the ice, respectively.  $U_i$  is zero for intact ice cover.

The model needed to be modified to incorporate breakup criteria. During each simulation, the model evaluates the breakup criterion being tested throughout the model domain. If the criterion is met at a certain location, the breaking front is set at this location. In the case where the criterion is met by multiple locations, the most downstream one is chosen as the breaking front. Downstream of the breaking front, the ice cover remains intact and the ice velocity is zero. Upstream of the breaking front, the ice velocity is set to increase linearly from zero to the water velocity over a distance of several channel widths. It has been observed in the field that there exists a transition zone between the rubble ice run from the released jam and the sheet breaking front generally of several river widths in length. Within the transition zone ice sheets shift position and close open water area. The ice in this reach is clearly not free drifting thus is expected to provide some

resistance to the water flow underneath. She and Hicks (2006b) applied this mechanism when modeling the moving ice accumulation ahead of the sheet breaking front (see Figure 2-1). The breaking front continues to propagate downstream as long as the breakup criterion is satisfied.

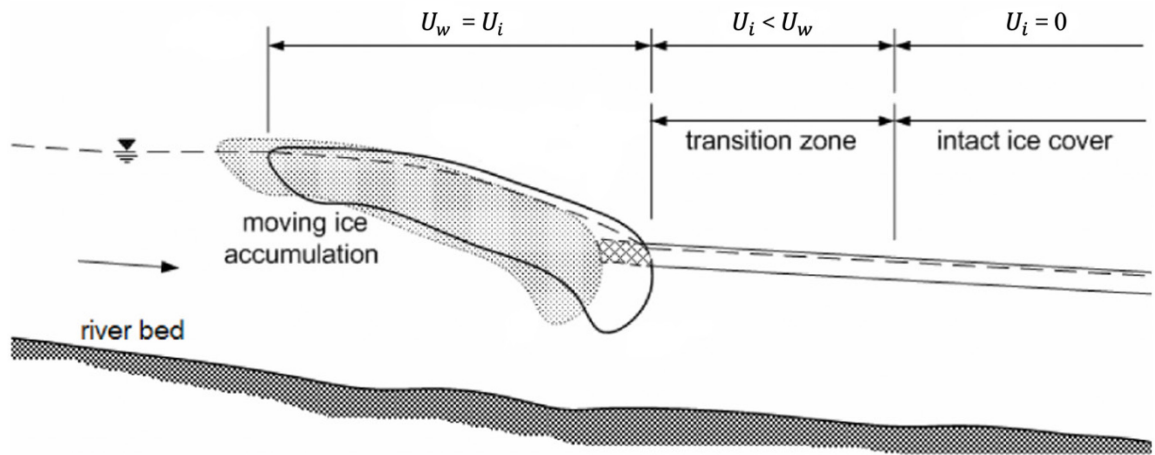


Figure 2-1. Definition diagram of ice movement near the breaking front (adapted from She and Hicks 2006a).

For each of the three field breakup events on the Athabasca River and the Peace River, the ice cover breakup was induced by a jave. The ice jam and the corresponding water surface profile before release are needed to quantify the shape and magnitude of the jave. *River1D* has a module to calculate the ice jam profile, however only for rectangular channel geometry. Therefore, HEC-RAS model (5.0.5 version) was used to simulate ice jam and water surface profiles before release. HEC-RAS solves the ice jam force balance equation at a constant carrier discharge using standard step method (HEC-RAS Hydraulic Reference Manual). The force balance equation is expressed as below:

$$\frac{d(\bar{\sigma}_x t_i)}{dx} + \frac{2\tau_{bn} t_i}{B_i} = \rho_i g S_w t_i + \tau_{iw} \quad [2-6]$$

where  $\sigma_x$  is the longitudinal stress along stream direction;  $\tau_{bn}$  is the shear resistance of the banks;  $B_i$  is the ice accumulation width;  $\rho_i$  is the density of ice;  $S_w$  is the water surface slope;  $\tau_{iw}$  is the shear stress applied to the underside of the ice by the flow.

HEC-RAS ice jam modeling requires the following inputs (Beltaos and Tang 2013):

1. The head and toe locations of an ice jam. This information is available from filed observations for all three events.
2. The Manning's coefficient of the bottom of the jam was calibrated for each individual event.
3. The thickness of ice cover prior to ice jam formation. This parameter was set according to field measurements of ice thickness in late winter or otherwise estimated based on other year's measurement if such information is not available.
4. The porosity of the rubble comprising the jam. A default number of 0.4 was used.
5. The friction angle of the rubble comprising the jam. A default number of  $45^\circ$  was used.
6. The ratio of lateral-to-longitudinal normal stresses within the rubble mass. A default number of 0.33 was used.
7. Maximum allowable flow velocity underneath the jam. A default number of 1.524 m/s was used for all events except for the 2007 Athabasca River ice jam, where a bigger value of 5 m/s was used instead to obtain a good match between the modeled and observed ice jam profile.

The HEC-RAS computed water surface profile before the ice jam release was then used as the initial condition in *River1D* for simulating the subsequent jave-induced ice cover breakup. For the

Athabasca River 2007 breakup event, field measurements of ice surface elevation within the released ice jam were available for calibrating the ice jam profile model. While for the Peace River 2014 and 2018 breakup events, such measurements were not available. Instead, the water levels recorded by the only hydrometric station upstream as the ice jam released was used to calibrate the ice jam profile. Thus, the calibrations were conducted through comparing the stage drop after the ice jam release. For simplicity, the rubble ice from the released ice jam was neglected. This approximation is considered acceptable as the focus of this study is the sheet breaking front, which is farther downstream from the ice rubble except for a very short period of time following the ice jam release.

## **2.2 Incorporating Breakup Criteria into *River1D***

### **2.2.1 Water level criterion**

Water level is empirically known to be a good indicator of breakup initiation. The water level criterion tested takes the form of equation [1-1] and is shown here again to facilitate discussions:

$$H_B - H_F > K\eta - F(\sum_5) \quad [1-1]$$

The freeze-up water level  $H_F$  was taken as the water surface elevation in the receiving channel prior to the ice jam release. This is because the freeze-up level was only available at a couple of gauged locations along the study reach. The breakup water level  $H_B$  is the model calculated water level after ice jam release and updated at every time step. The ice cover thickness  $\eta$  is set according to available information. The  $F(\sum_5)$  term was estimated through calculating the accumulated degree-days of thawing (ADDT) with a base temperature of  $-5^\circ\text{C}$  until the time of breakup. The temperature data were obtained from Alberta Climate Information Service (ACIS). For the Athabasca River 2007 ice jam release event, the value of ADDT is  $40^\circ\text{C-days}$ . As for the 2014

and 2018 breakup events of Peace River, the results of both years are quite similar, with 48.9 °C-days for 2014 and 56.1 °C-days for 2018. An adapted form of Stephan’s equation was used here to approximate the site-specific function  $F(\sum_5)$  (adapted from Ashton 1986):

$$\Delta ti = a\sqrt{ADDT} \quad [2-7]$$

where  $a$  is a site specific coefficient;  $\Delta ti$  is the ice thickness decreased due to warm weather. Instead of using accumulated degree-days of freeze-up (ADDF) to calculate the ice cover accretion due to thermal growth (original Stephan’s equation), this adapted equation uses ADDT to estimate the ablation caused by warm weather. Michel (1971) proposed a range of typical values for  $a$ , in which the values vary from 0.0014 to 0.0017 for an average size river with snow. Therefore, the ice thickness reduction between the time of late winter ice thickness measurement and just prior to breakup is between 0.009 m to 0.011 m for the 2007 Athabasca River breakup event, 0.01 m to 0.012 m and 0.01 m to 0.013 m for the 2014 and 2018 Peace River breakup events respectively. For simplicity, 0.01 m was chosen as the final input to substitute the  $F(\sum_5)$  term in equation [1-1] for the 2007 Athabasca River breakup event. And 0.012 m was used for both events on the Peace River.

The dimensionless site-specific coefficient  $K$  was the only calibrated parameter when using this criterion. The model evaluates equation [1-1] at every computational time step to determine the location of the breaking front. Ice velocity upstream of the breaking front was then set accordingly depending on whether the location is within the transition zone or not.

### 2.2.2 Discharge criteria

Two discharge based empirical criteria were tested in this study. One specifies a threshold discharge ( $Q_{br}$ ); the ice cover breaks up when  $Q_{br}$  is exceeded. The model compares the computed

discharge with the specified threshold value at each computational node at every time step. The other one considers the rate of change of discharge. This is an option that is available in *CRISSPID* (*CRISSPID Programmer's Manual Version 1.0*). The ice cover is considered breaking up when the calculated rate of change of discharge ( $R_Q$ ) exceeds a specified threshold for a given period of time ( $T_A$ ).  $R_Q$  was calculated through dividing the local discharge increment of each computational node over one time step. Considering the physics,  $T_A$  should not be a constant value. Smaller and slower change of discharge may have to build up the breaking power while big fast change likely does not need to persist long to break an ice cover. However, the criterion can become impractical to use if varying  $T_A$  for different  $R_Q$ . In this study, two sets of  $T_A$  and  $R_Q$  values were used: one for the early stage of the jave propagation when discharge changes rapidly and significantly; and one for the time when the jave had attenuated and the change of flow characteristics had reduced. The range of  $R_Q$  during an event was calculated by the model and used to determine its two threshold values. Afterwards, two  $T_A$  values were calibrated to obtain a best agreement between the modeled and observed breaking front trajectory.

### 2.2.3 Side resistance criterion

The side resistance criterion was implemented in the model in the following form (Ferrick and Mulherin 1989):

$$\tau_s = \frac{\bar{\omega}_i W_i}{2\eta} \quad [1-2]$$

The tractive stress  $\bar{\omega}_i$  includes the flow shear stress and the weight of the ice cover per unit area. Both are calculated in *River1D*. The flow shear stress underneath the ice was calculated with equation [2-5] shown above, and the equation for the calculation of the weight of the ice cover per unit area ( $G_i$ ) takes the following form:

$$G_i = \rho_i g S_w t_i \quad [2-8]$$

The width of ice sheet between hinge cracks  $W_i$  was taken as the initial width of the water surface just prior to the ice jam release, which can be calculated by the model based on geometric data and water level at each computational node. The ice cover is considered breaking up when  $\tau_s$  exceeds a threshold value which was calibrated against the observed breaking front location as it propagates downstream.

#### 2.2.4 Boundary constraint criterion

The boundary constraint criterion was incorporated into *River1D* in the form of equation [1-3] (Beltaos 1990a, 2008). The equation is shown here again to discuss how it was implemented in the model:

$$\frac{8(W-W_i)\bar{\omega}_i m^2}{(m-0.5)\eta_0} > \Phi_{B0} F(\Sigma_5) = \Phi_{B0} f_{ic} \quad [1-3]$$

The water surface width  $W$  when breakup occurs is computed by the model at every simulation time step using the modeled water level and the geometric data;  $W_i$  and  $\bar{\omega}_i$  were determined the same way as in the side resistance criterion. The thickness of winter ice cover just prior to the beginning of thaw  $\eta_0$  was taken as the user-defined ice cover thickness based on field measurement. The ice competence  $f_{ic}$  was set to 0.7 for the 2007 breakup event of Athabasca River considering the ice cover was only slightly deteriorated before the ice jam released. For the two events of Peace River, a value of 0.6 was used for both years given that their thermal deteriorations were similarly minor.

The variable  $m$  equals to the radius of channel curvature divided by  $W_i$ . The calculation of the radius of curvature was carried out in the Stream Restoration Toolbox of the National Center for Earth-surface Dynamics (NCED) on the ArcGIS platform (Marr et al. 2005). ArcGIS Desktop

(version 10.5.1) was used to facilitate this calculation. It provides a system to process maps and geographic information which also allows the extension of add-in tools. The Stream Restoration Toolbox consists of many sub-toolboxes which includes the Channel Planform Statistics Toolbox used here. It is capable of interpolating the centerline of a river and calculate the local radius of curvature. The final values of  $m$  were decided through dividing the output of the radius of curvature by  $W_i$ .  $m$  value changes with the spatial resolution used. In this study, the spatial resolution was selected based on the length of each river bend and was usually several kilometres for both the Athabasca River and Peace River. The only calibrated parameter when applying the boundary constraint this criterion was the reference composite parameter  $\Phi_{B0}$ .

### **2.2.5 Flexural and buckling criterion**

With regard to criteria based on ice cover flexure and buckling, the breakup criterion developed by Nzokou et al. (2009) in terms of the minimum required wave amplitude ( $a_{min}$ ) and water surface slope ( $S_W$ ) to initiate ice breakup was implemented in this study. Figure 2-2 shows the criterion as presented in Nzokou et al. (2009) for ice cover with a Young's modulus ( $E$ ) of 7 GPa and critical bending stress ( $\sigma$ ) of 0.7 MPa. The amplitude of javes is typically very large and is unlikely a limiting factor. Therefore, the flexural and buckling criterion was simplified to a water surface slope criterion. The wavelength of a jave is usually way bigger than the range considered by Nzokou et al. (2009). Thus, the plateaued value of water surface slope is taken as the threshold value.

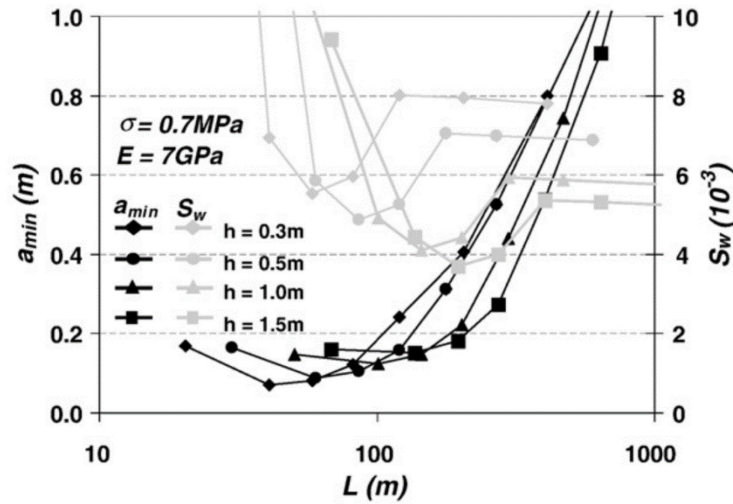


Figure 2-2. Minimum required wave amplitude and water slope to initiate ice rupture for ice cover of various thickness ( $h$ ) for  $E = 7$  GPa and  $\sigma = 0.7$  MPa (Nzokou et al. 2009).

## 2.3 Validation of Proposed Modeling Method

To validate the proposed modeling method, the hypothetical cases simulated by Jasek et al. (2005) with CRISSP1D model were modeled and the results were compared.

### 2.3.1 Case description

As in Jasek et al. (2005), two rectangular channels were set up for these simulations. One is 600 m wide, 500 km long with a bed slope of 0.0003. The other one is 600 m wide, 1000 km long with a bed slope of 0.00005. The lower 400 km portion of the 500 km long channel was covered by a 0.7 m thick ice sheet, and the ice cover with the same thickness was put on the lower 800 km portion of the 1000 km channel. The bed and ice roughness were 0.03 and the steady-state carrier discharge was 1600 m<sup>3</sup>/s for all simulations. Different triangular waves with the rising limb 3 times steeper than the falling limb were introduced at the upstream boundary condition to initiate breakup. As for the downstream boundary condition, the version of *River1D* applied in this study

does not support a steady state rating curve which was used by Jasek. Instead, a constant water level was specified at the downstream boundary, and two channels were extended 200 km downstream of the last cross-sections to minimize the effect of inaccurate water level at this boundary.

The discharge breakup criterion with a single threshold value was used to be consistent with Jasek et al. (2005). The ice cover is considered breaking up when local discharge exceeds a specified critical value (breakup initiating discharge  $Q_{br}$ ). In a prismatic rectangular channel with uniform ice cover thickness, the critical condition in terms of water level or shear stress would equally be exceeded when the critical discharge is exceeded. Thus, the single-variable discharge criterion is rigorous for this case study.

### **2.3.2 Transition zone**

CRISSP1D model used by Jasek et al. (2005) simulates a wide range of ice processes. Particularly related to ice cover breakup, it simulates surface ice concentration, the breakup ice run and jam. In this study, however, the proposed modeling method does not simulate the transport of ice and only considers the resistance effect of the ice on river flow. The broken ice was treated as either freely drifting with water or moving at a velocity slower than flow velocity within the transition zone (see Figure 2-1). This difference in the two models led to some discrepancy in the modeling results, which is affected by the length of the transition zone. She and Hicks (2006) reported that the length of the zone is generally several channel widths based on field observations. They chose to use 3 and 5 times of river width (B) when performing numerical experiments, and the same values were used in this study.

### 2.3.3 Results and discussions

Figure 2-3 shows an example of the typical results in terms of the discharge in the model domain at different simulation time. Both breakup (solid line) and the parallel no breakup cases (dashed line) are shown to depict how the storage release from the broken ice cover enhanced the incoming wave. This particular run was conducted in the steeper channel with a base flow  $Q_o$  of 1600 m<sup>3</sup>/s, and an incoming wave with a peak discharge of 1800 m<sup>3</sup>/s and a 3-hour duration. The breakup initiating discharge  $Q_{br}$  was set at 1620 m<sup>3</sup>/s. It can be seen that in the no breakup case, the incoming wave gradually attenuates as it travels downstream. While in the breakup case, the discharge waveform is greatly amplified. Water comes out from storage as the ice cover continues breaking up. Subfigures a)-c) in Figure 2-3 show that the shape of the discharge wave is maintained with a steep front and a flat crest, which is the feature of an SSW. The breaking front is sustained for hundreds of kilometres. The model results for a number of scenarios are compared with those in Jasek et al. (2005) and summarized in Table 1-1.

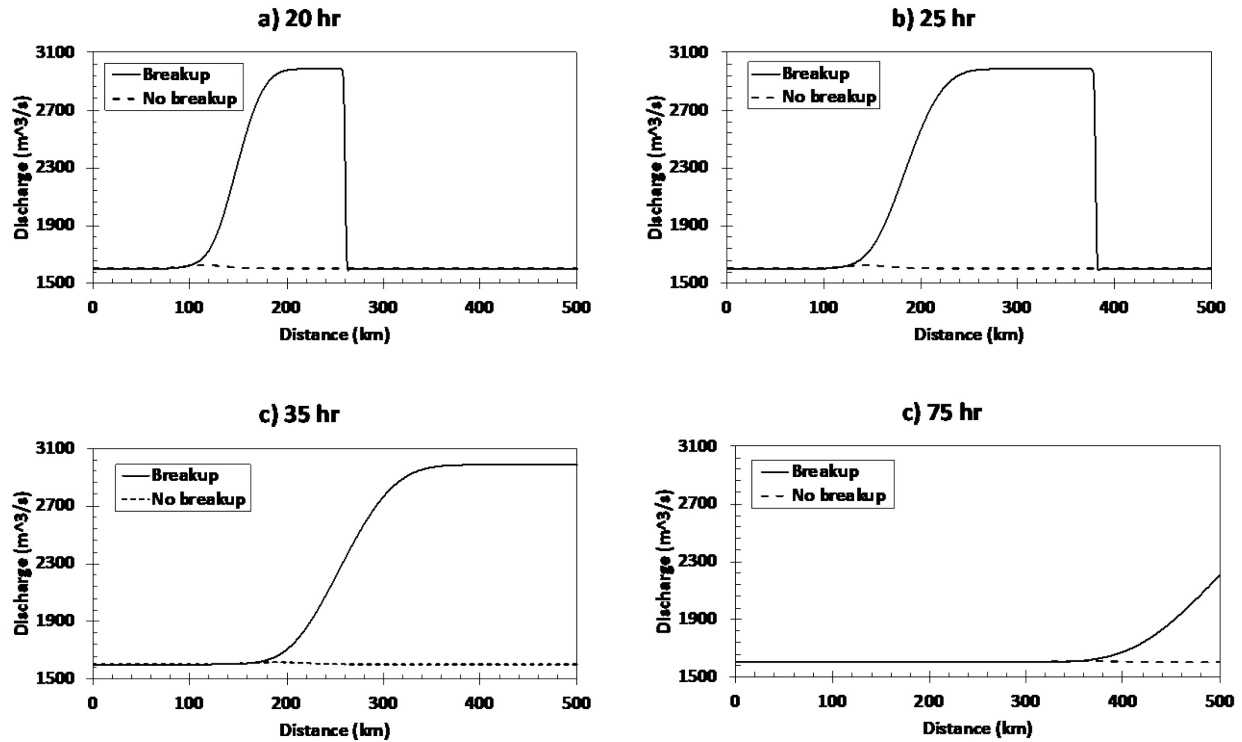


Figure 2-3. Comparison of discharge domain snapshots of the breakup and no breakup cases (Run 1 in table).

Table 2-1. Summary of modeling runs by CRISSP1D and *River1D*

Run #	Input					Output					
	Bed Slope	Q <sub>0</sub>	Q <sub>br</sub>	Incoming wave		Q at leading edge			Q sustained		
				Peak discharge	Wave duration	CRISSP1D	River1d 5B	River1d 3B	CRISSP1D	River1d 5B	River1d 3B
1	0.0003	1600	1620	1800	3 hours	1631	1697	1728	2900	2980	2960
2			3200	3400	4 days	3260	3520	3542	4300	4930	4700
3			2400	2600	4 days	2430	2652	2682	3600	4000	3800
4			2400	3000	18 hours	2430	2656	2684	3640	4000	3775
5			2000	2100	4 days	2055	2191	2225	3350	3500	3370
b1	0.00005	1600	1620	2100	6 hours	1629	1707	1713	2670	2684	2681
b2			3200	4600	4 days	3230	3294	3305	3530	3620	3627
b3			2400	3600	4 days	2673	2534	2546	3000	2950	2925
4b			2400	8000	18 hours	2498	2531	2543	3000	2940	2925

The discharge at the leading edge, which is the discharge at the breaking front, is usually slightly higher (by 2.9~11.8%) than the breakup initiating discharge  $Q_{br}$  for the cases tested. It can be seen that the values obtained using the proposed method are generally higher than those of Jasek et al.

(2005), and is slightly affected by the length of the transition zone. Shorter transition zone (3B) is associated with higher values as compared to the case with a longer transition zone (5B). Overall, these leading edge discharges produced by the proposed method are generally consistent with those in Jasek et al. (2005).

$Q_{sustained}$  is the self-sustaining discharge which was obtained after an SSW had formed. As shown in Table 2-1, results of the proposed method and CRISSP1D agree well for the cases in the mild slope channel, with only 0.5~1.7% difference. For the steep slope channel, the values of  $Q_{sustained}$  obtained from the proposed method are generally larger. The difference between the two ranges between 0.4~2.7% when using a transition zone of 3B and 0.5~2.5% when using a transition zone of 5B. These differences were considered acceptable given that the methods used to simulate ice are different in the two models.

This case study shows that in prismatic rectangular channels, storage release from ice breaking up greatly enhances the incoming wave, leading to the formation of SSW. As both the  $Q_{sustained}$  and  $Q_{br}$  exceed the base discharge  $Q_o$ , Beltaos (2017a) used excess ratios to explore the characteristics of SSW. The excess ratios were defined as  $(Q_{sustained}/Q_o - 1)$  and  $(Q_{br}/Q_o - 1)$ , respectively. The excess ratio offers a direct view of the flow discharge contributed by storage release from ice breakup. In the same way, the excess ratio of sustained discharge is plotted against the excess ratio of breakup discharge in Figure 2-3. Both the results from Jasek et al. (2005) and this study are shown for comparison. Some linear trendlines are added, and it can be seen that the excess sustained discharge increases with the increase of the excess breakup discharge. The storage release can amplify the flow by up to 210%. This amplification effect is more prominent in the steeper channel as compared to the milder one.

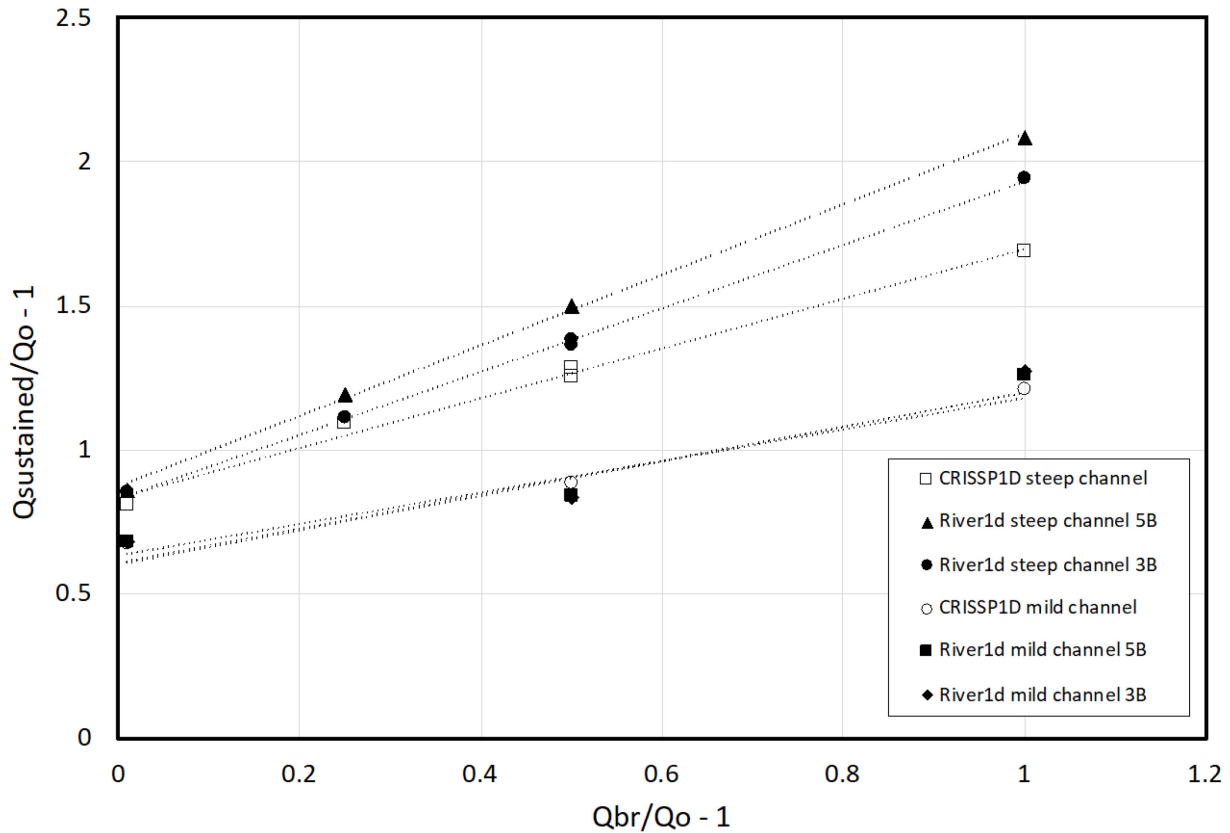


Figure 2-1. The variation of sustaining wave discharge and breakup initiating discharge. Both excess ratios were normalized with base discharge and subtracted by 1 to show the storage release amount (adapted from Beltaos 2017a).

This case study shows that the proposed modeling method produced comparable results to those of Jasek et al. (2005) with less sophisticated ice simulation. The transport of broken ice in a sheet breaking front was simplified with setting the velocity of ice based on where it is within or upstream of a transition zone. A sensitivity study was conducted with the typical range of the length of the transition zone (3B vs 5B). It was shown that the length of the transition zone affects the magnitude of SSW more in the steep slope channel but has little effect in the cases of the mild slope channel. The proposed method was then used to assess different breakup criteria using the

field data obtained during three breakup events that occurred on the Athabasca River and the Peace River. The results are presented in the following chapters.

## **Chapter 3 2007 Breakup Event on the Athabasca River**

The proposed modeling method was applied to simulate a documented ice jam release event that occurred during the Athabasca River 2007 breakup. The six breakup criteria were compared in terms of their capability of capturing the observed propagation of the sheet breaking front resulted from the ice jam release. The characteristics of SSW caused by jave-induced breakup were also explored. This chapter first introduces the study reach, followed by a description of the simulated ice jam release event. The model configuration and results are then discussed.

### **3.1 Study Reach**

The Athabasca River originates from the Jasper National Park of Alberta (AB), Canada, and is known as the longest river in Alberta. It travels 1,231 km and drains into the Peace-Athabasca Delta (PAD) near Lake Athabasca (data from Alberta Environment and Parks). The entire Athabasca River basin takes about 24% of Alberta's landmass with an area of 159,000 km<sup>2</sup> (data from the Athabasca Watershed Council). The basin supports around 5% of the provincial population, various natural resources in addition to the surface water and groundwater, and biodiversity such as bird nesting habitat and migration.

Figure 3-1 illustrates the map of the whole Athabasca River basin, as well as a zoom in the map of the area near the City of Fort McMurray, one of the most populated residential areas along the river. Breakup on the Athabasca River near Fort McMurray is usually a mechanical type and highly dynamic. The river is relatively steep with an average bed slope of  $\sim 0.001$  upstream of the city and flattens considerably to  $\sim 0.0003$  downstream of the location where the Clearwater River joins. A consistent breakup pattern is often observed from year to year (She et al. 2009). Breakup starts in the upper reach in the south and the broken ice forms small accumulations which toe-out over the many rapids. These ice movements lead to water level fluctuations which break more ice off the

intact ice cover and cause the small ice accumulations to lengthen. They finally become large enough to slip over these rapids and result in ice runs. In this manner, a cascade of ice jam formation and release events propagate down the river. The ice runs from the released ice jam upstream often become arrest near the Clearwater River confluence due to the sudden reduction in river slope and many large islands and bars just downstream of the confluence. The resulted ice jam can obstruct and back up the Clearwater River outflow, flooding downtown Fort McMurray. For example, Andres and Doyle (1984) documented three ice jams of over 20 km long with their toe located just downstream of the Clearwater River confluence, in consecutive years 1977, 1978 and 1979. Release of the 1979 ice jam caused a 3.6 m water level increase at the MacEwan Bridge in the City of Fort McMurray. The 2002 breakup involved a series of ice jam release events and was documented by Kowalczyk and Hicks (2003). The water level was recorded at several hydrometric stations. A station approximately 30 km upstream of the city recorded a water level rise of 4.1 m with a maximum rise of 0.81 m/minute, and one in the city recorded an increase of 1.4 m.

Numerous ice jam formation and release events have been documented by previous study on the Athabasca River near the City of Fort McMurray. In particular, the 2007 breakup involved release of an ice jam just upstream of the Clearwater River confluence. The resulted jave instigated a sheet breaking front which was tracked by helicopter, allowing this numerical exploration.

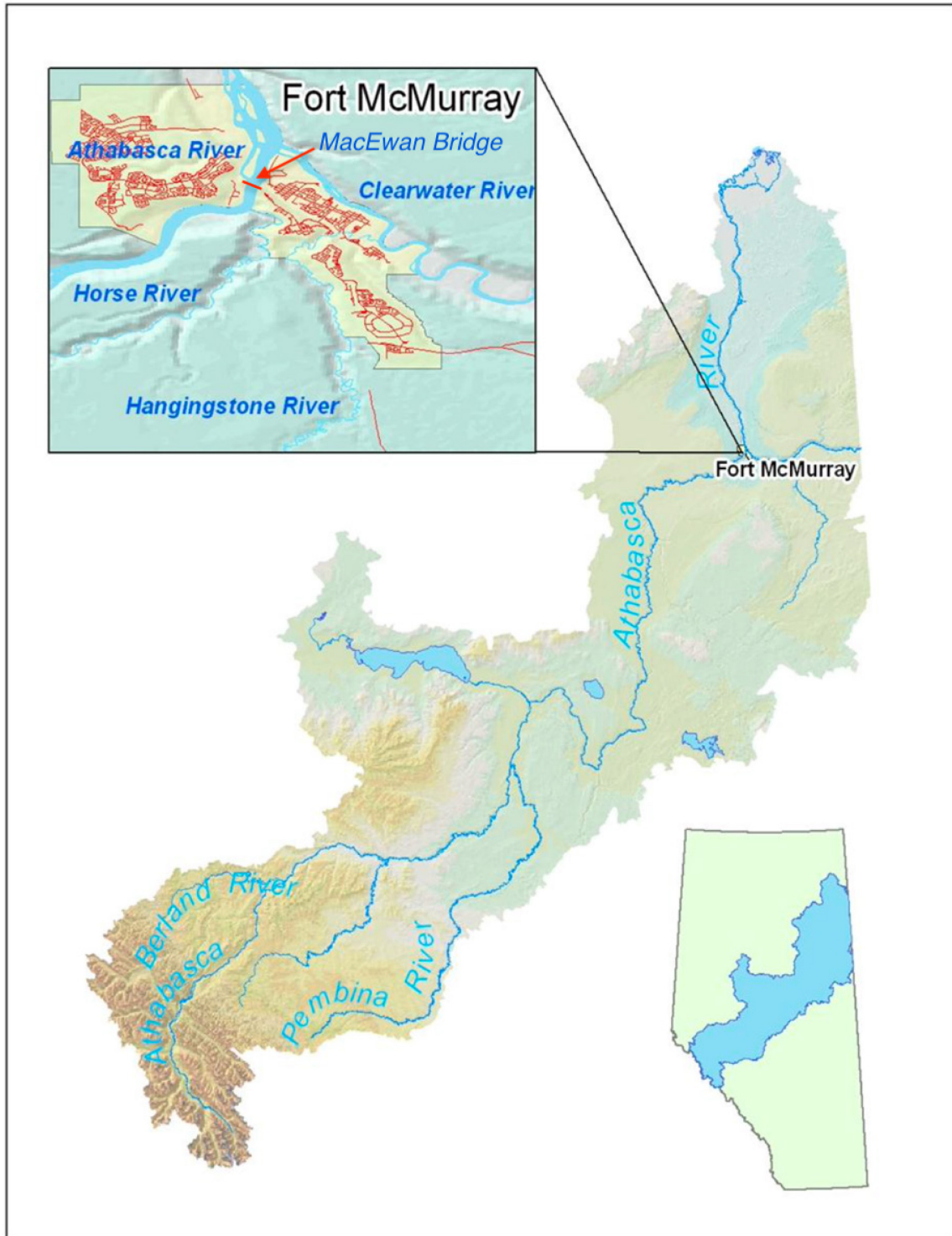


Figure 3-1. Map of Athabasca River basin and river reaches in the vicinity of Fort McMurray  
(Adapted from Friesenhan et al. 2008).

### **3.2 2007 Ice Jam Release Event Description**

The 2007 breakup on the Athabasca River was highly dynamic, resulting in multiple ice jam events along the river. This event was documented by She et al. (2009) in detail. Figure 3-2 shows the monitoring stations along the river in the vicinity of Fort McMurray in that year, which included meteorological data monitoring, ice and water level monitoring and photographic monitoring. The water or ice level hydrographs at several stations were recorded by this monitoring network. Other aerial and ground observations were also conducted to provide complementary data about ice conditions.

In the late afternoon of April 17th, all the rapids between Fort McMurray and Crooked Rapids were experiencing small ice jams. These ice jams all lengthened by 8:00 on April 18th. During the late evening of April 18th and early morning of April 19th, several hundred kilometres of ice cover broke up which led to a series of ice runs, ice jam formation and release events. In particular, an 11 km long ice jam formed against lengthy intact ice cover, with its toe at the water intake site (at 296.1 km) and its head near the Mountain Rapids (near 308 km). During the day of April 19th, an extensive ice run over 30 km long traveled from upstream and hit the head of the ice jam, causing the jam to release at 20:00. A sheet breaking front formed as the ice cover in the receiving channel was broken into large ice sheets and pushed ahead by the propagating jave. The jave was recorded by 3 stations downstream of Fort McMurray: Water Survey of Canada (WSC) gauging station Athabasca River below Fort McMurray (RATHMCM, 289 km), station M288.1 and further downstream at 268.1 km. The location and speed of this breaking front were tracked with GPS and video camera on a helicopter. It was observed that the breaking front was initially traveling at high speed at around 3.8 m/s but later slowed down to about 1.8 m/s near the islands downstream of the Clearwater River confluence (293.0 km).

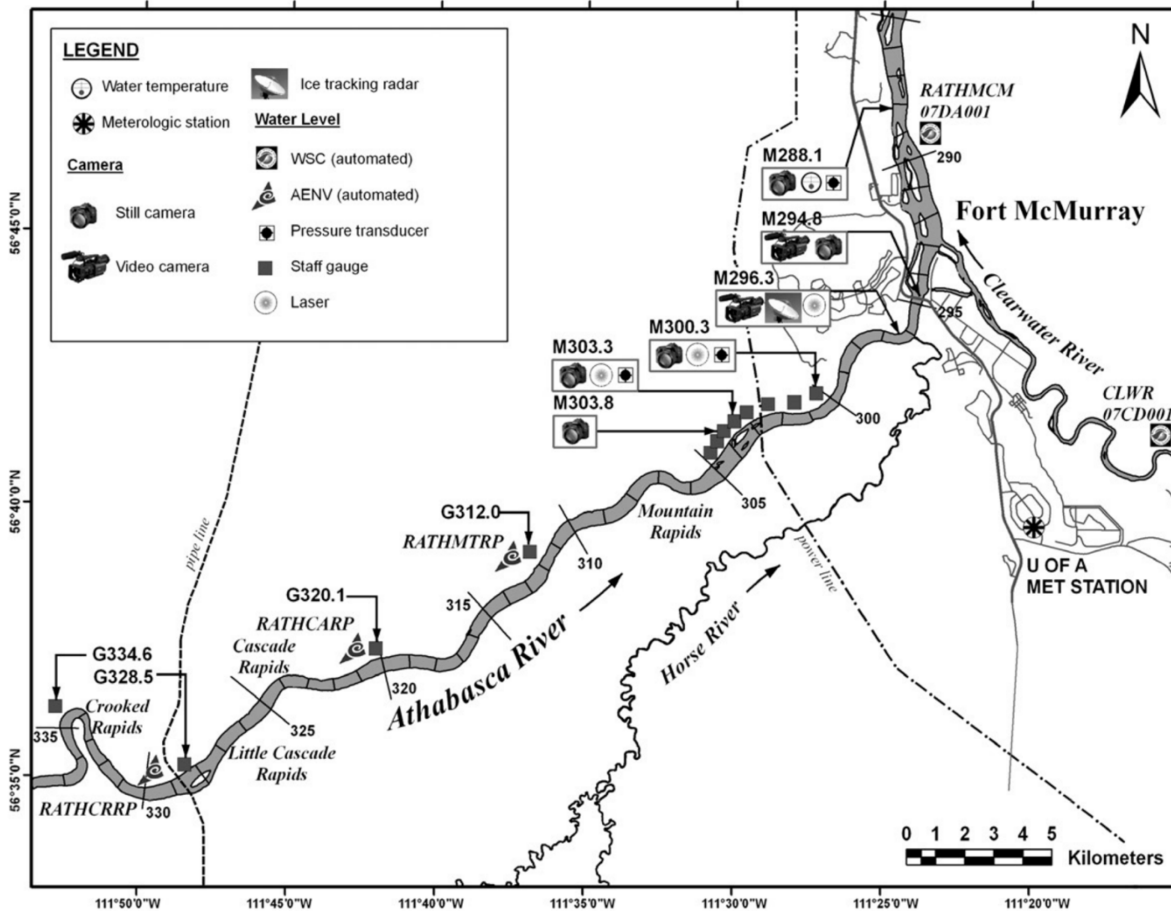


Figure 3-2. Monitoring stations in the vicinity of Fort McMurray in 2007 (She et al. 2009).

The top of the ice jam was measured by a laser rangefinder at the water intake site (M296.3), as well as by photographing the staff gauges installed along the remote reach upstream of Fort McMurray just prior to its release. The ice cover was measured to have an average thickness of around 0.5 m in the late winter and was only slightly deteriorated by the time the water intake ice jam released. She et al. (2009) analyzed the water intake ice jam release event and the subsequent breaking front propagation using *River1D* ice jam release modeling component based on rectangular channel geometry approximation (She and Hicks 2006a). Effects of the ice in the original ice jam were included empirically. The sheet breaking front was simulated with a

conceptual model (She and Hicks 2006b). Figure 3-3 shows the measured level of the top of the ice jam prior to its release, together with the tracked locations of the breaking front formed as a result of the release (She et al. 2009).

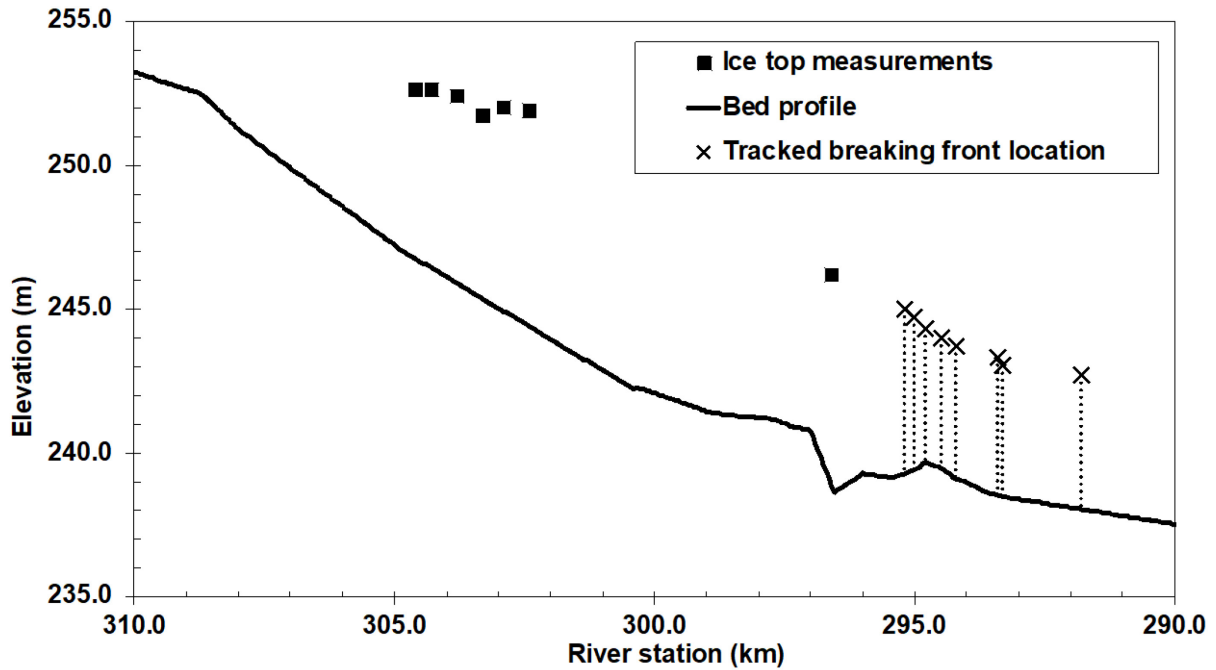


Figure 3-3. Measurements of the top of the ice jam prior to release on April 19, 2007 and locations of breaking front tracking (adapted form She et al. 2009).

### 3.3 Model Configuration

#### 3.3.1 Geometric model

The geometry used in this study is a combination of rectangular and natural cross sections. 50 surveyed cross sections are available in the section between ~340 km and 260 km. Most of these cross sections were obtained from Friesenhan (2004) which were based on different sources (Andres 1982; ARC SWE 1977, 1979, 1984, 1985; University of Alberta 1999, 2001, 2002) and 7 cross sections were provided by Alberta Environment and Parks (AEP). The bed elevation profile

of the interest area is shown in Figure 3-4, along with the locations of surveyed cross sections and key locations of the event. The propagation of the sheet breaking front was tracked until ~ 290 km and the most downstream gauge station which recorded the jave was at 268.1 km. The model domain was extended by over 200 km downstream so that a fixed water level can be used as the downstream boundary condition and does not affect the hydraulics of the river section of interest. The extended reach had rectangular cross-sections which are the same as those used in She et al. (2009). At the upstream boundary, a constant discharge of 950 m<sup>3</sup>/s was used based on She et al. (2009), estimated from two WSC gauging stations: RATHMCM and Clearwater River at Draper (RCLEDRAP). The cross sections in the section of interest were interpolated at a 50 m space interval. The Manning's n used for bed was 0.035 upstream of 319.45 km and 0.03 downstream based on She et al. (2009).

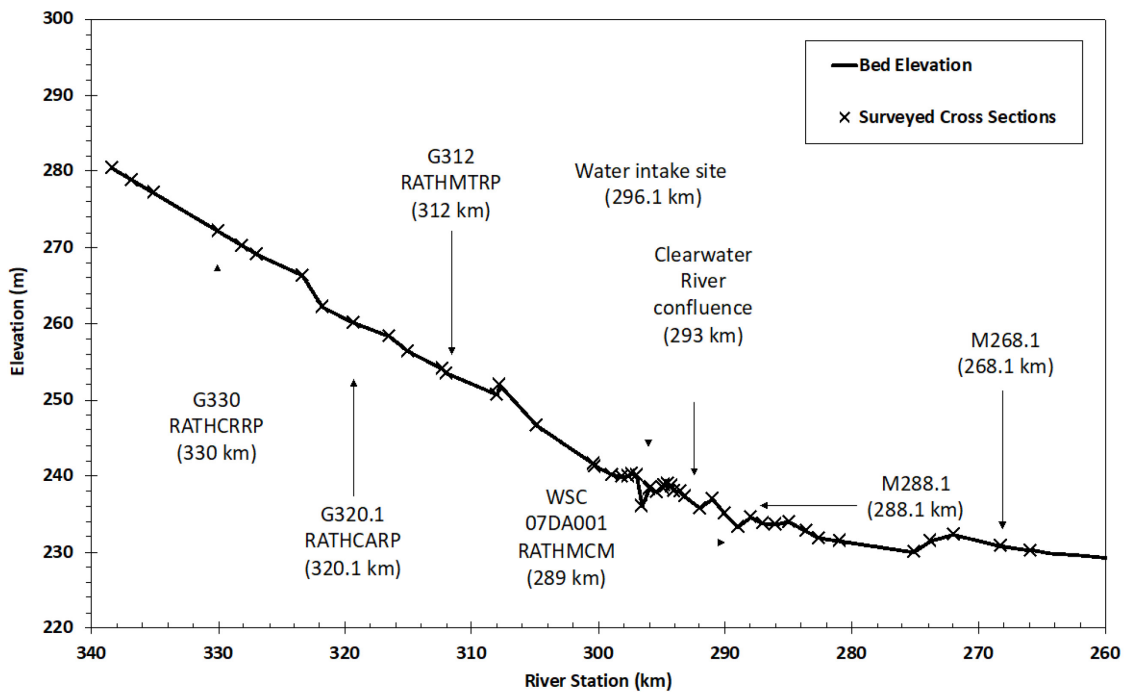


Figure 3-4. Bed profile of the interest area on the Athabasca River with available surveyed cross sections and key locations.

### 3.3.2 Initial condition

HEC-RAS model was used to calculate the water surface profile and the associated ice jam profile prior to release. It was noticed that a space interval of 50 m produced an unrealistic ice jam profile. Beltaos and Tang (2013) had noted the issue that too large or too small spacing can both cause HEC-RAS to calculate implausible ice jam profile, and the optimal spacing appears to be site specific. Through trial and error, a spacing of 200 m was found to provide a reasonable ice jam profile. The ice roughness was calibrated to be 0.043 for the bottom of the ice jam and 0.015 underneath the solid ice cover downstream. As shown in Figure 3-5, the modeled and observed top of ice elevations agree well.

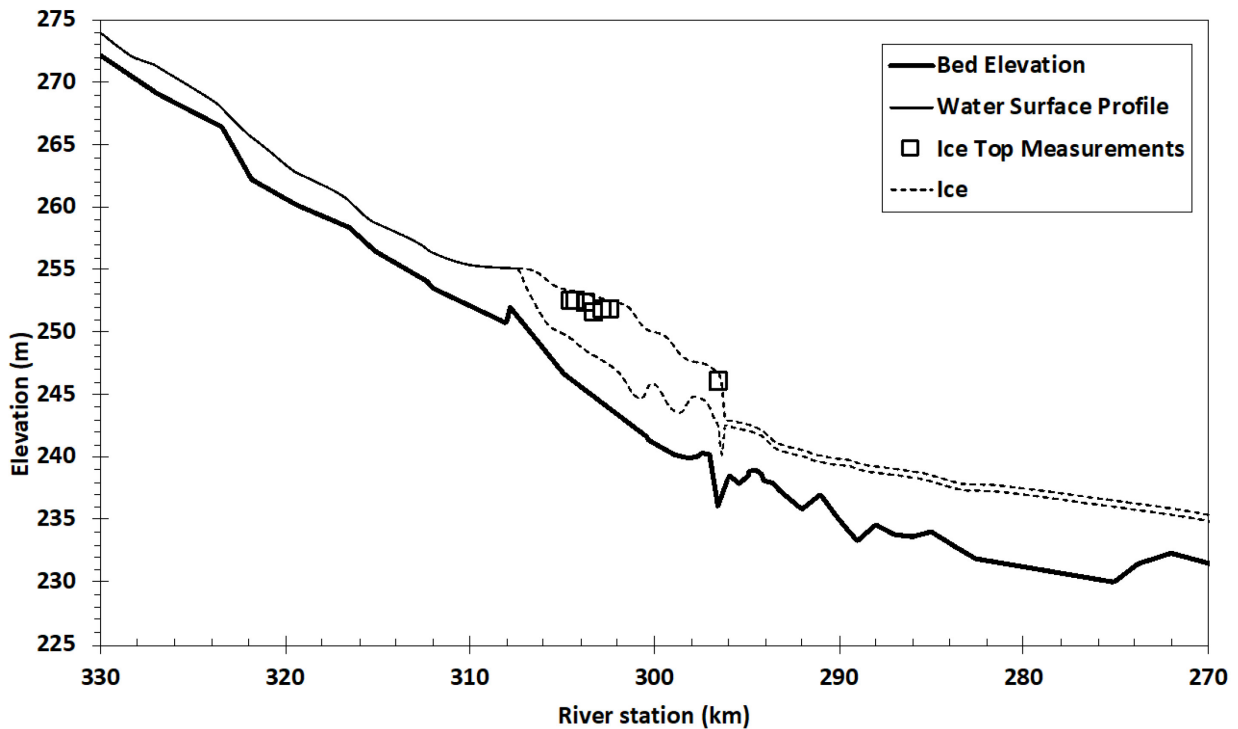


Figure 3-5. The computed profile of the 2007 Athabasca River water intake ice jam.

### 3.3.3 Other considerations

As can be seen from Figure 3-4, the Athabasca River in the vicinity of the Clearwater River confluence and downstream is relatively flat with an average bed slope of  $\sim 0.0003$ . It had been shown that the length of the transition zone can affect the model results for steep channels, but the difference between using three channel widths (3B) and five channel widths (5B) is only marginal. Therefore, the length of the transition zone was set as five times of the channel width (5B) in all simulations of the Athabasca River 2007 event.

The river reach upstream of the Clearwater River confluence is relatively steep single channel with narrower cross sections, while downstream of the confluence the river is a lot flatter and with wide and braided channels. Example surveyed cross sections in these two reaches are shown in Figure 3-6. It is plausible to think that this difference in geometric features also affects some of the hydraulic and ice features such as flow drag underneath an ice cover and type of the ice cover. Therefore, the study reach was divided into two sub-reaches at the confluence when setting the values of parameters used in certain breakup criteria, for example, the threshold value of side resistance. Details of the parameter calibration are discussed for each of the specific breakup criterion in the following section.

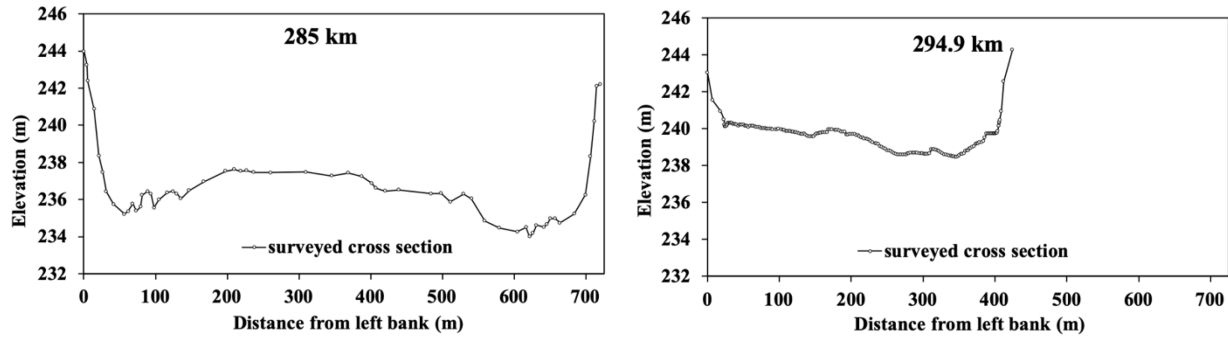


Figure 3-6. Cross section geometry downstream (285 km) and upstream (294.9 km) of the Clearwater River confluence (293.0 km).

### 3.4 Results and Discussions

#### 3.4.1 Breakup criteria assessment

The aforementioned six breakup criteria were assessed in the context of the 2007 water intake ice jam release event. Parameters of each criterion were calibrated against the documented breaking front location. Figures 3-7 – 3-12 show the comparison between the modeled and observed locations of the sheet breaking front following the water intake ice jam release, when different breakup criterion was used.

In the water level criterion (equation [1-1]), the coefficient  $K$  was calibrated to be 3 which is at the high end of the range of 2 – 3 obtained by Beltaos (1990a) using field data of six river sites. This is likely due to the relatively low bed slope near Fort McMurray, resulting in lower tractive stresses ( $\bar{\omega}_i$ ) acting on the ice cover. It can be seen that the modeled breaking front propagation overall matches well with the GPS and video tracked breaking front locations (Figure 3-7). The difference between the modeled and observed breaking front location is within 200 – 400 m. Since the breaking front is relatively close to the toe location of the original ice jam (the last recorded location is only 4.3 km or 0.39 jam length downstream), it is expected that the jave is highly

dynamic and the effect of the ice rubble from the released jam on the water wave is significant. Therefore, this discrepancy between the model and the observed is considered acceptable. The modeled breaking front kept propagating downstream (not shown in the figure) and eventually stopped at 249.3 km at 02:30 on April 20<sup>th</sup>. The arrest of the breaking front was not observed in the field; but the hydrographs recorded at gauge stations RATHMCM (289 km) and M288.1 suggest the ice run had stalled (at least briefly) between these two stations. Model results may possibly be fine-tuned by setting different threshold values for different segments of the study reach. However, it would result in many calibrated parameters and there is no justification for doing so.

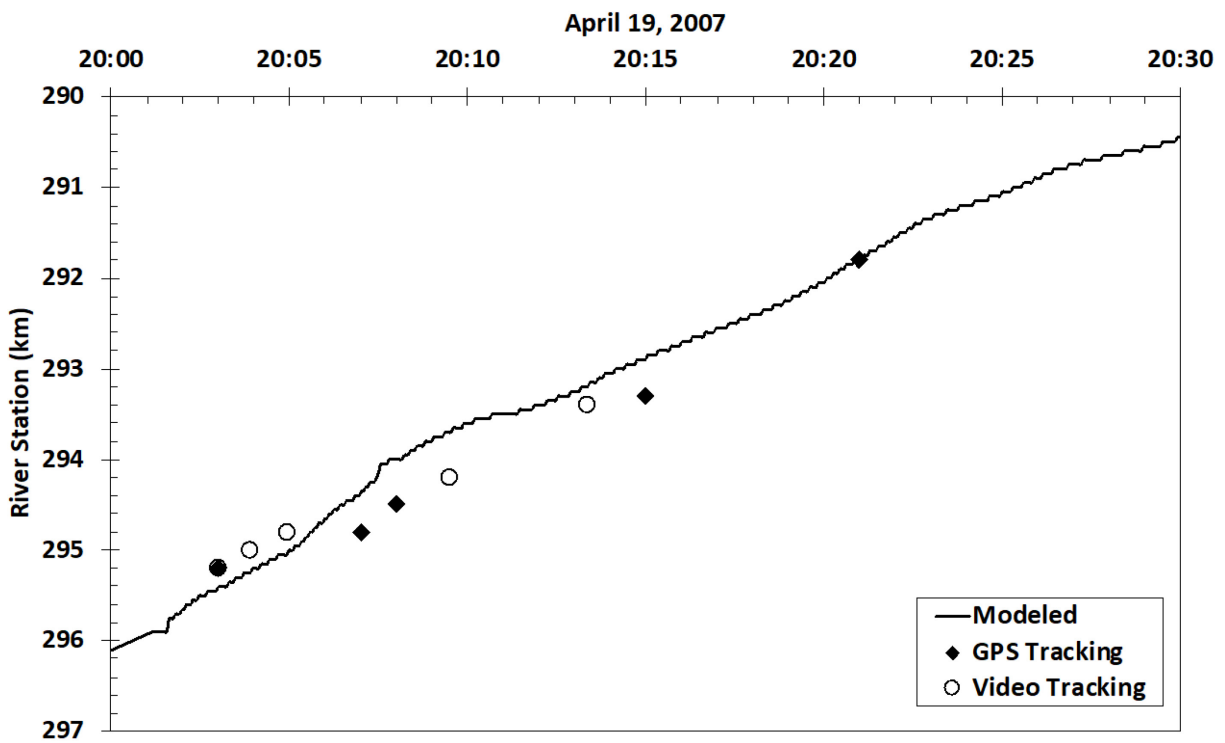


Figure 3-7. Comparison of observed and modeled breaking front location in 2007 on the Athabasca River (water level criterion).

The modeled breaking front progression based on the discharge criterion is shown in Figure 3-8. A range of values of the breakup initiating discharge ( $Q_{br}$ ) was tested and it was found that 4000 m<sup>3</sup>/s produced the best agreement with the observed breaking front trajectory. The modeled and observed breaking front agree almost perfectly in the first 10-minute travel time, then the modeled became 350 – 800 m ahead than the observed. At 21:20, the modeled breaking front stopped at 283.6 km (not shown in the figure). To see the effect of selecting different  $Q_{br}$  value, the result for  $Q_{br} = 5000$  m<sup>3</sup>/s is also shown in the figure for a comparison. It can be seen that the modeled breaking front lagged behind the observed until around 15 minutes after the jam release, and then agreed well afterwards. This indicates that the modeled breaking front propagation is sensitive to the threshold discharge. Using different threshold discharge values for different segments may produce better results, but again there is no physical basis and the calibrated values would not be transferable to other sites. The unperturbed-flow discharge prior to the ice jam release was 950 m<sup>3</sup>/s and the peak discharge of the jave was 6180 m<sup>3</sup>/s as computed by *RiverID*.

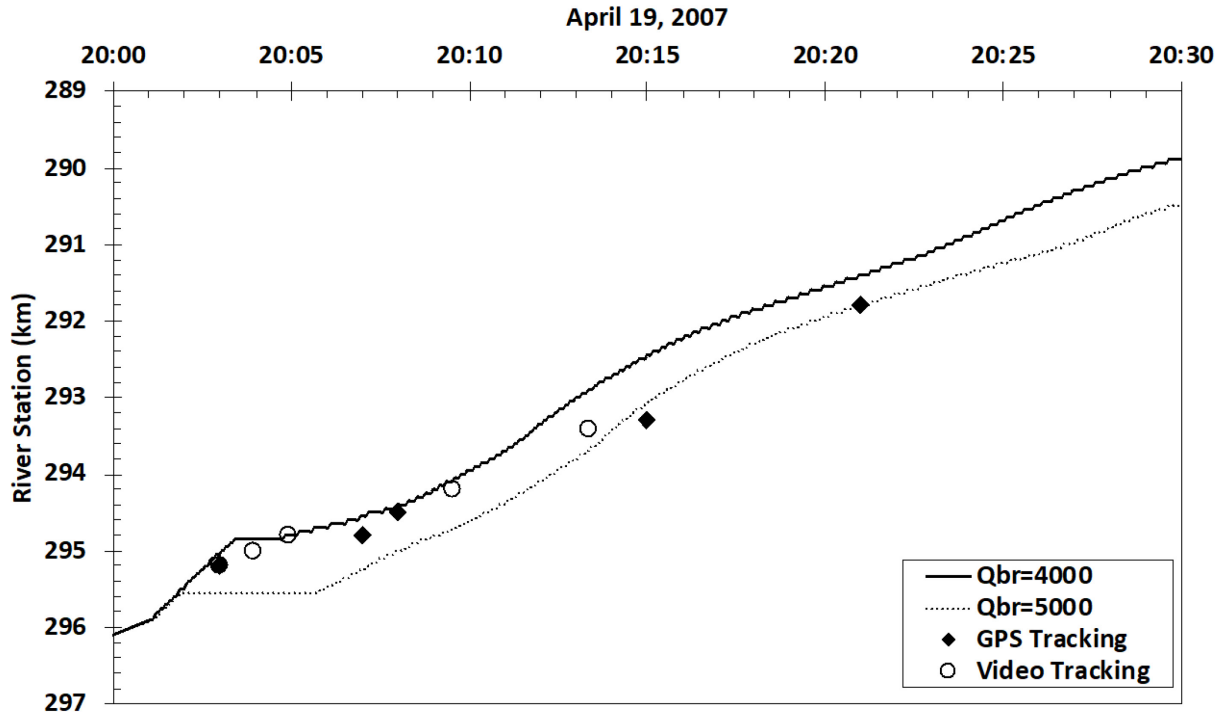


Figure 3-8. Comparison of observed and modeled breaking front location in 2007 on the Athabasca River (discharge criterion).

The peak value of the rate of change of discharge  $R_Q$  was computed to be in the range of  $\sim 150 - 360 \text{ m}^3/\text{s}^2$  within the first 5 minutes of the ice jam release. At around 15 minutes, the peak  $R_Q$  reduced to about  $10 \text{ m}^3/\text{s}^2$  and continued to decrease as the jave attenuated. These values provided the basis for calibrating the discharge rate breakup criterion. To produce the results shown in Figure 3-9, the ice cover was set to breakup immediately ( $T_A = 0$ ) if  $R_Q$  exceeds  $250 \text{ m}^3/\text{s}^2$  or when  $R_Q$  persisted beyond  $2 \text{ m}^3/\text{s}^2$  (but below  $250 \text{ m}^3/\text{s}^2$ ) for 5 minutes or more. It can be seen that the modeled breaking front stopped for 5 minutes near 294.7 km, then resumed downstream movement at 20:08. GPS/video tracking data also showed that the breaking front slowed down significantly near 294.7 km, which lends credibility to the theory that smaller and slower change of discharge

have to persist some time to break an ice cover. The modeled breaking front eventually stopped near 281.75 km at 21:02.

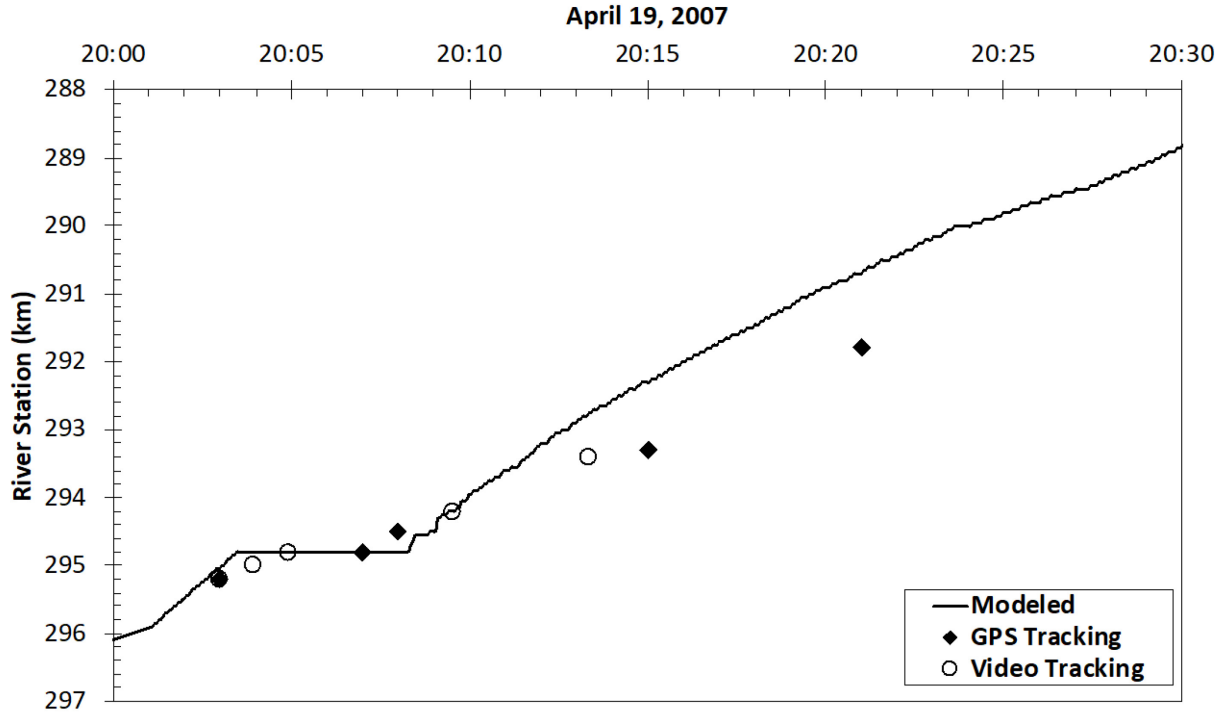


Figure 3-9. Comparison of observed and modeled breaking front location in 2007 on the Athabasca River (discharge rate criterion).

Two values of 21 kPa and 18 kPa were calibrated for the threshold side resistance, for reaches upstream and downstream of the Clearwater River confluence, respectively. The smaller threshold value for the downstream reach is likely due to the channel and the ice cover is much wider and the bed slope is milder here. However, the calibrated threshold values are way bigger than those found by Beltaos (1997a), which ranged from 0.2 to 7 kPa for five river sites. The side resistance criterion does not appear to work well as the modeled breaking front only captured the observed at some certain locations (Figure 3-10). The modeled front traveled faster than the observed during the first 6 minutes and then paused at 293.65 km for roughly 10 minutes. And it stopped

permanently around 20:18 near 291.45 km. These two stalls were inconsistent with field evidence. This is likely due to the highly site and time dependent nature of the side shear resistance. Side resistance at the onset of breakup calculated by Beltaos (1997a) with field data showed large variability for different sites. The cross sections near and after the confluence change dramatically within a short reach, with the channel width doubled and larger islands appearing in the channel. It is also unclear how side resistance changes with the progression of thawing. For these reasons, Beltaos (2008) suggested that the side resistance criterion is more suitable for one site only at one time.

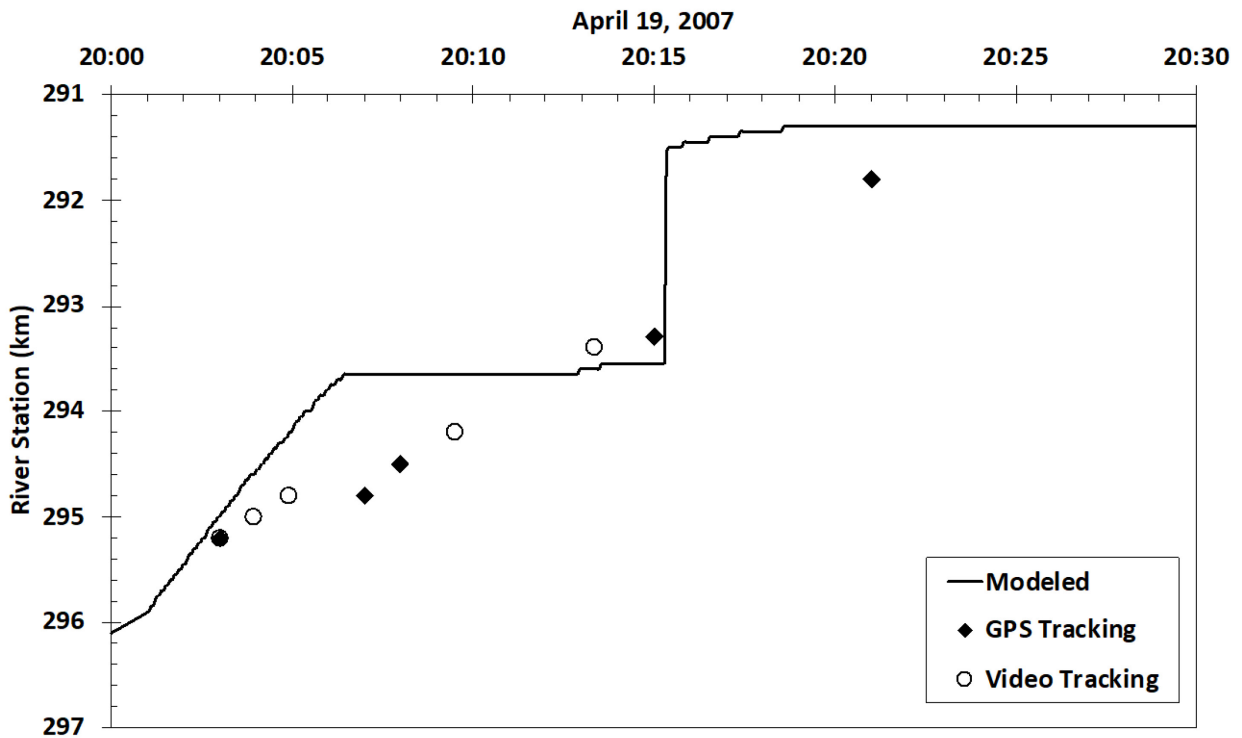


Figure 3-10. Comparison of observed and modeled breaking front location in 2007 on the Athabasca River (side resistance criterion).

In the boundary constraint criterion (see equation [1-3]), the dimensionless radius of curvature  $m$  was determined using the Stream Restoration Toolbox as described in Chapter 2. Beltaos (2013b)

pointed out that  $m$  is a dominant factor in equation [1-3] thus it was deemed necessary to assess the effect of using different spatial interval when computing  $m$ . Two spatial intervals were used, a constant 1 km and the length of individual river bend or crossover section (usually several kilometres), resulting in two sets of  $m$  values. Figure 3-11 shows a comparison of the two sets of computed  $m$  values, focusing on the reach within which the ice jam was in place and the breaking front had traveled. It can be seen that the values computed at 1 km interval are over a wider range and more scattered than those calculated at individual bend and crossover, but there is no huge difference between the two sets. These values appear to be consistent with the values presented by Beltaos (1997a) for five river sites (Table 2-1). A Large percentage of the values fall between 5 ~ 7. The largest  $m$  values are seen near 295 km where the river is relatively straight single channel. Smaller  $m$  values are around 290 km where the channel is very wide with islands and bars. The large range of  $m$  values in the reach is due to the variable channel geometry.

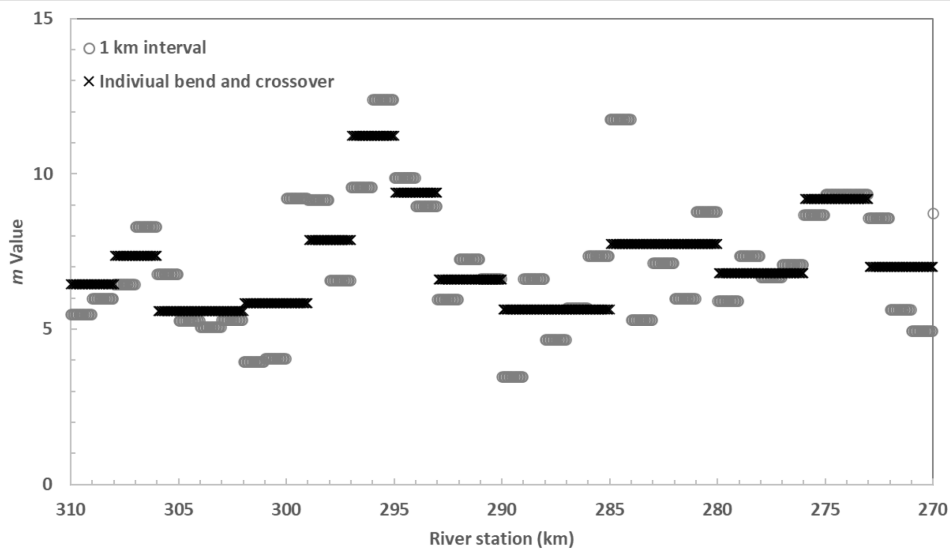


Figure 3-11. Comparison of  $m$  values computed using different spatial interval.

The composite parameter  $\Phi_{B0}$  was calibrated to be 80 kPa when using the  $m$  values computed at individual bend and crossover and 70 kPa when using the  $m$  values computed at 1 km interval, respectively. Both values are considered reasonable for a typical large northern river and within the range of  $\sim 70 - 120$  kPa found by Beltaos (2013b). The modeled breaking front propagation trajectories are very similar between the two cases. The breaking front temporarily stopped several times with its location always ahead of the field observations. All of the stalls happened near or downstream the confluence, where the steep banks of the cross sections lead to small  $W - W_i$  values. As a result, the left hand side of equation [1-3] is very small at these locations and the boundary constraint criterion cannot be met. When the jave traveled to location further downstream where the channel banks are less steep, equation [1-3] can be satisfied and the breaking front “jumped” to this location. In this way, the modeled breaking front continued moving downstream until it finally stopped at 288.55 km at 21:28.

The scale of individual river bend and crossover section may be more representative of the geometric/morphologic characteristics, while it is more straightforward to just use a constant interval. These results show that although  $m$  values are different when computed using different spatial interval, similar modeled breaking front propagation can still be achieved by calibrating the composite parameter  $\Phi_{B0}$ . The modeled breaking front does not match the observed as good as some of the empirical criterion (e.g. water level, discharge), but it is still promising as it demonstrates that the breaking front stalls or slows down in responding to geometric constraint. This is known to be the main cause of the arrest of an ice run and the formation of an ice jam. Thereby the boundary constraint criterion may have the potential to predict ice jam occurrence and associated flood. The limitation may be with applying such criterion with a 1D model, especially when river channel characteristics are highly complex (e.g. steep banks, large islands and bars). A

1D model may not be adequate to account for the real effects of large islands and bars (presented in the study reach downstream of the confluence) when considering the ice segment to move past the river bend. This issue may potentially be addressed through applying the boundary constraint with a 2D model.

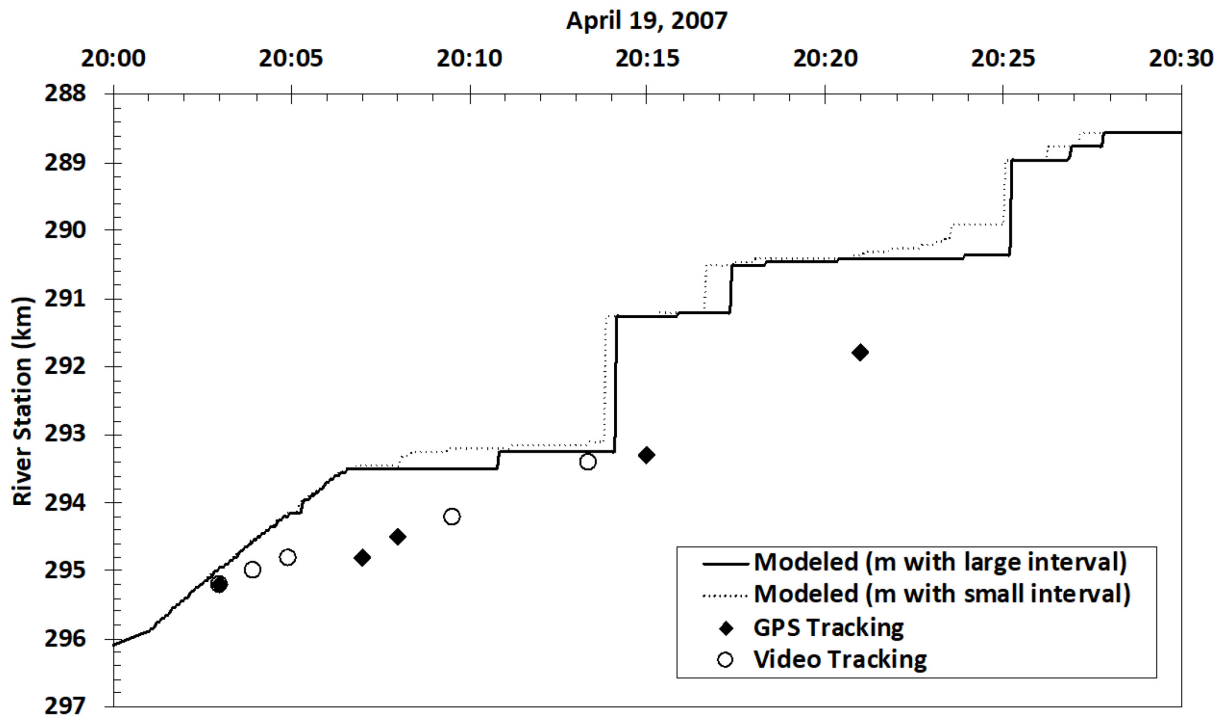


Figure 3-12. Comparison of observed and modeled breaking front location in 2007 on the Athabasca River (boundary constraint criterion).

Table 3-1. Channel characteristics of five river sites (adapted from Beltaos, 1997a)

Site and years of record	Chanel description	m
Thames River at Thamesville, 1980 - 1986	Straight single channel, deep, steep banks	31.4
Grand River near Marsville, 1981 - 1984	Moderate bends, single channle shallow	6.4
Moose River at Moose River, 1961 - 1980	Straight channel, islands, wide	14.4
Nashwaak River at Durham Bridge, 1965 - 1983	Straight channel, large island above gauge	21.6
Restigouche River above Rafting Ground Brook, 1970 - 1992	Wider meander, single channel	7.9

Billfalk (1982) and Beltaos (1985) suggested based on theoretical analysis that flood waves with water surface slope of 0.005 or more can break ice cover by vertical bending. Nzokou et al. (2009) also showed that the required water surface slope to break an ice cover plateaued at  $\sim 0.005 - 0.007$  as the wavelength of the incoming wave increases. This large water surface slope may persist for a short period of time following the release of a major ice jam. For the 2007 water intake ice jam release event, the water surface slope was between 0.005-0.008 during the first 5 minutes and  $\sim 0.001-0.005$  thereafter as computed in the model. A range of breakup initiating water surface slopes (0.001-0.005) was tested, but none seemed able to capture the breaking front progression observed in the field (Figure 3-13). When using larger threshold water surface slopes, the modeled breaking front stopped completely not long after the ice jam released; while for small threshold water surface slope (0.001), a long stretch of the river (over 2 km) broke up instantaneously. Beltaos (1990a) noted that during a major ice jam release event, the flow velocities can increase dramatically, amplifying the flow shear stresses applied on the ice cover. As a result, many other breaking mechanisms in addition to vertical bending may come into play. Thus, using the water surface slope as a single-variable threshold may not be adequate for jave-induced breakup.

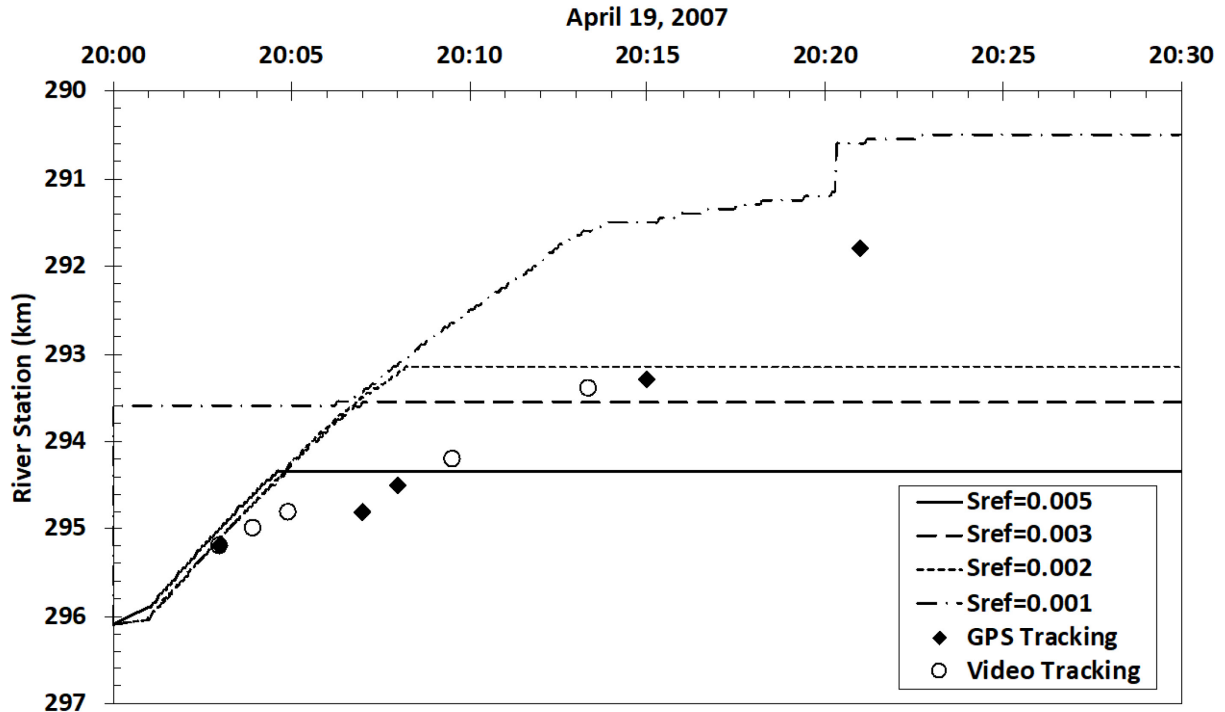


Figure 3-13. Comparison of observed and modeled breaking front location (flexural and buckling or water surface slope criterion).

### 3.4.2 Stage hydrographs

The water level hydrographs were recorded at five gauge stations after the water intake ice jam release and were compared with the model results. The hydrographs produced by the model using different breakup criteria were very much the same. Therefore, results generated using the discharge criterion are shown in Figure 3-14 as an example. It was not expected that the model would be able to capture the wave propagation since the rubble ice from the released jam was neglected in the proposed model. Previous studies had shown that the effect of the rubble ice on water levels is significant within a travel distance of 1-2 jam lengths, in particular decreasing the peak and changing the shape of the falling limb of the wave (Jasek 2003; She and Hicks 2006a). It can be seen that, except for the stations upstream (303.3 km) and at the jam toe location (296.3

km), the recorded hydrographs all show two peaks. This is because the ice from the released jam moves at the surface water velocity, which is much slower than the wave speed. The first smaller peak is associated with the water wave passing these stations, and the second peak occurs when the rubble ice passes subsequently.

The modeled water level at station M303.3 captured the timing of the water drop caused by the ice jam release very well but returned to a level much lower than the measured after release. This is likely due to the remaining ice in the channel backing up the water level, which is not captured in the model. Station M296.3 locates right at the toe of the jam. Again, the modeled hydrograph was able to capture the wave form but with increasing discrepancy in water level after the jam release, which was also conceivable due to the backwater caused by the remaining ice. The datum of gauge stations M289, M288.1 and M268.1 were unavailable and thus a different constant value was added to the measured water level at each of these three stations to match the modeled value at 20:00 of April 19<sup>th</sup>. The modeled water level hydrographs at these three stations all have a single peak, with a steep rising limb and a gradual falling limb. The model captured the timing of water level increase but was not able to capture the second peak or the shape of the falling limb of the measured hydrograph. This is again due to neglecting the effect of the rubble ice from the released jam.

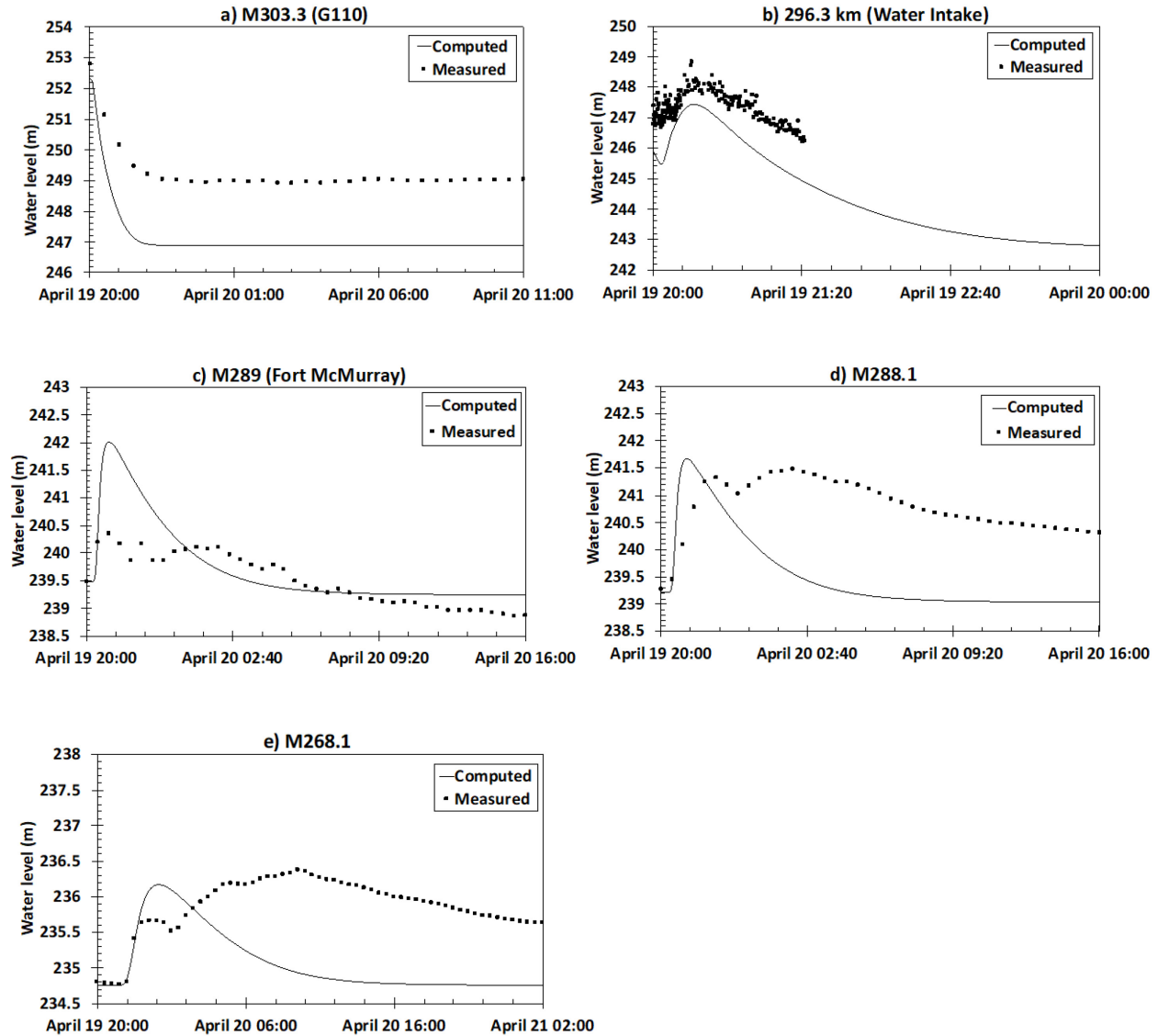


Figure 3-14. Stage hydrographs by model compared with record at various stations on the Athabasca River (discharge criterion with  $Q_{br} = 4000 \text{ m}^3/\text{s}$ ).

### 3.4.3 Self-sustaining wave (SSW)

A number of studies had postulated that the storage release leads to the formation of a non-attenuating, i.e. self-sustaining wave (SSW), which likely is the source sustaining the rapid sheet breaking front propagation over long distance. Both Jasek et al. (2005) and Beltaos (2017a) investigated the properties of SSW formed in prismatic rectangular channel during ice breakup

caused by different kind of incoming wave or jave. Beltaos (2017a) also established a theoretical framework and applied it to an event of rapid ice breaking over hundreds of kilometres observed on the Peace River during 2014 breakup. The SSW theory only partially explained the highly dynamic breakup event in an average sense, likely because the natural river conditions were not accounted for in the theoretical framework. This study further explored the postulation about the existence and role of SSW during ice breakup, taking into consideration of the effect of natural river conditions. The tested criteria, particularly those explicitly account for the river irregularities, all showed that the breaking front sped up or slowed down/stopped depending on local hydrodynamic and geometric conditions. This suggests that the resistance to ice breaking varies along the study reach.

To visualize the wave generated from storage release, the same ice jam release event was modeled without ice breaking up in the receiving channel and the resulted water depth between the breakup and no-breakup cases were compared in Figure 3-15 at various simulation time up to 5 hours after the water intake ice jam release. The solid triangle symbol in the figure indicates where the breaking front located at the plotted time for the breakup case. Similar wave properties were observed regardless the choice of the breakup criteria and thus one example (using the discharge breakup criterion with  $Q_{br} = 4000 \text{ m}^3/\text{s}$ ) is shown to facilitate the following discussions. It can be seen that up to 10 minutes after ice jam release, there is no noticeable difference in water depth between the breakup and no-breakup cases. Afterwards, the water depth for the breakup case becomes greater for a reach in the vicinity of the breaking front, extending both upstream and downstream. As time goes, this reach lengthens and the magnitude of the depth difference between the two cases also increases. At 1 hour, the water depth for the breakup case is about 0.4 m greater in a ~5 km long reach. When using the discharge criterion, the breaking front stopped at about 1

hour and 20 minutes after release time. The difference in water depth between the two cases began to diminish afterwards (see 2 hours and 5 hours) and became almost invisible at around 10 hours. Unlike the SSW in prismatic rectangular channel as shown by Jasek et al. (2005) and Beltaos (2017a), the SSW formed in this case did not develop a flat crest and cannot even be visualized on discharge hydrographs. Therefore, the self-sustaining discharge  $Q_{sustained}$  could not be determined. The discharge at the breaking front (leading edge) was taken from the model to be  $4086 \text{ m}^3/\text{s}$ . This value only slightly exceeded the breakup initiating discharge, which is consistent with previous numerical studies.

These results suggest that the storage release associated with jave-induced ice breakup can lead to the formation of SSW. SSW takes time to develop ( $\sim 10$  minutes in this case). The majority of the wave travels upstream of the sheet breaking front but a portion of it is under the intact ice cover. Unlike the properties presented in previous numerical studies regarding prismatic channels, SSW formed under natural channel conditions in this event does not seem to take on a constant shape or become self-sustaining. This may be explained by the variations of resistance to breaking along the study reach in a natural channel environment. In places where the resistance is high, the breaking front gets arrested and SSW begins to attenuate as it moves under the intact ice cover. This has important implications to ice jam formation. It is worth noting that the results presented may be limited by the relatively short travel distance of this event. More numerical simulations and field data are needed to obtain a more comprehensive view of SSW in natural channels.

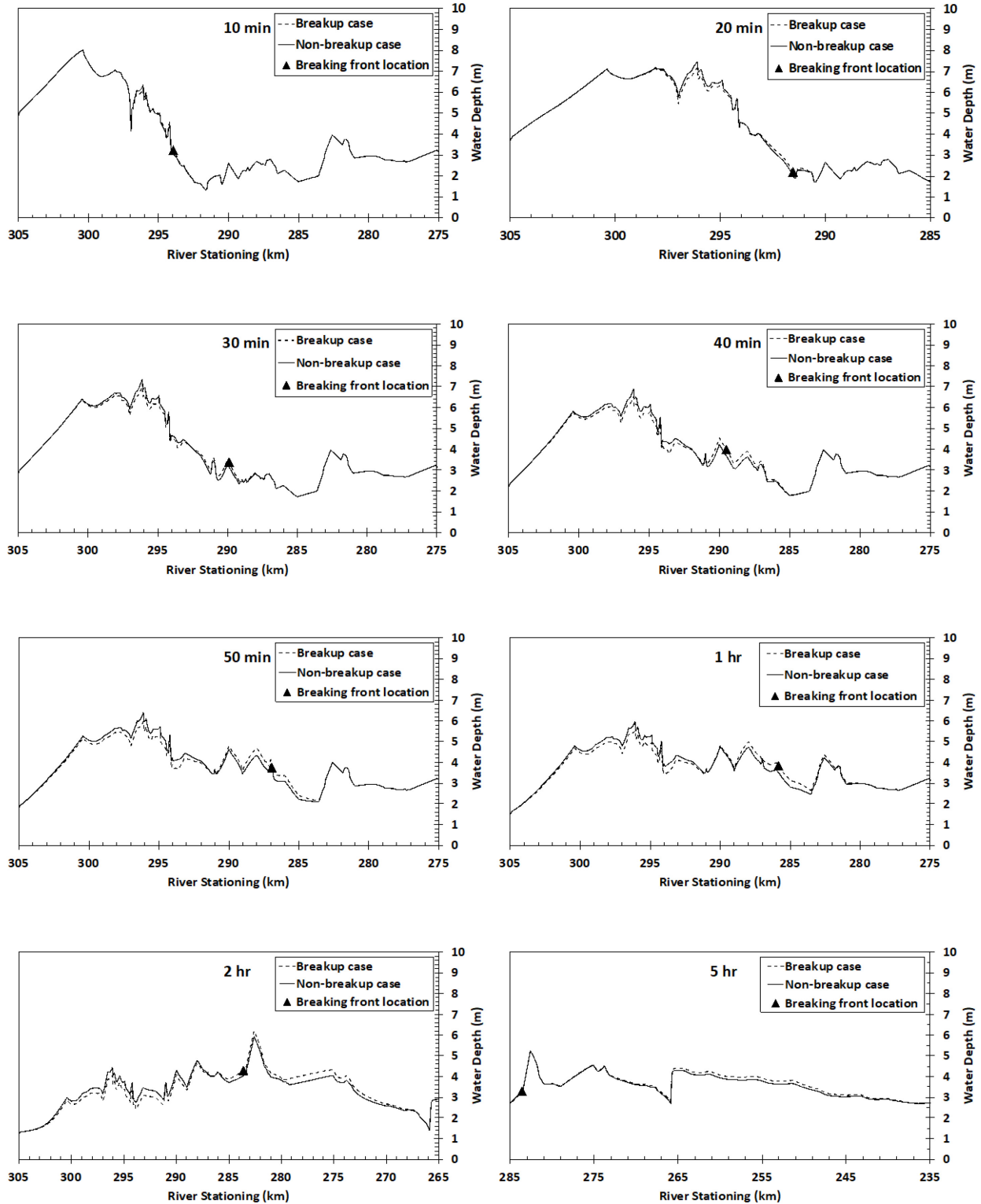


Figure 3-15. Comparison of water depth between cases with and without ice breakup at various times after the ice jam release on the Athabasca River.

## **Chapter 4 2014 and 2018 Breakup Events on the Peace River**

The proposed modeling method was then applied to simulate the 2014 and 2018 ice jam release events that occurred on the Peace River. In addition to comparing the six breakup criteria and exploring the characteristics of the SSW, the transferability of the breakup criteria is also evaluated. This chapter first introduces the study reach, followed by a description of the 2014 and 2018 ice jam release events. Before simulating the two breakup events, calibration and validation of the model are first achieved by modeling four open water events in 1987, 2009, 2011 and 2019.

### **4.1 Study Reach**

The Peace River originates in the Rocky Mountains of northern British Columbia and flows to the northeast through northern Alberta. This river is 1,923 kilometres long (from the head of Finlay River to Lake Athabasca) and drains an area of approximately 302,500 square kilometres (data from Natural Resources Canada). The Peace River basin is Alberta's largest watershed, which accounts for about 28% of the provincial landmass (Mighty Peace Watershed Alliance 2015) and supports around 165,000 people within Alberta (2011).

Peace River is regulated by the W.A.C Bennett Dam and the Peace Canyon Dam, which are roughly 20 km apart from each other (Friesenhan et al. 2008). Figure 4-1 shows the map of the Peace River from the Bennett Dam (0 km) in British Columbia to the Peace-Athabasca Delta (PAD) (1200 km) in Alberta. Some key locations are noted and distances from the Bennett Dam are marked every 100 km. About 5 km upstream of Town of Peace River (TPR), the Smoky River enters the Peace River. It is the key tributary which determines the breakup mode of the Peace River. It is observed that when the snowpack in the Smoky River basin is above normal, the snowmelt runoff can progress downstream and initiate dynamic breakup on the Peace River near the TPR, causing flooding in adjacent communities. Many years have seen occurrence of such

events (1963, 1965, 1973, 1974, 1979, 1997, for example). Andres (1996) showed that the calculated maximum capacity of dykes of TPR is 3500 m<sup>3</sup>/s with ice jam presence, severe flooding can occur at TPR if this threshold is exceeded. Much of the previous research focused on ice jams near the PAD (e.g. Beltaos 2017), because the region is one of the largest inland freshwater delta with unique ecosystems and ice jam flood is believed to play an essential role replenishing the higher elevation areas in the delta (Jasek 2019a). However, Jasek (2017b) found that storage released from breakup upstream between TPR and Vermillion Rapids have great contributions in increasing the channel discharge, which facilitates the breakup propagation further downstream. This upper reach is the focus of this study.

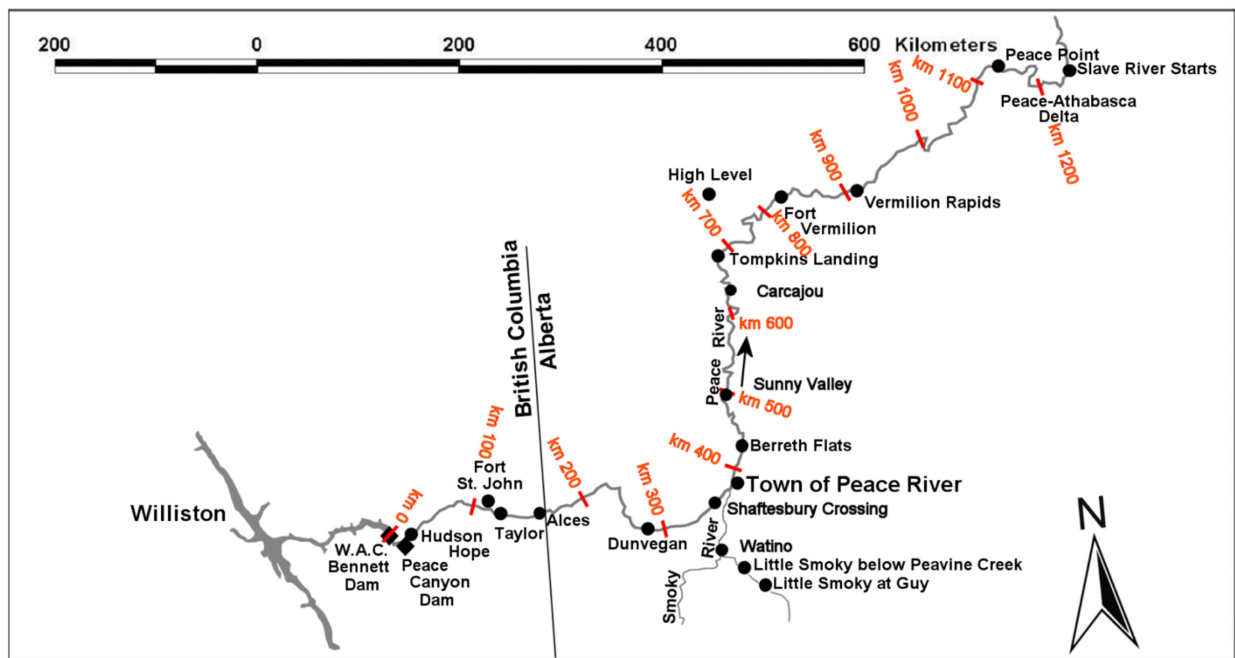


Figure 4-1. Map of the Peace River basin with pertinent locations (Jasek 2017b).

## 4.2 Geometric Model

Hicks (1996) developed a hydraulic routing model for the Peace River from Hudson Hope to Peace Point using limited cross-section survey supplemented with topographic map data. Approximated rectangular cross sections were used in the ~1100 km reach at a 1-km interval. The channel widths were measured from the National Topographic System (NTS) maps and then smoothed. The mean bed elevation at each surveyed cross section was calculated by subtracting the hydraulic mean depth (flow area/top width) during the 1:2 year flood from the corresponding water level. A best-fit line was then drawn through these data points to establish the effective bed profile. Between the surveyed reaches, the effective bed profile was estimated by projecting the effective bed of the surveyed reaches parallel to the water surface slopes obtained from the NTS maps. The model was shown to capture water level and discharge hydrographs in reasonable agreement with those measured during the 1980 and 1987 flood events. Blackburn and Hicks (2002) added some natural cross sections into the Peace River geometric model developed by Hicks (1996) and used it to reproduce the 1987 flood event. The available surveyed cross sections were in three subreaches, Dunvegan, TPR and Fort Vermillion. This hybrid geometry appeared to greatly improve the model's capability to predict peak flood level in the three communities.

The geometric model used in this study is based on the one from Blackburn and Hicks (2002). The study reach extends from the South Gauge of TPR (394 km) to ~932 km. Figure 4-2 illustrates the bed profile in the study reach. The locations where surveyed cross sections were available are noted in the figure. Besides the 43 surveyed cross sections (18 near TPR and 25 near Fort Vermillion) which were available to use in Blackburn and Hicks (2002), 30 new cross sections between 415.83 km and 660 km were added in this study (collected between October 2015 and September 2016 for Peace River Hazard Study, provided by AEP). It was noticed that the modeled

water velocity was unreasonably high within the ~3 km subreach upstream of 847.69 km where the natural cross sections transition to rectangular cross sections. The channel bed downstream of 847.69 km was moved up by 4 m to reduce the modeled velocity to reasonable range. This shift is justifiable given the way how the effective bed was estimated. Hicks (1996) also stated that the estimated effective bed elevation can be several meters different from the surveyed bed. This shift caused no change to the water level of the closest and the last available hydrometric station at Fort Vermillion.

As the geometry used contains information obtained from both ~20 years ago and very recent years, the stationing of key locations along the study reach as presented in Hicks (1996) and Jasek (2017b) are compared in Table 4-1. It can be seen that the stationing is relatively consistent between TPR and Carcajou, but there is a ~20 km difference for the reach starting Fort Vermillion. This difference is likely due to change in river morphology. The stationing used in this study is consistent with that presented in Jasek (2017b).

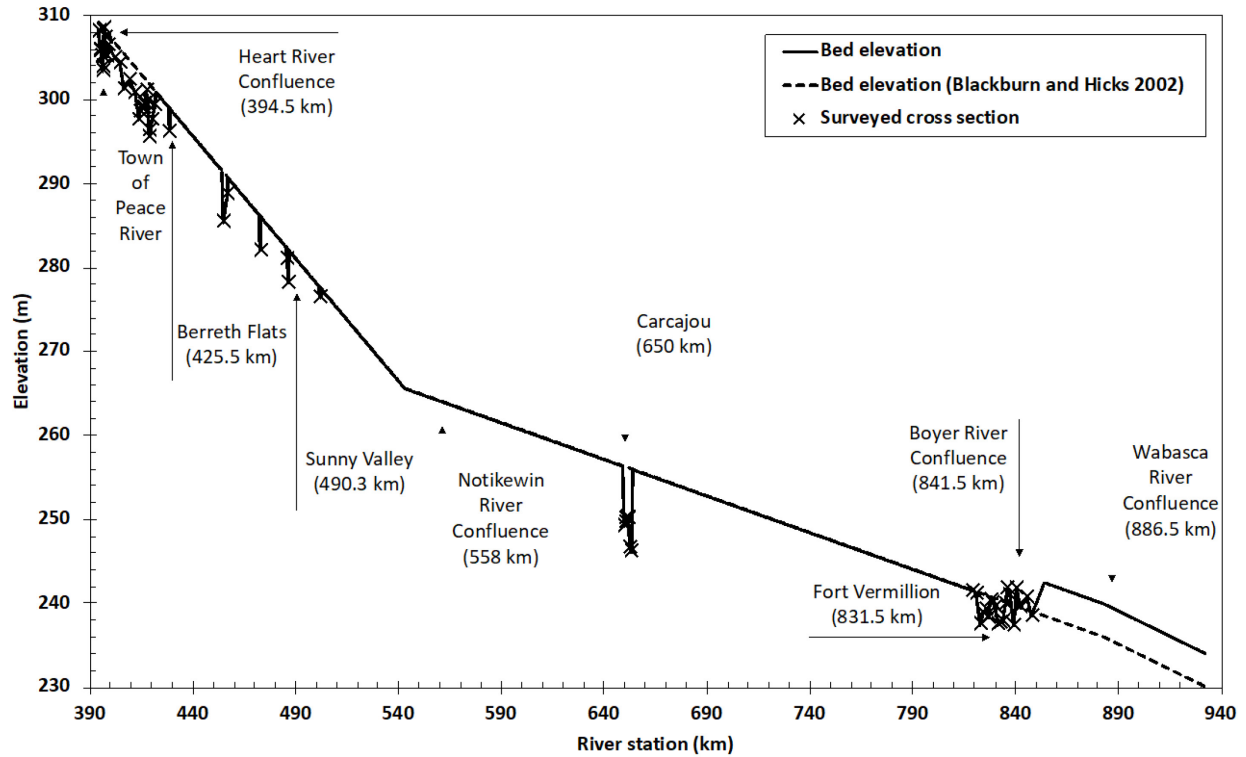


Figure 4-2. Bed profile of the Peace River with surveyed cross sections and key locations.

Table 4-1. A comparison of key locations along the Peace River

Location	Station (Hicks 1996)	Station (Jasek 2017b)
South Gauge at Town of Peace River	-	394 km
Heart River Confluence	394.5 km	394.5 km
Peace River at Peace River (07HA001)	395 km	397 km
Notikewin River confluence	558 km	558 km
Peace River near Carcajou (07HD001)	650 km	650 km
Peace River at Fort Vermilion (07HF001)	808 km	831.5 km
Boyer River confluence	819 km	841.5 km
Wabasca River confluence	865 km	886.5 km

The spatial discretization used in this study is 500 m. All gauge stations operated by WSC and AEP/BC Hydro within the study reach are listed in Table 4-2. The availability of hydrometric data is also marked for each of the open water events and the breakup events. It should also be noted

that the discharge data near TPR obtained by BC Hydro during the breakup events of 2014 was recorded at the South Gauge, and the flow data near TPR for the 2018 breakup and other years' flooding events (1987, 2009, 2011, 2019) were measured at Peace River at Peace River gauge (07HA001). Hence, the upstream boundary was set at the South Gauge (394 km) for 2014 event and at Peace River at Peace River gauge (397 km) for other events.

Table 4-2. List of all gauge stations and the corresponding data availability for each year's event

Station		1987	2009	2011	2014	2018	2019	
Peace River at South End of Townsite (394km)	BCHYDRO-007	Stage	x	x	x	✓	x	✓
		Discharge	x	x	x	✓	x	x
Peace River at Peace River (397 km)	07HA001	Stage	✓	✓	✓	✓	✓	✓
		Discharge	✓	✓	✓	x	✓	✓
Peace River at Berreth Flats (425.5 km)	BCHYDRO-004	Stage	x	x	✓	✓	✓	x
		Discharge	x	x	x	x	x	x
Peace River at Sunny Valley (490.3 km)	BCHYDRO-005	Stage	x	x	✓	✓	✓	✓
		Discharge	x	x	x	x	x	x
Peace River at Carcajou (650 km)	07HD001	Stage	x	x	✓	x	x	✓
		Discharge	x	x	x	x	x	✓
Peace River at Fort Vermillion (831.5 km)	07HF001	Stage	✓	✓	✓	✓	✓	✓
		Discharge	x	✓	✓	x	x	✓

Table 4-3 presents all the tributaries considered in this study, and the corresponding multiplication factor used by AEP to transpose the tributary gauge data downstream to the confluence with the Peace River (Taggart 1995). The factor is a linear adjustment, which is the ratio of the catchment area at the confluence to the catchment area at the gauge. Some tributaries were not used in this study nor the previous two (i.e. Hicks 1995; Blackburn and Hicks 2002) due to the lack of the multiplication factor.

Table 4-3. Peace River tributaries considered in this study (adapted from Hicks, 1996)

Heart River near Mampa	07HA003	1.00
Notikewin River at Manning	07HC001	1.39
Boyer River near Fort Vermilion	07JF002	1.00
Ponton River above Boyer River	07JF003	1.26
Wabasca River at Walden Lake Road	07JD002	1.10

### 4.3 Open Water Calibrations

The 1987, 2009, 2011 and 2019 flood events were used to calibrate Manning's  $n$  for the channel bed and validate the new hybrid geometry used in this study. Table 4-4 presents the boundary conditions used for each event. A fixed water level was set at the downstream boundary and the values were selected to ensure minimal backwater effects based on a sensitivity analysis. All simulations were conducted with a time step of 0.01 hr. The model results were compared to water level and discharge recorded at WSC, AEP and BC Hydro gauges. Two values of Manning's  $n$  were calibrated to be 0.025 and 0.02 for the reach upstream and downstream of the bed slope break at 545 km, respectively. Kellerhals et al. (1972), Hicks (1996) and Blackburn and Hicks (2002) used a single value of 0.02 for the reach between 345 km to 1107 km.

Table 4-4. Initial and boundary conditions of all flood events

Event	Steady state discharge ( $\text{m}^3/\text{s}$ )	Downstream boundary conditions (m)
1987	2344	Fixed water level 236.5
2009	1567	Fixed water level 235.5
2011	3012	Fixed water level 236.5
2019	1510	Fixed water level 235.5

Figure 4-3 presents the results of the 1987 flood. Discharge was only available at TPR and water level hydrographs were recorded by gauges at TPR and Fort Vermillion. The results of Blackburn and Hicks (2002) are also shown in the same figure for comparisons. It can be seen that the new hybrid geometry produced consistent results with the previous study. The new stationing of Fort Vermillion (831.5 km) was used when producing output of this study, and the results seemed to be reasonable when compared with that of 808 km (Blackburn and Hicks 2002). In both studies, the computed peak water level at TPR is considerably lower than the measured value for the peak and the receding portion of the hydrograph.

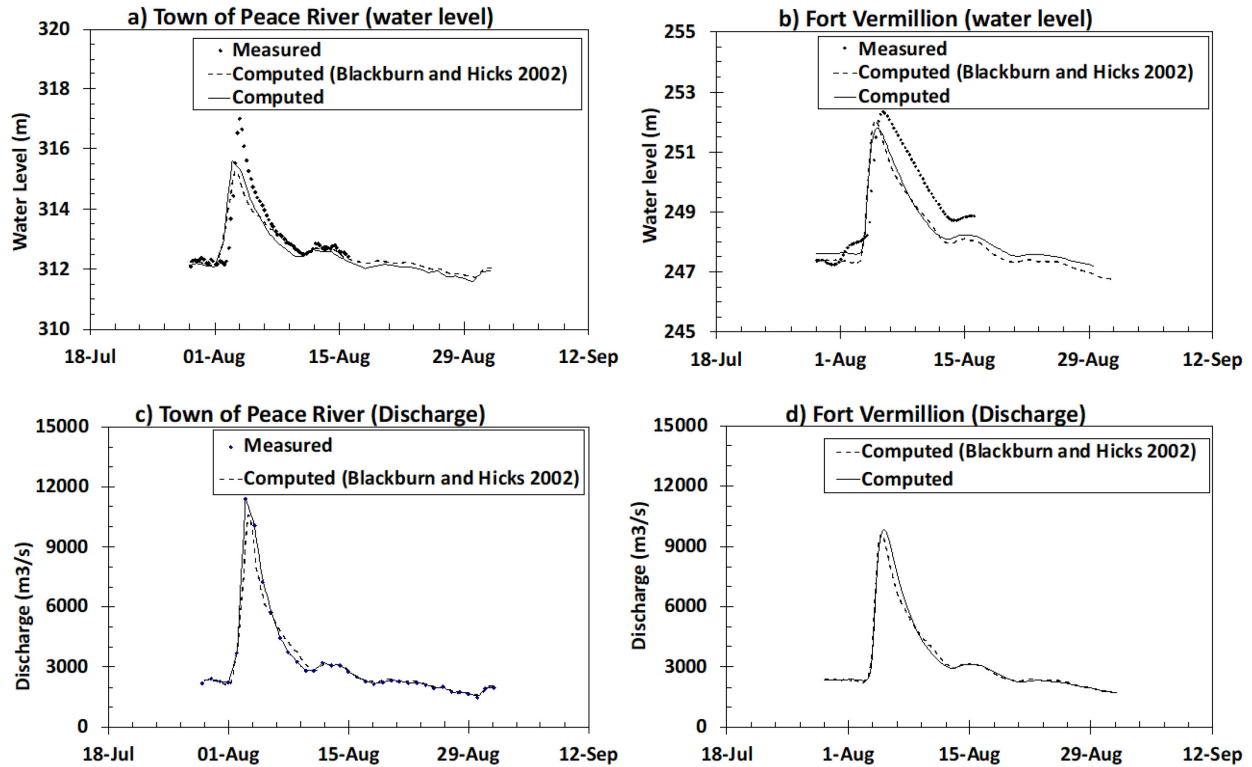


Figure 4-3. Comparisons of measured and computed discharge and water level hydrographs of the 1987 open water event.

The results of 2009, 2011, 2019 events are shown in Figures 4-4, 4-5 and 4-6, respectively. It can be seen that the computed water levels and discharges at TPR match the measured ones well in all years. At Fort Vermillion, the modeled peak discharge is always lower than measured which is consistent with the 1987 event. The recorded discharge and water level hydrographs at Fort Vermillion in 2011 seem to be questionable since their magnitudes are even larger than those of TPR which indicates that the wave amplified rather than attenuated as it travelled from TPR to Fort Vermillion. Water level data were also available at Sunny Valley and Carcajou in 2011 and 2019 and Berreth Flats in 2019. The historical data published by WSC at the gauge of Carcajou (07HD001) was based on an assumed datum. The hydrometric data of gauges at Berreth Flats and Sunny Valley were obtained from AEP, and neither of these two stations presented data on a

geodetic datum. The stage data of these two stations were based on an assumed datum to see relative changes in water level. Due to the unknown gauge datum at these locations, the measured water levels were moved so that the first datapoint between the measured and modeled match. This allows a direct comparison between the model results and the measurements. The calculated water levels at Sunny Valley and Carcajou successfully captured the wave forms with stage differences around 0.2 – 0.6 m at Sunny Valley and 0.2 – 0.7 m at Carcajou. The model also predicted the wave form at Berreth Flats but with a large deviation in water level which is between 0.2 to 1.4 m when compared with the measured. These larger discrepancies of water level are likely due to the scarce natural geometry near these stations (only 2 at Berreth Flats and Sunny Valley and 5 at Carcajou). Additionally, the flow data were also available at Carcajou in 2019 and the calculated discharge appeared to match the recorded very well.

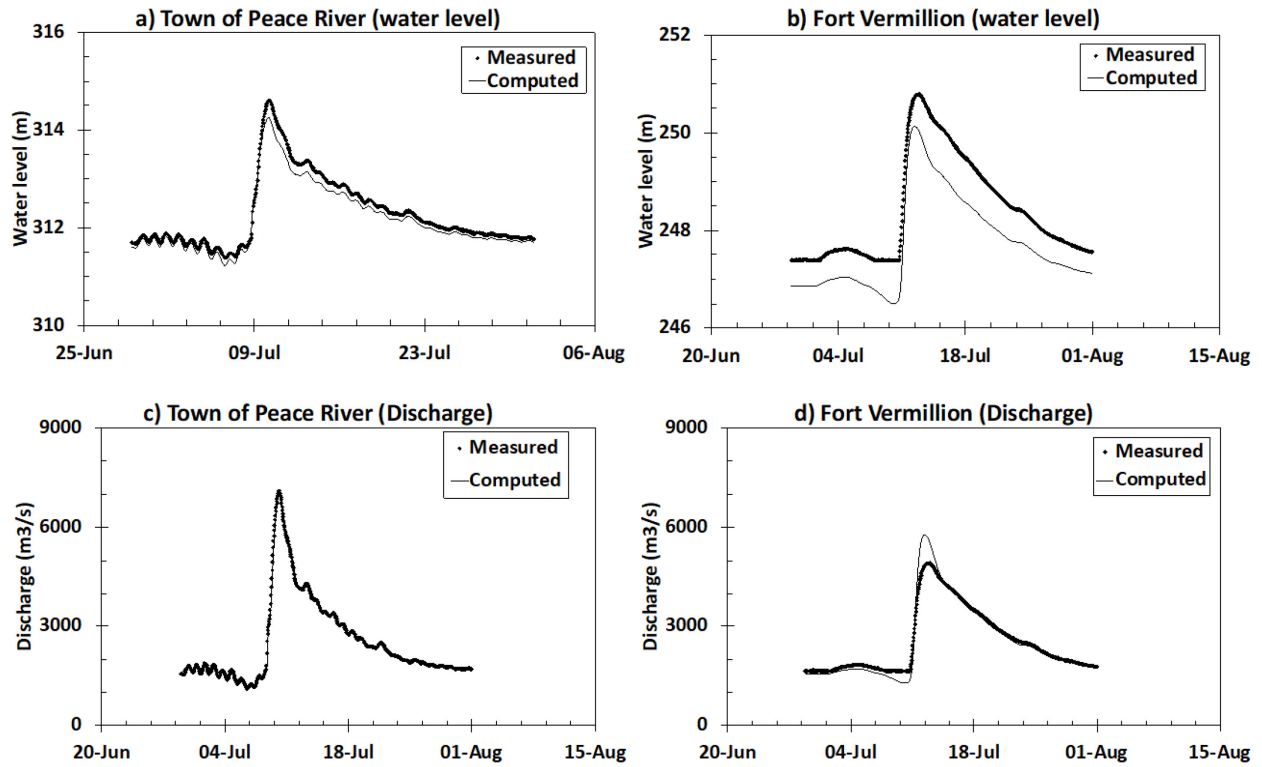


Figure 4-4. Comparisons of measured and computed discharge and water level hydrographs of the 2009 open water event.

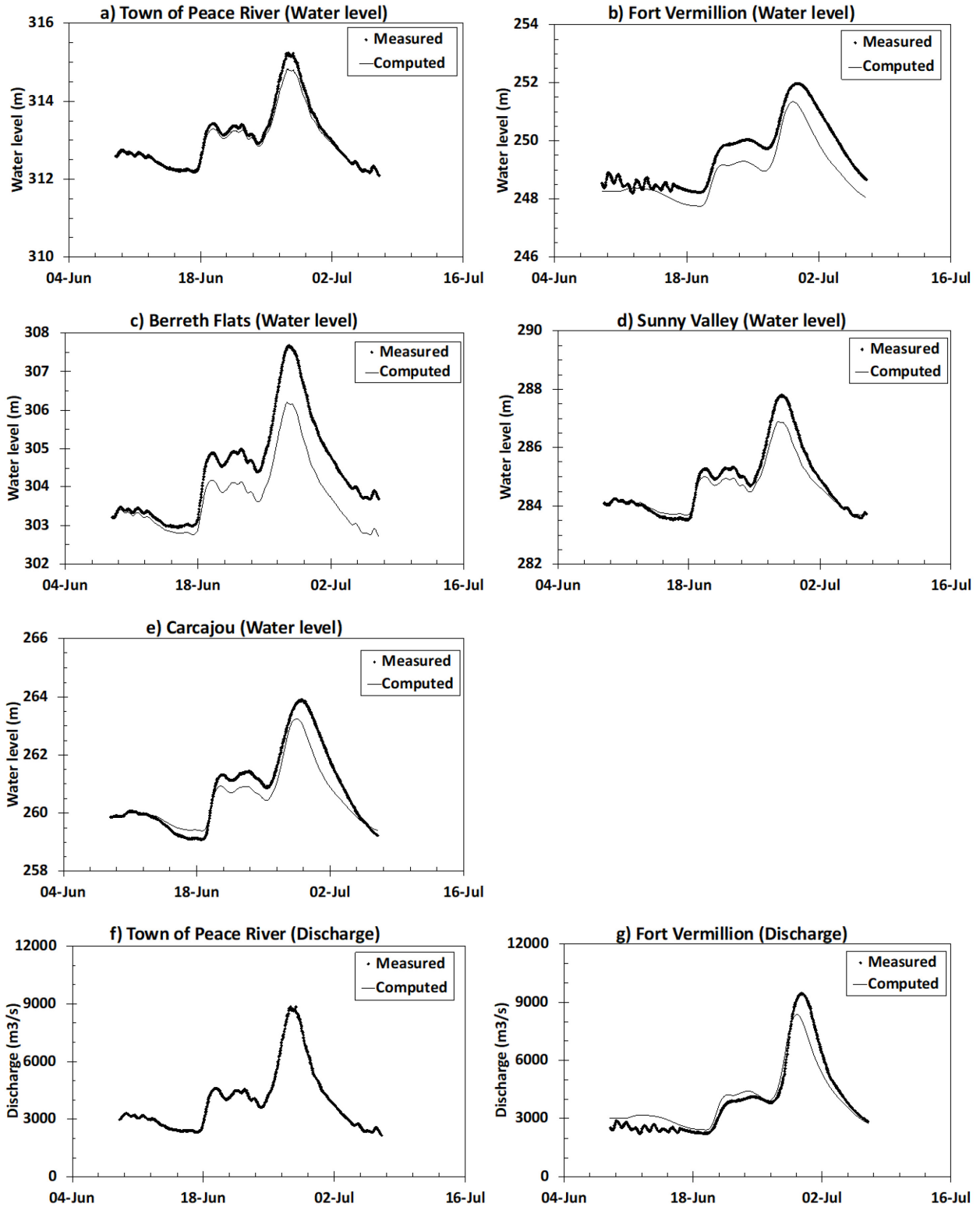


Figure 4-5. Comparisons of measured and computed discharge and water level hydrographs of the 2011 open water event.

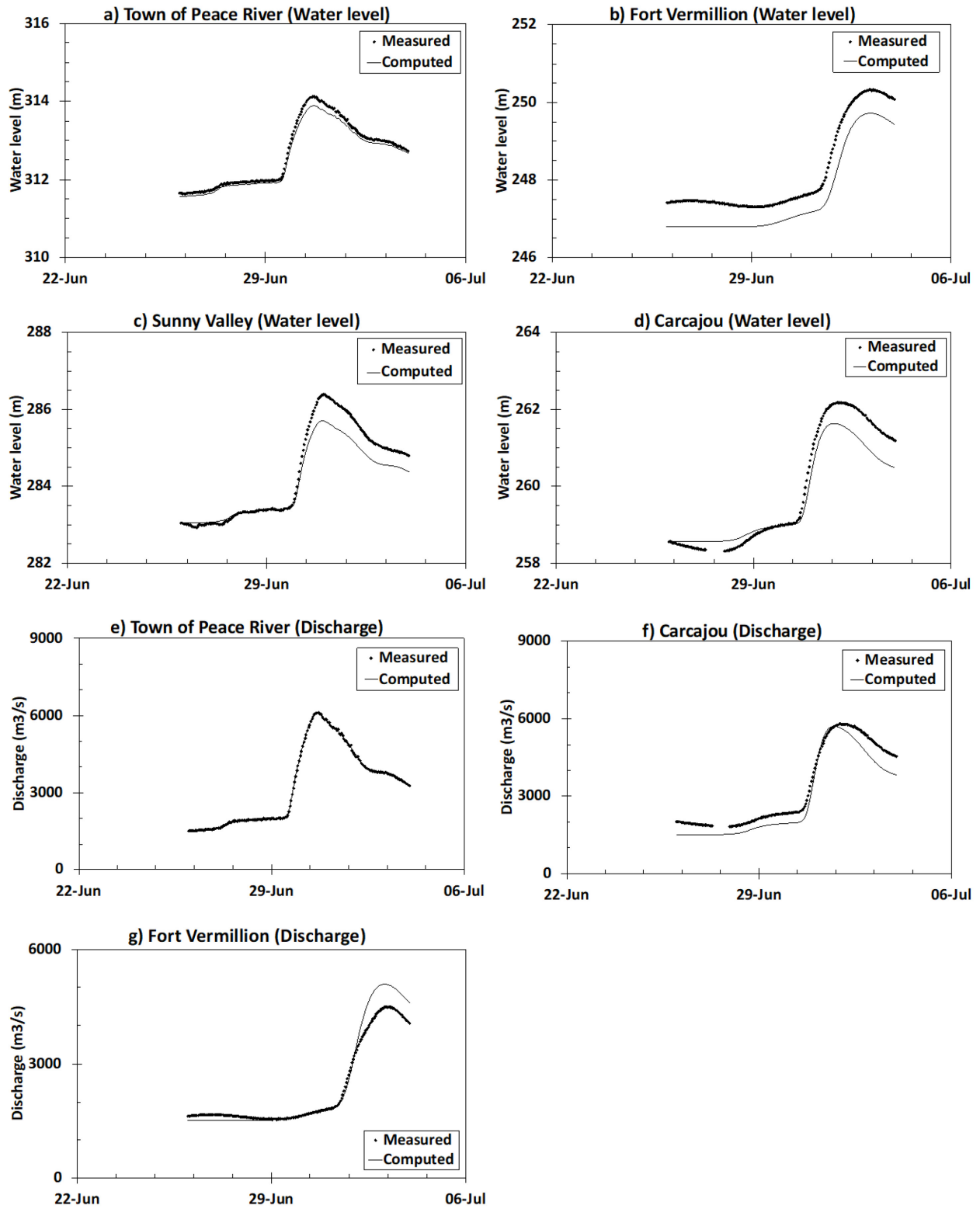


Figure 4-6. Comparisons of measured and computed discharge and water level hydrographs of the 2019 open water event.

Table 4-5 summarizes the results of all open water validations, providing a more comprehensive view of how the model behaved when predicting stage and discharge hydrographs at TPR and Fort Vermillion. Results of other stations were not analyzed here since their records were based on assumed datums and there was only very limited number of surveyed cross sections nearby. Overall, the modeling results are quite promising and the calibrated values of Manning’s n are credible.

Table 4-5. Overview of validation results at Town of Peace River and Fort Vermillion

Events		Town of Peace River			Fort Vermillion		
		Model	Data	Difference	Model	Data	Difference
1987	Steady water level (m)	312.29	312.4	-0.11	248.22	248.87	-0.65
	Peak water level (m)	315.6	317	-1.4	251.8	252.29	-0.49
	Root Mean Square Error (RMSE) of discharge (m <sup>3</sup> /s)	-			268.535		
	Root Mean Square Error (RMSE) of water level (m)	0.545			0.884		
2009	Steady water level (m)	311.76	311.85	-0.09	247.13	247.55	-0.42
	Peak water level (m)	314.24	314.6	-0.36	250.14	250.77	-0.63
	Root Mean Square Error (RMSE) of discharge (m <sup>3</sup> /s)	-			236.345		
	Root Mean Square Error (RMSE) of water level (m)	0.104			0.681		
2011	Steady water level (m)	312.38	312.45	-0.07	247.76	248.25	-0.49
	Peak water level (m)	314.78	315.15	-0.37	251.34	251.98	-0.64
	Root Mean Square Error (RMSE) of discharge (m <sup>3</sup> /s)	-			616.695		
	Root Mean Square Error (RMSE) of water level (m)	0.144			0.681		
2019	Steady water level (m)	311.56	311.65	-0.09	246.85	247.33	-0.48
	Peak water level (m)	313.88	314.12	-0.24	249.72	250.33	-0.61
	Root Mean Square Error (RMSE) of discharge (m <sup>3</sup> /s)	-			289.632		
	Root Mean Square Error (RMSE) of water level (m)	0.127			0.614		

#### 4.4 Breakup events modeling

Alberta Environment and Parks (AEP) and BC Hydro have been closely monitoring freeze-up and breakup on the Peace River throughout each ice season since 1973. Most of the observations were carried out between the Bennett Dam and Vermillion Rapids (~900 km) (Beltaos 2017a). Fast moving sheet breaking fronts triggered by jave were documented within the reach between TPR and Vermillion Rapids in both 2014 and 2018 breakup seasons, which makes breakup events in

these two years perfect options for assessing the breakup criteria. All times in the following descriptions are in Mountain Standard Time (MST).

#### **4.4.1 Event descriptions**

##### **4.4.1.1 2014 ice jam release event**

Jasek (2017b) documented the 2014 breakup of the Peace River from the TPR to the PAD, as well as the breakup of the Smoky River. There were multiple ice jam formation and release events in that year and two sheet breaking fronts were documented. The one used for modeling happened between Sunny Valley (490.3 km) and Fort Vermillion (831.5 km). The breakup between Vermillion Rapids and PAD was not modeled due to the lack of geometry data.

In 2014, the breakup process on the Smoky River started on April 6<sup>th</sup>. An ice jam formed on the Smoky River just upstream of the Peace River confluence on April 11<sup>th</sup> and let go on April 21<sup>st</sup>. The released water and rubble ice pushed into the Peace River but did not trigger a mechanical breakup on the Peace River near TPR. The breakup on the Peace River was mainly thermal from April 21<sup>st</sup> to April 26<sup>th</sup> with the ice front receding at an average rate of 25 km/day (0.29 m/s). A 7 km long ice jam formed during this period and was observed to be upstream of the ice front at 468 km on April 25<sup>th</sup>. The ice jam moved slowly downstream in short starts and stops and reached Sunny Valley in the late evening of April 25<sup>th</sup>. The slow drop of the gauge record at Sunny Valley on April 26<sup>th</sup> showed that the ice jam was still moving slowly downstream during the day (as shown in Figure 4-7). At this time, the breakup had not gone fully dynamic and the breaking front was moving downstream slowly. The suddenly dropped water level at 20:30 on that day indicates the possible release of the jam and the occurrence of a fully dynamic breakup. The 1.5 m high wave peaked at 3:00 of April 27<sup>th</sup> at Sunny Valley was possibly originated from the breakup of an upstream river called the Cadotte River. Meanwhile, the gauge record at Carcajou (650 km)

indicated that the mechanical breakup could have passed this location at 16:30 of April 26<sup>th</sup> which was earlier than the jam release. Jasek (2017b) noted that the gauge at Carcajou was not recording the water level accurately since April 24<sup>th</sup>, but the big stage drop at 16:30 of April 26<sup>th</sup> showed the evidence of breaking front movement (Figure 4-8). The ice front was captured by ground observation at Tompkin’s Landing (694 km) at 22:00 of April 26<sup>th</sup>. The gauge record at Fort Vermillion (831.5 km) showed that the ice front arrived at this location at 0:00 of April 27<sup>th</sup>. Finally, a flight observation at 20:00 of April 27<sup>th</sup> found that breaking front passed Fort Vermillion and reached 897 km and two new ice jams appeared to form between Fort Vermillion and Vermillion Rapids. Table 4-6 summarized the documented propagation of the ice front.

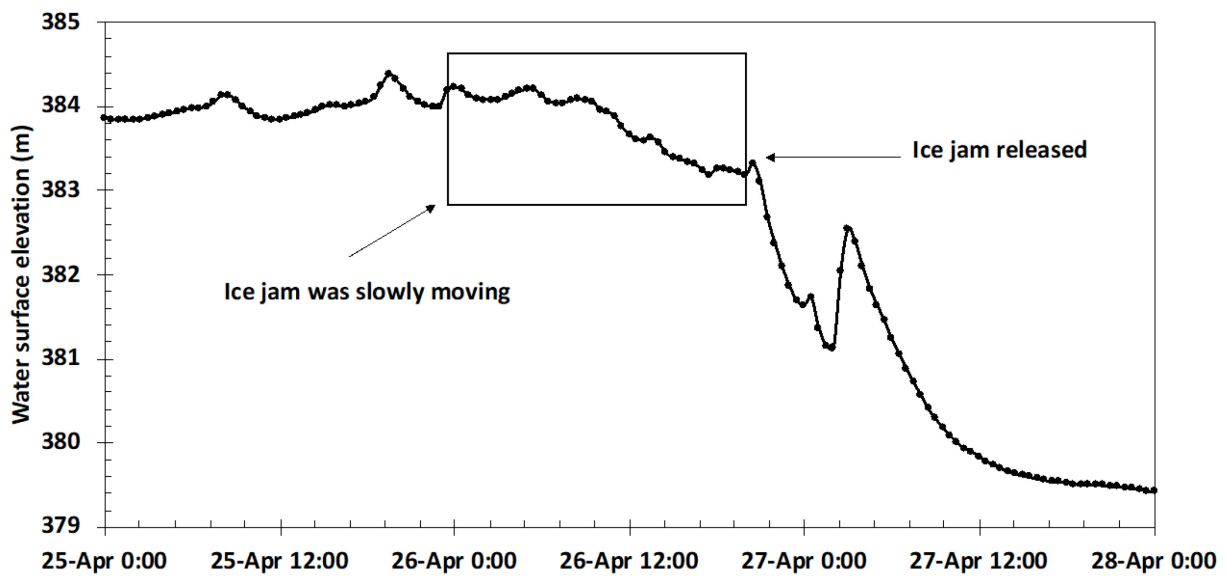


Figure 4-7. Water surface elevation at Sunny Valley indicating the ice jam movement (Data obtained from AEP).

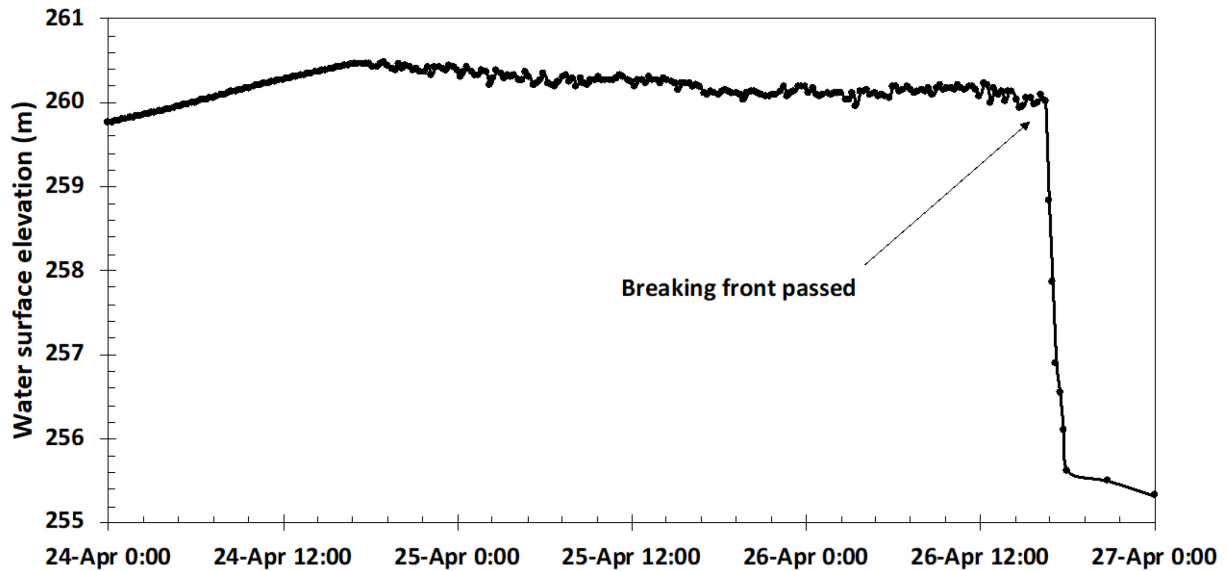


Figure 4-8. Water surface elevation at Carcajou indicating the breaking front movement (Data before 16:45 April 26<sup>th</sup> from AEP and afterwards digitized from Jasek 2017b).

Table 4-6. Documented ice front location of breakup between Sunny Valley and Fort Vermillion in 2014 (source: BC Hydro)

Date/Time (MST)	Ice Front Location (km)	Notes/Comments
2014-04-26 9:00	490.3	Sunny Valley gauge starts to drop gradually indicating thermal breakup passing the gauge
2014-04-26 20:30	502.1	Extrapolated downstream until Sunny Valley gauge water level started dropping rapidly, breakup went dynamic
2014-04-26 16:30	650	Carcajou gauge drops suddenly and flat-lined indicating dynamic breakup
2014-04-26 22:00	694	Ground observation at Tompkin's Landing
2014-04-27 0:00	831.5	Fort Vermillion gauge data indicate ice front passing
2014-04-27 20:00	897	Flight observation

As can be seen from Figure 4-9 and the previous description, there appear to be multiple breaking fronts during this period and they seem to be non-sequential. It was also observed that although

the breaking front triggered by the jave released from the Sunny Valley ice jam produced an ice jam upstream of Fort Vermillion, the jave did break up the ice cover downstream of Fort Vermillion. The breaking front locations at 502.1 km and 897 km are thus related as one jave-induced breakup event (shown as triangles connected with a solid line in Figure 4-9). The gradual drop of water level at Sunny Valley indicates that the ice jam was slowly moving or maybe partially released. This may possibly be the cause of another breaking front, shown as circles with dashed lines connecting four observed or deduced breaking front locations. Therefore, the proposed modeling method was applied to simulate the propagation of the two separate breaking fronts during the 2014 breakup, one following the partial release of the Sunny Valley ice jam and the other one following the complete release.

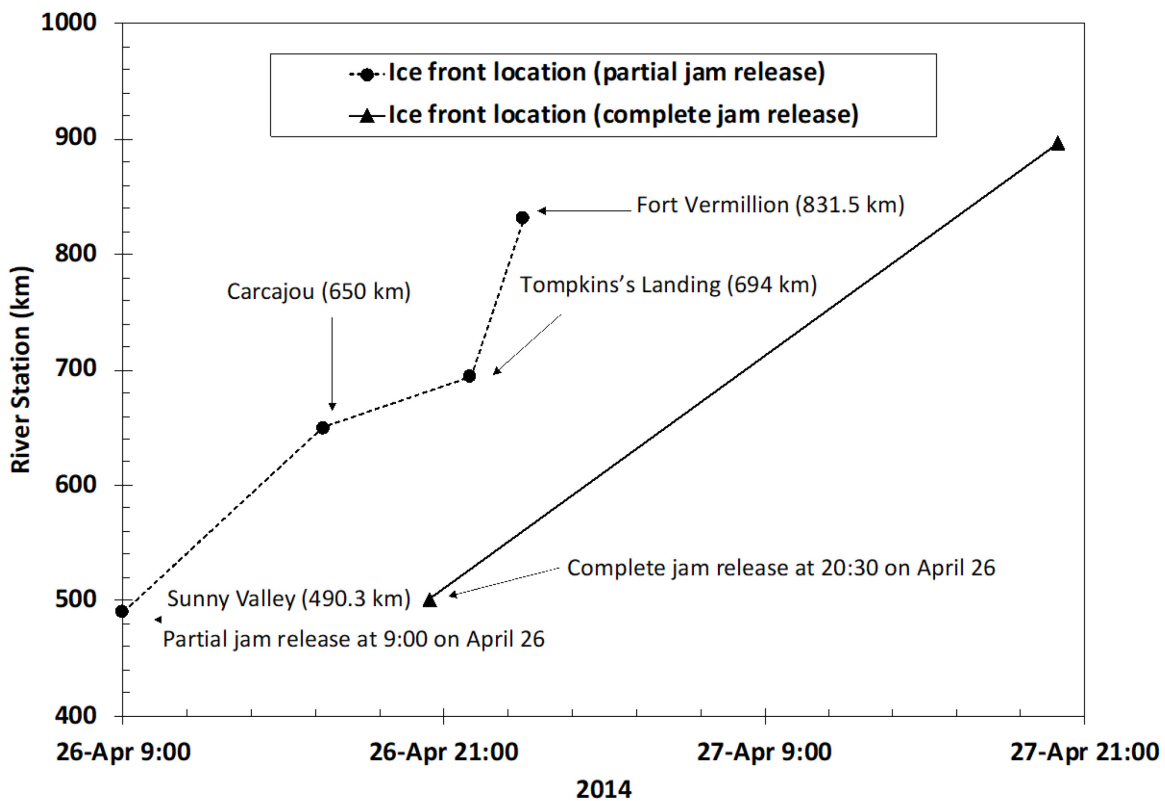


Figure 4-9. Documented ice front location of breakup between Sunny Valley and Fort Vermillion (Data provided by BC Hydro).

#### 4.4.1.2 2018 ice jam release event

Jasek (2019a) reported that the 2018 breakup was extremely dynamic with high discharges and severe ice jam related flooding. A sheet breaking front happened between Sunny Valley (490.3 km) and Fort Vermillion (831.5 km) was successfully documented. The weather started to warm up on April 18<sup>th</sup> and caused remarkable snowmelt runoff in the Smoky River basin by April 22<sup>nd</sup>. A series of ice runs and ice jams were observed on April 22<sup>nd</sup>, and an 18 km long ice jam formed just 2 km upstream of the Smoky-Peace River confluence by April 24<sup>th</sup>. This jam released at around 18:00 on April 24<sup>th</sup>, increasing discharge in the Peace River significantly. The ice run came to a rest upon encountering the solid ice cover on the Peace River, forming a new ice jam just downstream of Sunny Valley on April 25<sup>th</sup>. From the evening of April 25<sup>th</sup> and to the morning of April 26<sup>th</sup>, the ice jam consolidated and caused flooding at Sunny Valley. On April 26<sup>th</sup>, another large jave from the Smoky River entered the Peace River. The arrival of the jave was coincided with the release of the Sunny Valley ice jam at 8:00 of April 26<sup>th</sup>. The jave released by the Sunny Valley ice jam proceeded to break up the solid ice downstream and created a sheet breaking front. At 11:44 on April 26<sup>th</sup>, the front was observed at 605 km for the first time via a flight by BC Hydro. Approximately 3 hours after, the breaking front was captured by photographs taken at Carcajou. A flight operated by AEP observed the front at 702 km about 2 hours after it passed Carcajou. The front was found to be arrested at 723 km at 10:19 on April 27<sup>th</sup>. Based on these observations, the breakup rate calculated ranged from 4.0 to 7.1 m/s. The observed breaking front locations are summarized in Table 4-7.

Table 4-7. Sheet breaking front locations observed over a 214 km reach of the Peace River in 2018 (adapted from Jasek 2019a)

<b>Date/Time of Observation</b>	<b>Location (km)</b>	<b>Comment</b>
26-Apr-2018 08:00	510	Estimated ice jam release time based on start of water level drop at Sunny Valley
26-Apr-2018 11:44	605	BC Hydro Flight
26-Apr-2018 14:52	650	BC Hydro ground observation at Carcajou
26-Apr-2018 17:05	702	AEP Flight Photographs
27-Apr-2018 10:19	723	Observed location of arrested breaking front

#### **4.4.2 Model configuration**

##### **4.4.2.1 2014 breakup event**

The Sunny Valley ice jam was first observed forming by noon on April 25<sup>th</sup> and the last observation prior to its partial release was in the late evening of April 25<sup>th</sup>. By that time, the ice jam was observed to be 7 km long with its toe near 490.3 km. Figure 4-10 shows the discharge hydrograph at the South Gauge from 5:30 on April 25<sup>th</sup> to the end of the breakup event. The peak discharge of 4770 m<sup>3</sup>/s during this period occurred at 5:30 on April 25<sup>th</sup> and was used to compute the ice jam profile using HEC-RAS. The ice jam formed against lengthy intact ice cover downstream. The solid ice cover thickness was taken as 1 m based on winter measurements of WSC on March 27<sup>th</sup>. Two values of Manning’s n were calibrated for the solid ice cover, which were 0.04 and 0.02 for the reach upstream and downstream of the slope break (545 km), respectively. The higher Manning’s n of the ice cover in the steeper reach is as expected since the ice cover tends to consolidate in this reach. As the discharge gradually decreased to approximately 4100 m<sup>3</sup>/s just prior to the partial release, the initial condition for the partial ice jam release event was simulated

by running the model with the inflow hydrograph and the computed ice jam profile in place until 9:00 on April 26<sup>th</sup> (time of partial release).

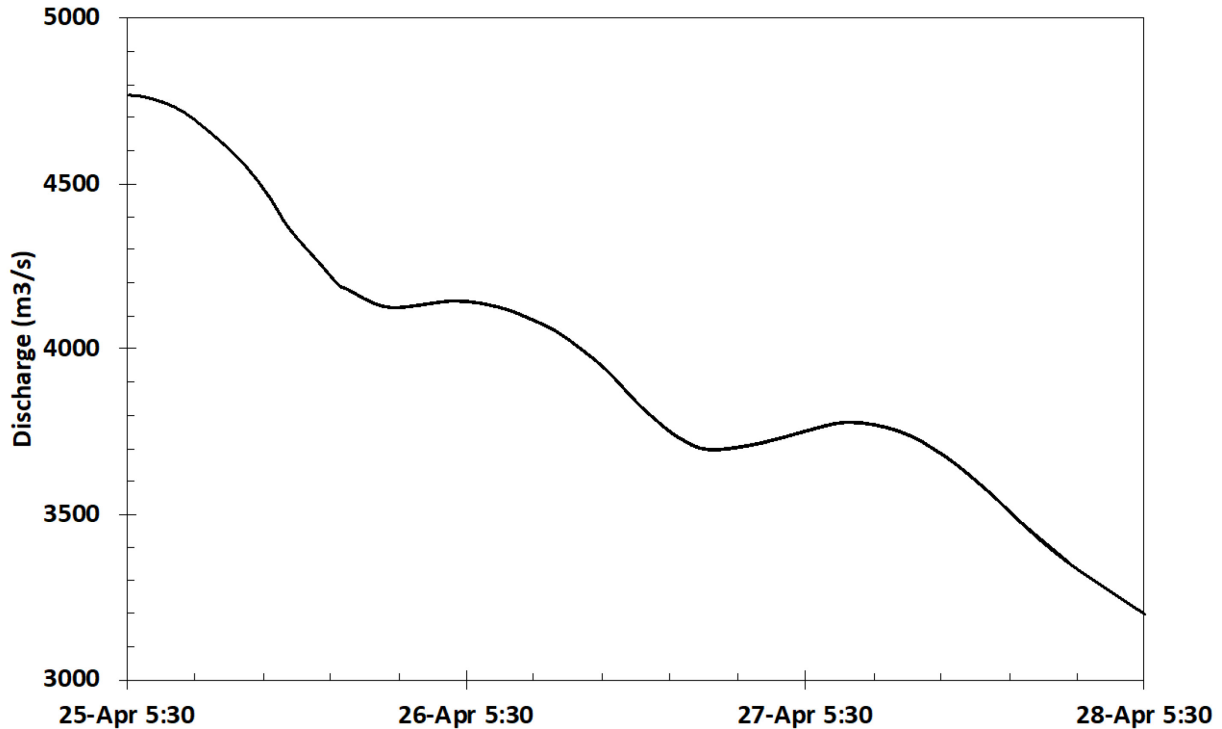


Figure 4-10. Discharge hydrograph of the South Gauge at Town of Peace River during the 2014 jam release (Digitized from Jasek 2017b).

According to field observation, the Sunny Valley ice jam pushed downstream during the partial release. The toe location after the movement was not observed; however, the breaking front location was extrapolated to be at 502.0 km on April 26<sup>th</sup> (personal communication with M. Jasek, BC Hydro). It was therefore set as the new toe location of the Sunny Valley ice jam just prior to its complete release. The same peak discharge of 4770 m<sup>3</sup>/s was used to compute the profile of the ice jam and water surface profile prior to the complete release event. Upstream of the ice jam the study reach was all open. Downstream the river was covered by solid ice but with a short open section between 498 km and 503 km. The thickness and roughness of the intact ice cover were set

the same as before for the partial ice jam release event. Similarly, the initial condition for the complete ice jam release event was simulated by running the model with the inflow hydrograph and the computed ice jam profile in place until 20:30 on April 26<sup>th</sup> (time of complete release).

Figures 4-11 and 4-12 show the initial condition prior to the partial and complete ice jam release events as computed by HEC-RAS, respectively. The ice jam roughness was calibrated to be 0.04. Since there was no measurement of the ice jam profile to compare with, the ice jam roughness was adjusted until the amount of water level drop due to jam release matches that measured at the Sunny Valley gauge, which was the only station that successfully recorded water level during the ice jam movement and release (Figure 4-13). Due to the uncertainty of the datum of the Sunny Valley gauge, the measured water levels were moved 94.888 m down to match the modeled to allow a better visual comparison of the stage drop. It can be seen that the calculated stage drops match the observed ones well in both cases, which indicates that the amount of water released from the modeled ice jams is reasonable. Therefore, water component of the jave can be properly captured with these simulated initial conditions, which is key to the simulation of jave-induced ice cover breakup.

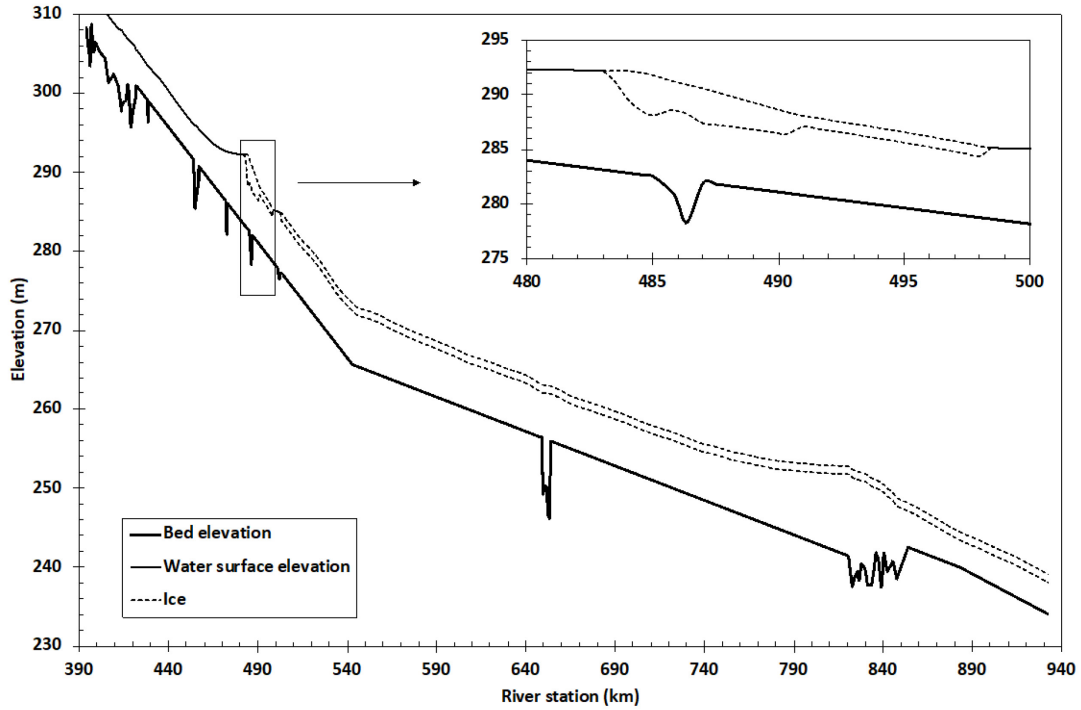


Figure 4-11. Initial condition of the 2014 partial ice jam release event.

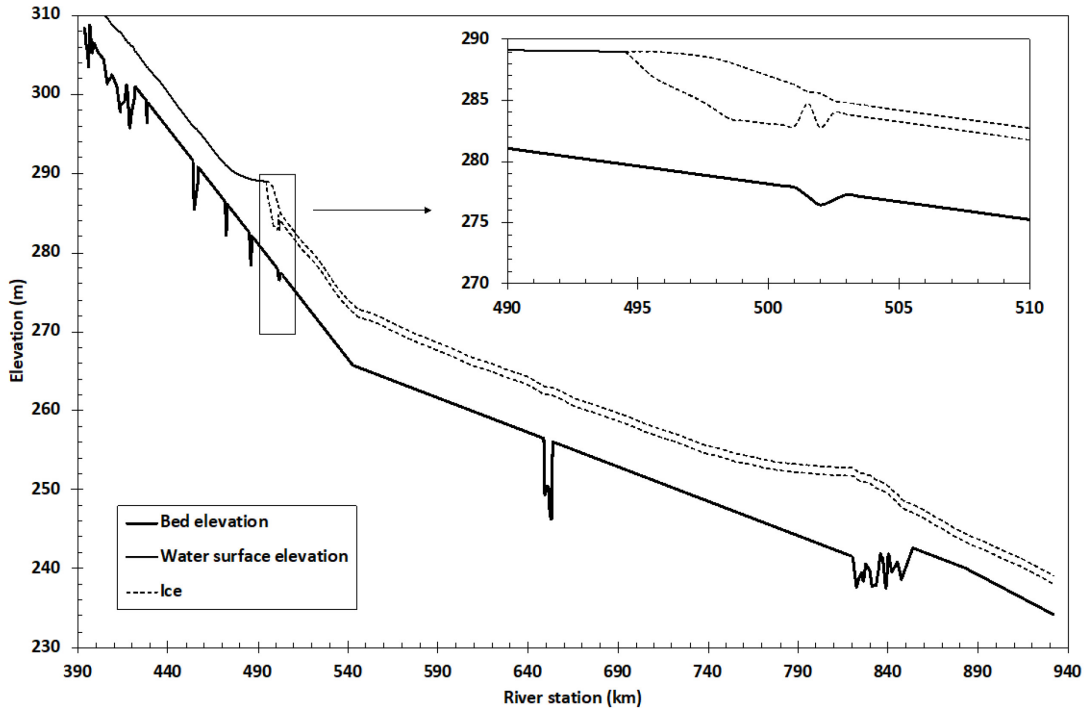


Figure 4-12. Initial condition of the 2014 complete ice jam release event.

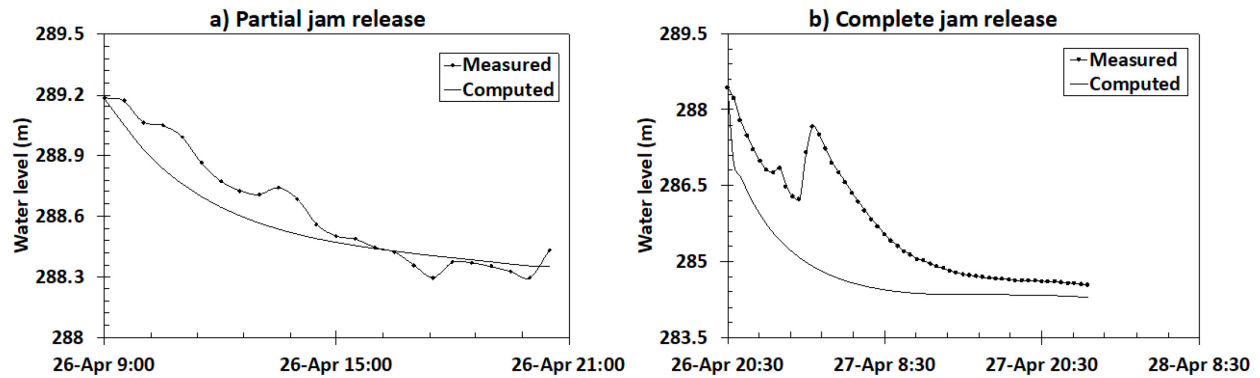


Figure 4-13. Comparisons of the computed and measured water levels at Sunny Valley during the 2014 jam release events.

#### 4.4.2.2 2018 breakup event

During 2018 breakup, an ice jam formed between 496 km and 510 km and was last observed at 19:30 on April 25<sup>th</sup> before its release at 8:00 on April 26<sup>th</sup>. There was lengthy ice cover downstream of the jam and the same thickness and roughness as those of 2014 were used. The discharge hydrograph recorded by TPR gauge from 9:00 April 25<sup>th</sup> until the end of the breakup event is shown in Figure 4-14. It can be seen that the discharge was relatively steady between 10:00 to 19:30 on April 25<sup>th</sup> during which time the ice jam formed. This discharge of 5200 m<sup>3</sup>/s was used to conduct the ice jam profile calculation. The discharge at TPR increased from 5200 m<sup>3</sup>/s to 8200 m<sup>3</sup>/s just prior to the ice jam release at Sunny Valley due to the incoming jave from the Smoky River. Therefore, the initial condition of the 2018 breakup event was computed through running the model with the inflow hydrograph and computed ice jam in place until 8:00 on April 26<sup>th</sup> (release time), assuming that the incoming jave did not cause the Sunny Valley ice jam to consolidate. Figure 4-15 depicts the initial condition of the 2018 breakup event. The ice jam roughness was also calibrated as 0.04 based on the stage drop at Sunny Valley gauge (Figure 4-16). Due to the unknown gauge datum, the measured water level was moved 94.975 m down to

enable the first data point of the measured and modeled water level hydrograph to match. It can be seen that the calculated water level decrease matched the observed very well, which indicates that the computed storage release, as well as the ice jam, is reasonable to proceed with breakup simulations.

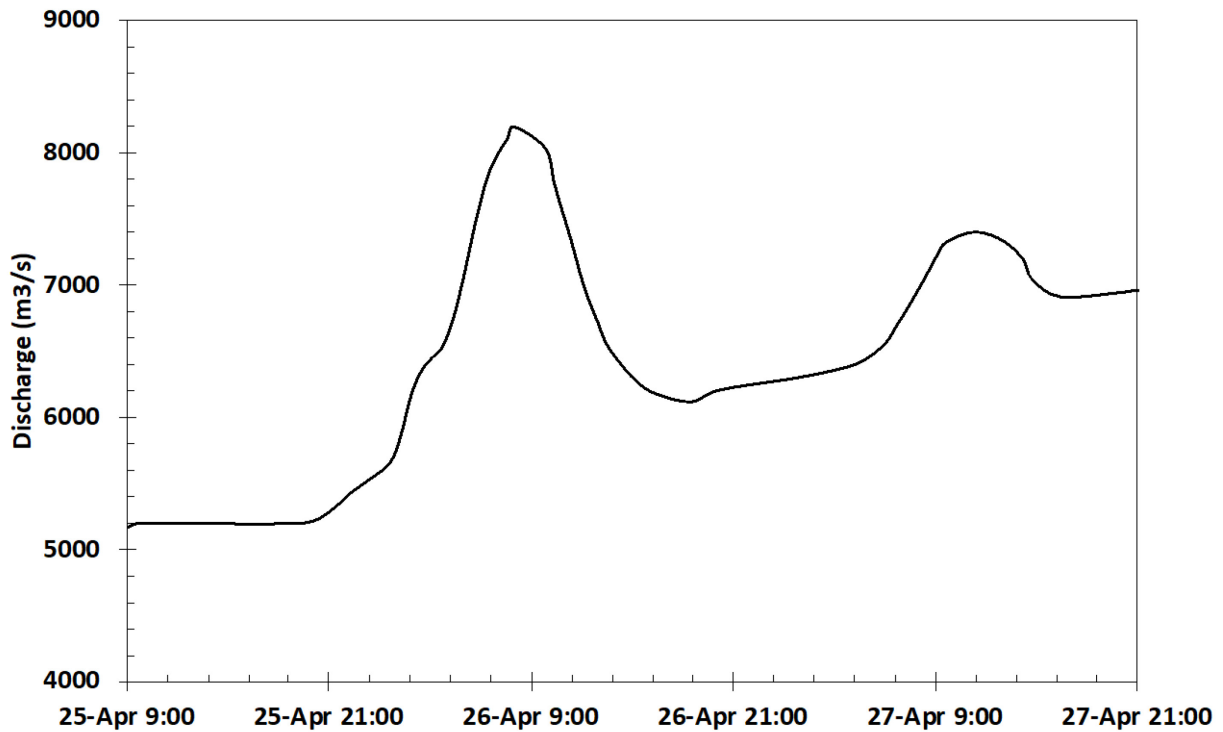


Figure 4-14. Discharge hydrograph of WSC gauge at Town of Peace River during the 2018 jam release (digitized from Jasek 2019a).

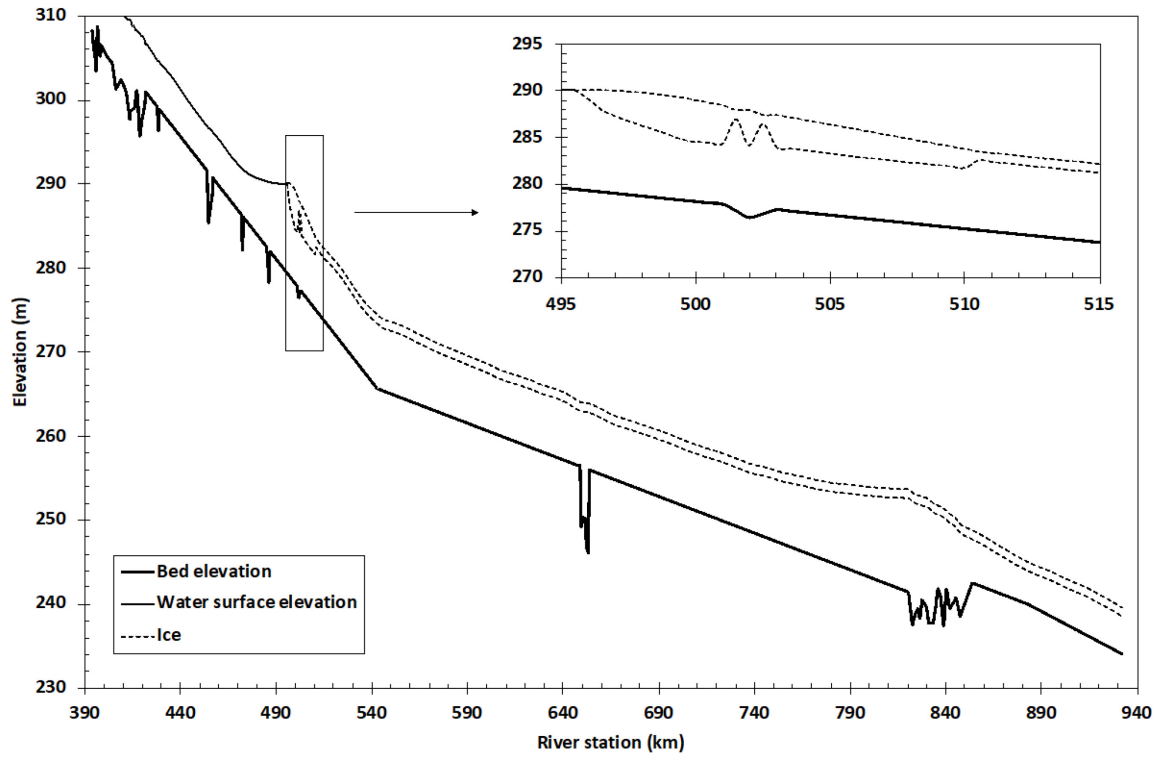


Figure 4-15. Initial condition of the 2018 ice jam release event.

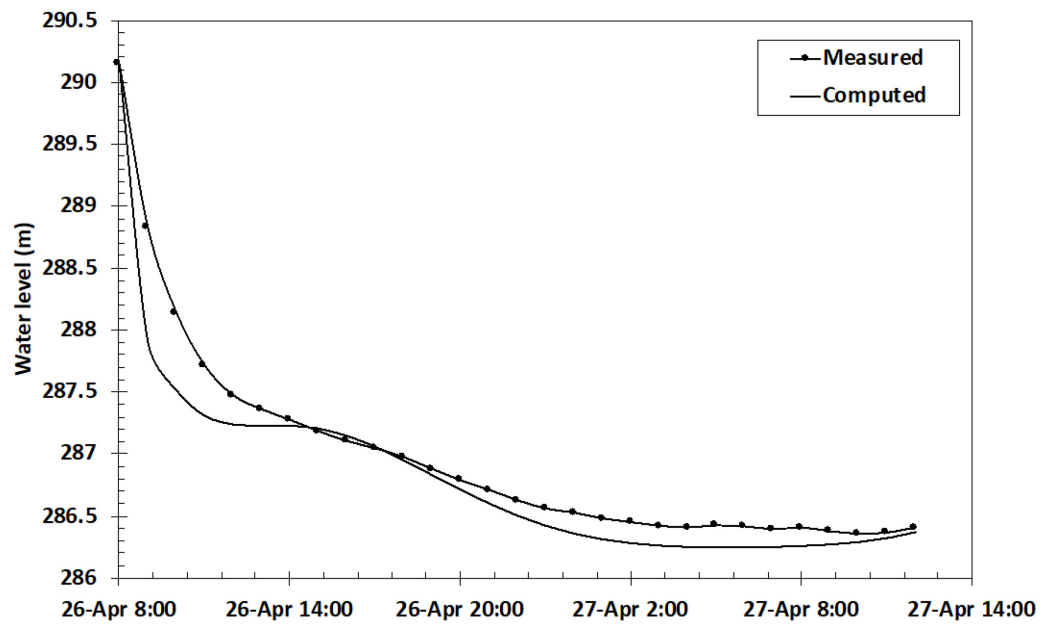


Figure 4-16. Comparison of the computed and measured water levels at Sunny Valley during the 2018 jam release event.

## 4.5 Results and Discussions

Once the initial conditions were obtained, each of the ice jam release and jave-induced breakup was then simulated using the proposed method. Ice in the original jam was neglected. The length of the transition zone was set to be five times of the channel width ( $5B$ ). This is because the breaking front propagations during the 2014 and 2018 events were primarily in the flatter lower reach (average bed slope is  $\sim 0.00005$ ) and the sensitivity analysis (in Chapter 2) showed that the model results are not sensitive to the length of the transition zone for mild-slope channels. The time step was set as 0.01 hour for all breakup simulations.

The ice jam release events on the Peace River were used to test the aforementioned six breakup criteria. For the 2014 breakup, the documented breaking front locations following the complete ice jam release event were used to calibrate the parameters of each breakup criterion; and the calibrated parameters were then used to simulate the partial release event. The parameters were calibrated separately for the 2018 breakup event considering they may be situation-specific.

### 4.5.1 Breakup criteria assessment

#### 4.5.1.1 Water level criterion

Figure 4-19 presents the results obtained using the water level criterion. The term  $F(\Sigma_5)$  which represents the thermal deterioration before breakup in equation [1-1] was approximated with an adapted form of Stephan's equation as previously mentioned. The reduction of ice thickness was calculated to be 0.012 m for both 2014 and 2018. The coefficient  $K$  was calibrated to be 1.2 for the 2014 complete ice jam release event. Only two observed points were available for the breaking front propagation and both were well captured by the model (Figure 4-17a). However, this criterion was not able to capture the breaking front following the partial release event, as the jave attenuated

and disappeared while traveling downstream without initiating any ice breakup. As for the 2018 breakup event, the coefficient  $K$  was calibrated to be 2. The modeled breaking front appeared to agree with the observations before ~700 km, but did not slow down as suggested by the front locations observed at 17:05 on April 26<sup>th</sup> and 10:19 on April 27<sup>th</sup>. The modeled breaking front kept traveling downstream while the actual breaking front got arrested at 723 km.

Beltaos (1990) showed that 2-3 is the typical range of the coefficient  $K$ . The calibrated value for the 2018 event falls on the low end of this range, while that of the 2014 events appears to be small and falls outside of the typical range. Beltaos (1990) also pointed out that this parameter is highly site-specific since it depends on several channel and flow characteristics. The flow condition and the released ice jam of the 2014 event were very different from those of 2018. This may explain why the calibrated values of  $K$  were different for the two years. Additionally, the reach over which the breaking fronts were tracked is around 400 km long. It may be an over-simplification to use a single value of  $K$  for the entire breaking front propagation event. It is thus plausible to see result improvements by calibrating different values of  $K$  for different sections of the reach. However, the number of parameters to be calibrated needs to be limited so that a criterion can be of practical use.

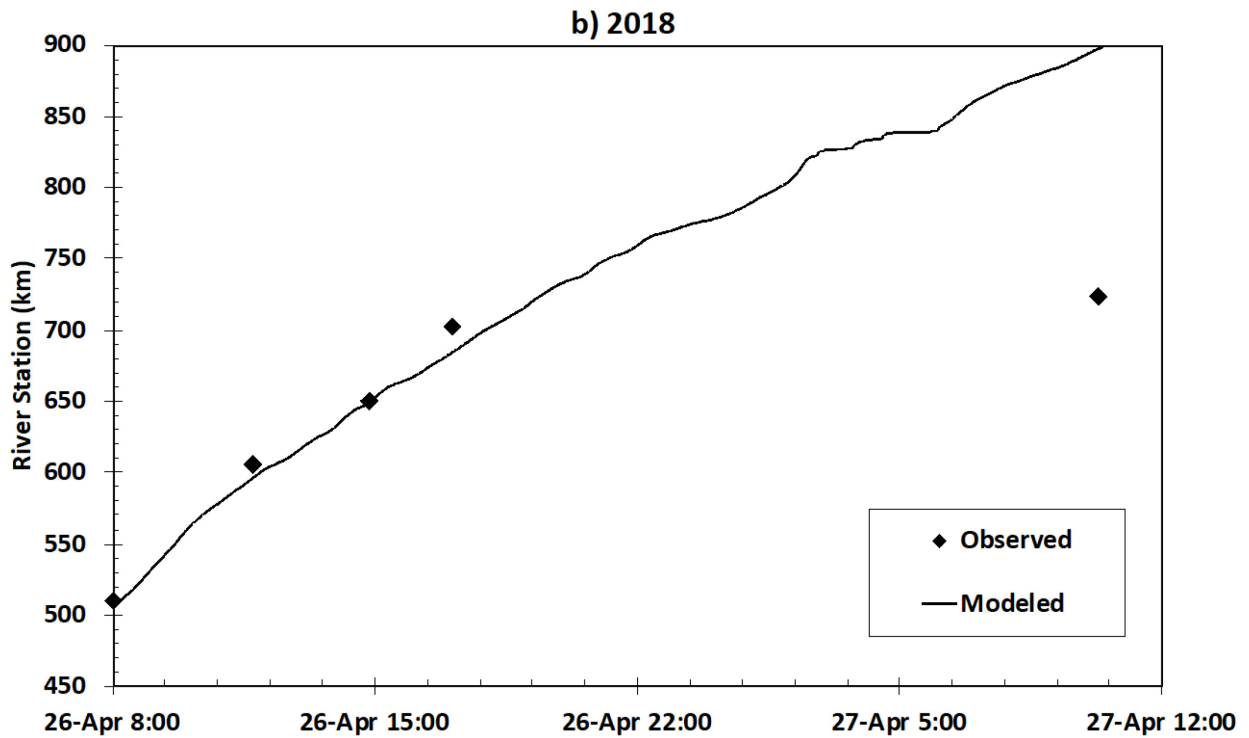
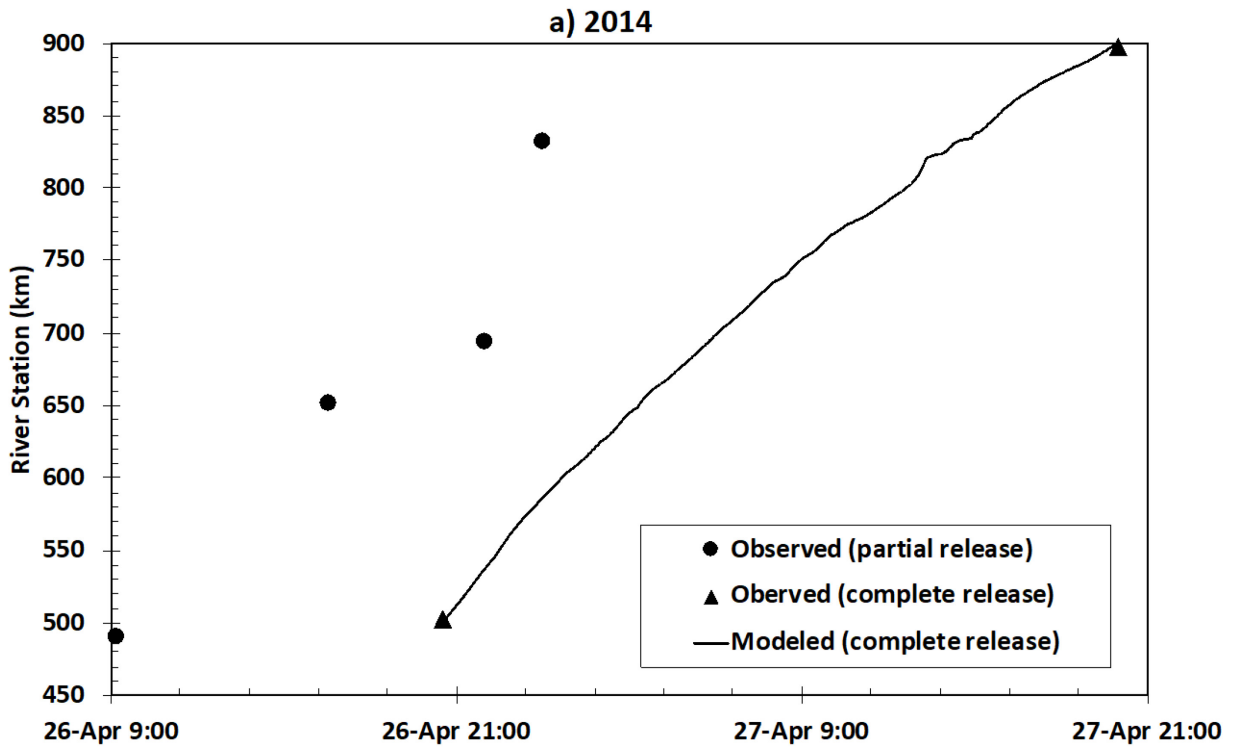


Figure 4-17. Comparison of observed and modeled breaking front location in 2014 and 2018 on the Peace River (water level criterion).

#### 4.5.1.2 Discharge criterion

The modeled front propagations based on the discharge criterion are shown in Figure 4-18. A value of 6500 m<sup>3</sup>/s was found to be the most promising breakup initiating discharge ( $Q_{br}$ ) for the 2014 complete ice jam release event. The modeled breaking front stalled 9 hours at 819.5 km. Field observations also noted that two ice jams formed, one located upstream of Fort Vermillion (831.5 km) and another one was downstream of it. The wave from the Sunny Valley ice jam release and any wave from storage release due to ice cover breakup was able to pass through and continued to break the ice cover further downstream. In the model, breakup was also able to restart at 17:30 on April 27<sup>th</sup>. Same as the water level criterion, the same breakup initiating discharge was not able to initiate ice breakup when modeling the partial ice jam release event.

The breakup initiating discharge of the 2018 ice jam release event was calibrated to be 9800 m<sup>3</sup>/s. The larger threshold may be due to the greater base flow in 2018. Also, the slope of the toe region of the 2018 ice jam was milder as compared to the 2014 jam. The peak discharge of the wave was computed as 11000 m<sup>3</sup>/s for 2014 major event and 17000 m<sup>3</sup>/s for 2018 event. The modeled breaking front travels along the trajectory of the observed before ~700 km, only that it was approximately 10-20 km ahead. The observed breaking front stopped at 723 km while the modeled continued until 817 km near Fort Vermillion. The model also showed a short stall of around 1 hour near Carcajou (650 km). It should be noted that within the lower 500 km of the study reach, the 5 km subreach near Carcajou and the 30 km subreach near Fort Vermillion are the only locations where there are surveyed channel data available. The rest cross sections are all rectangular approximations. The channel characteristics of these natural cross sections near Carcajou and Fort Vermillion are significantly different than the rectangular cross sections. The widths of the rectangular channel are generally within 600 – 1000 m, while the surveyed cross sections near Fort

Vermillion can be ~2200 m wide with large islands present inside the channel. The bed elevations of those natural cross sections near Carcajou are significantly different than the effective bed elevations of the sections with rectangular geometry. This may explain the stops of the modeled breaking fronts at these locations. The model results might get improved through calibrating different threshold values for these subreaches with natural geometry but again this would hamper the applicability of the discharge criterion.

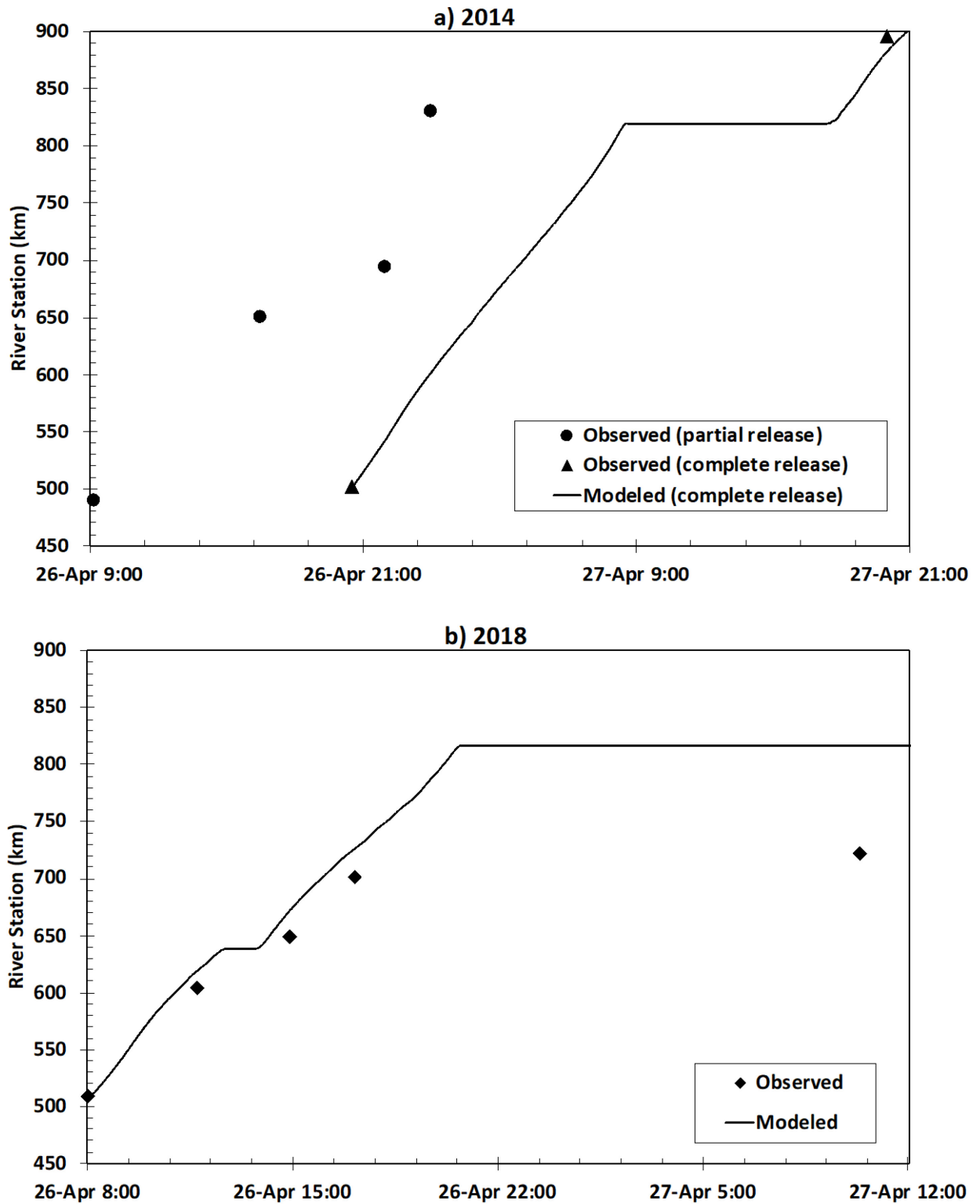


Figure 4-18. Comparison of observed and modeled breaking front location in 2014 and 2018 on the Peace River (discharge criterion).

#### 4.5.1.3 Discharge rate criterion

When calibrating the parameters of the discharge rate criterion for the 2007 Athabasca River breakup event, it was found that best agreement with field observation was achieved when the ice breaks up immediately ( $T_A = 0$ ) when the rate of change of discharge exceeds  $250 \text{ m}^3/\text{s}^2$  or when the rate of change of discharge persisted beyond  $2 \text{ m}^3/\text{s}^2$  (but below  $250 \text{ m}^3/\text{s}^2$ ) for 5 minutes or more. For the Peace River, the peak rate of change of discharge was calculated to be in the range of  $\sim 20 - 30 \text{ m}^3/\text{s}^2$  for the first 5 minutes after the complete ice jam release in 2014, and  $20 - 60 \text{ m}^3/\text{s}^2$  for the 2018 ice jam release event. The peak rate decreased rapidly to  $\sim 10 \text{ m}^3/\text{s}^2$  after 10 minutes or so for both events. These rates are not as high as those following the Athabasca River water intake ice jam release event and they may not be able to initiate breakup instantaneously. Therefore, the same two threshold  $R_Q$  values as in the Athabasca River breakup event were considered reasonable to be used here, leaving  $T_A$  to be the only calibrated parameter. The ice cover was considered broken instantly once the threshold  $R_Q$  of  $250 \text{ m}^3/\text{s}^2$  was achieved and the required durations of above  $2 \text{ m}^3/\text{s}^2$  were found to be different for two years' events.

After testing a series of  $T_A$  for the 2014 major event, it was found that 300 s (5 min) was able to produce the best result, which coincided with the calibrated values used for the 2007 Athabasca River event. As shown in Figure 4-19, the breaking front propagation ended up at 824.22 km and did not match the second observation. The same threshold value of  $T_A$  was applied to simulate the 2014 partial release event. The result shows that the jave could not initiate any ice breakup. To produce the result of 2018 shown in the figure, the parameter  $T_A$  was calibrated as 580 s (9 min 40 s). It can be seen that the modeled front traveled faster than the documented before  $\sim 700$  km. The modeled front propagation was terminated at 694 km which was 8 km behind the data point at 702 km and did not restart.

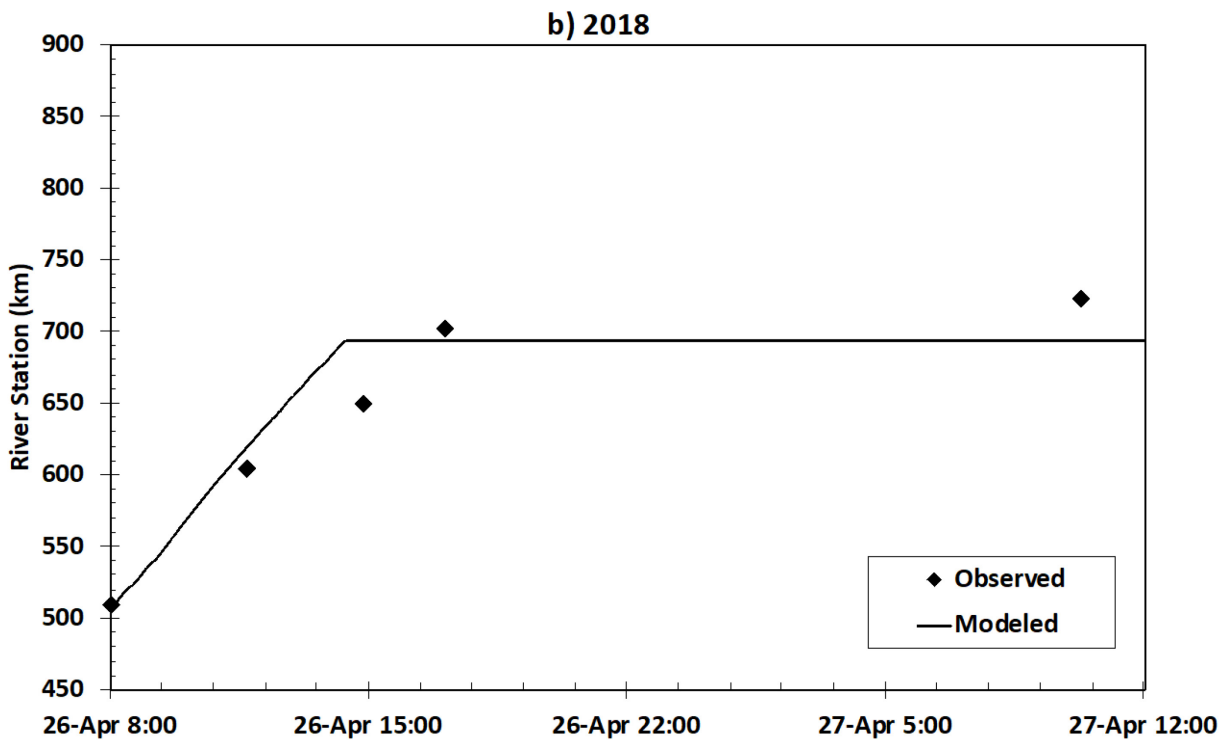
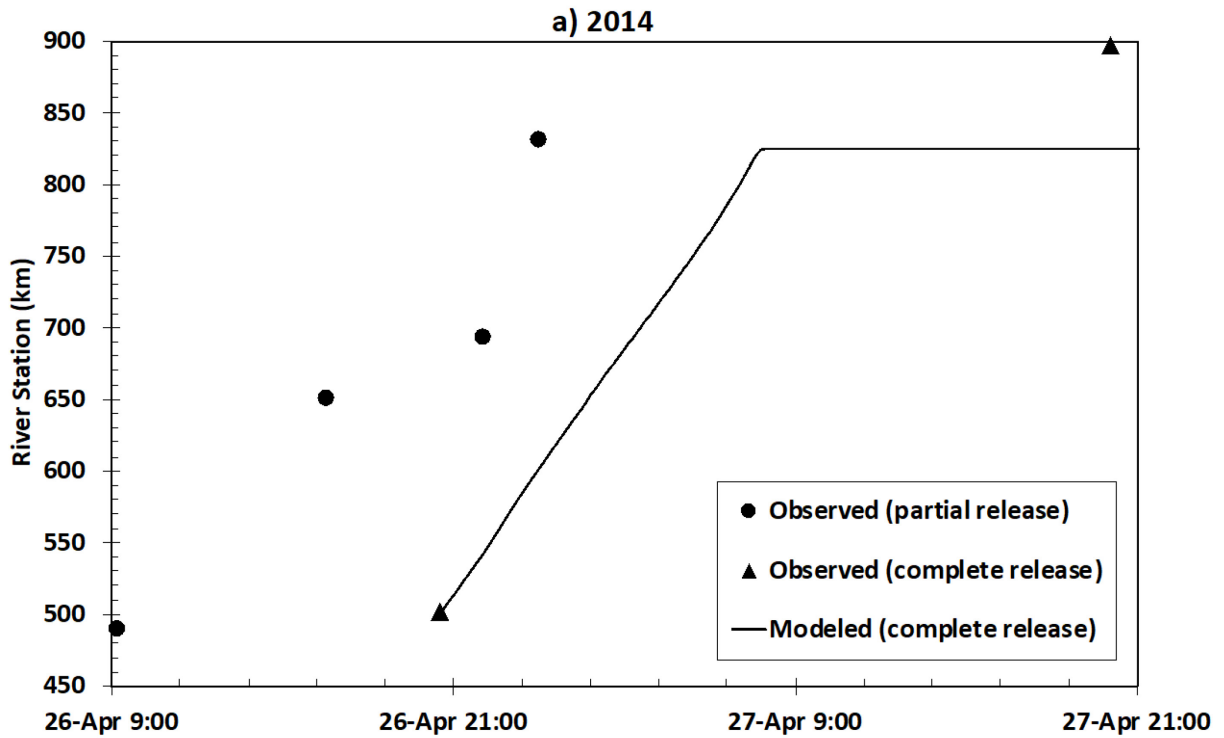


Figure 4-19. Comparison of observed and modeled breaking front location in 2014 and 2018 on the Peace River (discharge rate criterion).

#### 4.5.1.4 Side resistance criterion

The results based on the side resistance criterion are shown in Figure 4-20. The threshold values were calibrated to be the same for the 2014 complete ice jam release event and the 2018 event, which are 12 kPa and 4 kPa for the reach upstream and downstream of the slope break, respectively. It is justifiable to use two separate values as the upper reach is much steeper than the lower reach thus the flow drag acting on the bottom of the ice and the downslope component of the ice weight are bigger. The modeled breaking front following the complete release of the 2014 ice jam stopped several times and the one at 613 km was particularly long. The breaking front resumed movement at ~210 km downstream after nearly 15 hour and reached the second observed location one hour ahead. The result of the 2018 event is not as promising. The modeled front traveled ahead of the observed before it stopped at 682.5 km for approximately 4.5 hours. The breakup was reinitiated ~150 km downstream and proceeded until the end of the study reach. The unsuccessful prediction is likely due to highly dynamic nature of the breakup resistance along the river. Jasek (2019a) calculated the breakup rates of the 2018 jam release event and found the breaking front traveled faster at the beginning, slowed down and then sped up again. This might indicate the breakup resistance varies for different river reaches. The jave of the 2014 partial release event cannot cause any ice failure with applying these two values as threshold of side resistance.

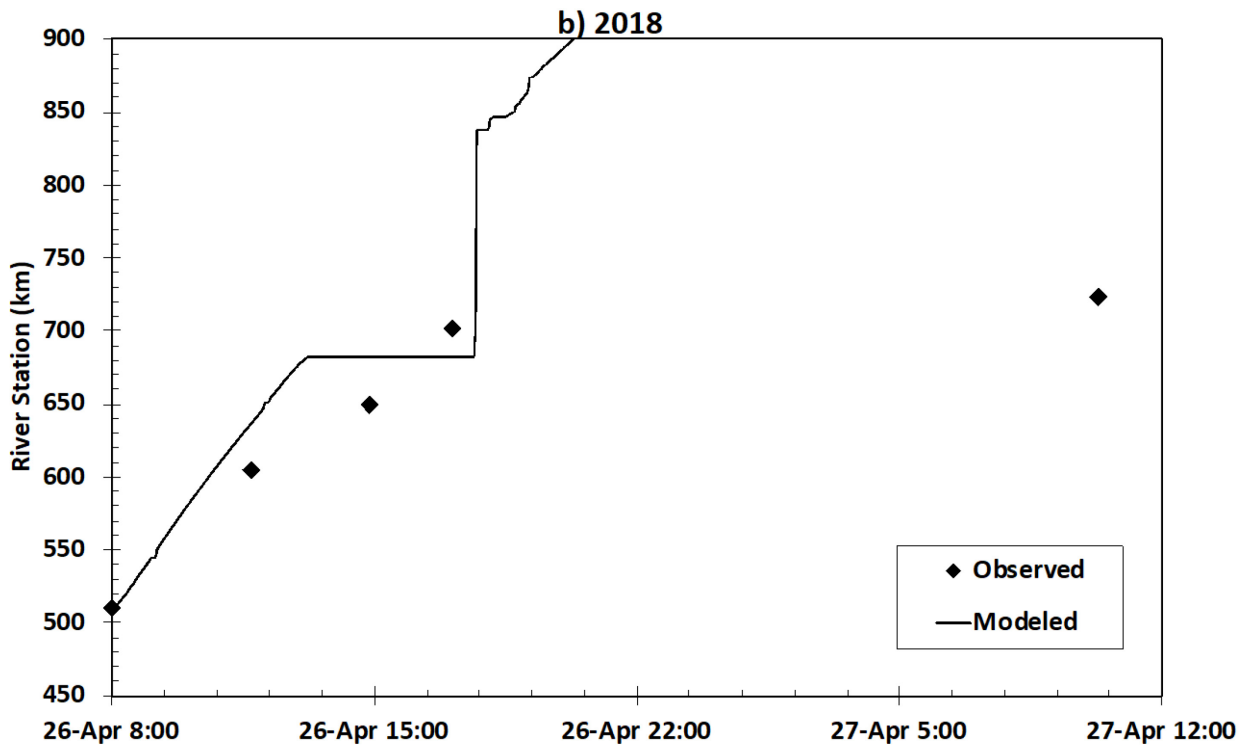
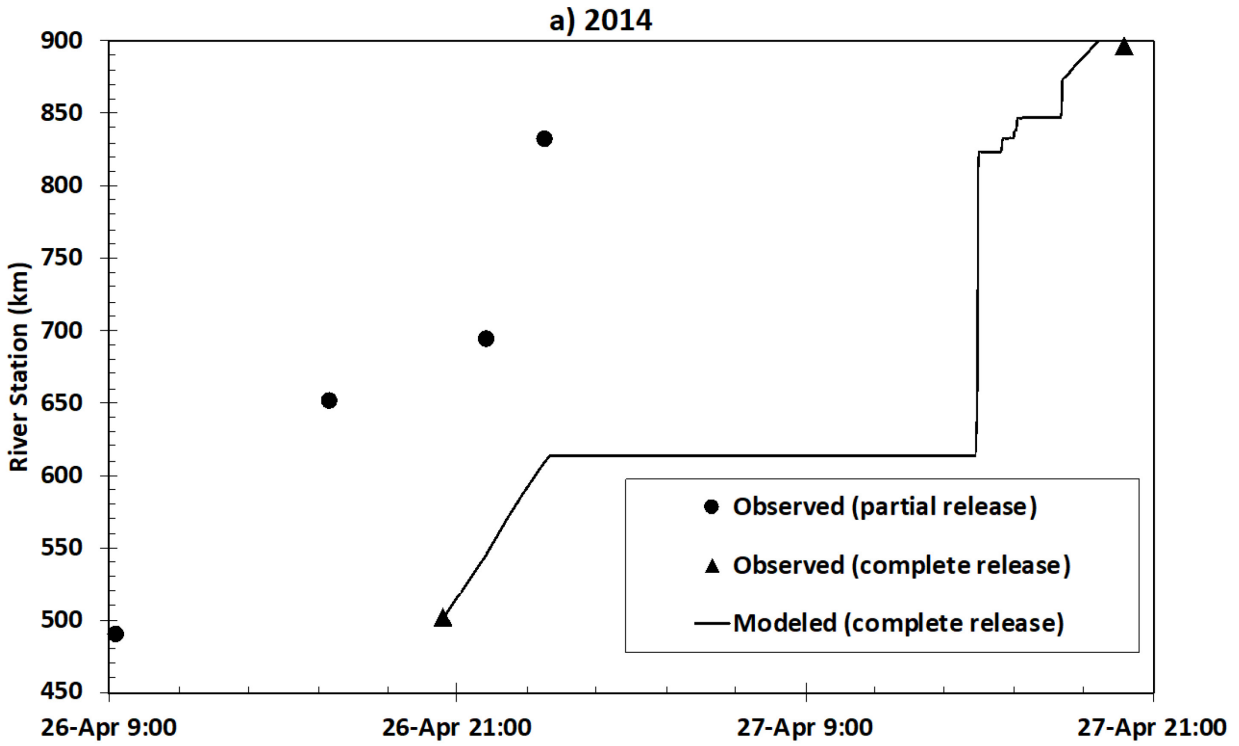


Figure 4-20. Comparison of observed and modeled breaking front location in 2014 and 2018 on the Peace River (side resistance criterion).

#### 4.5.1.5 Boundary constraint criterion

When applying the boundary constraint criterion (equation [1-3]), the difference between the water surface width and the distance between hinge cracks ( $W - W_i$ ) is computed in the model. The hybrid geometry of this study reach includes large portions of rectangular approximations. As a result, the values of  $W - W_i$  were extremely small, which led to a very small left-hand side of equation [1-3] and thus no breakup initiation. Therefore, an empirical value of 50 m (Beltaos 2013b) was used for the subreaches with rectangular cross sections. Similar to the 2007 Athabasca River jam release event, the calibrations of boundary constraint criterion for the Peace River events concentrated on the composite parameter  $\Phi_{B0}$ . It was found that a value of 55 kPa produced the best result for the 2014 complete ice jam release event. The modeled breaking front kept traveling downstream with brief starts and stops until it reached 740 km and stopped for 12.5 hours. Breakup was then reinitiated at 822 km downstream and the front location was about  $\sim 17$  km upstream of the location where the breaking front was last observed. It should be noted that the breaking front ‘jumped’ to 545 km instantly following the jam release, indicating that the ice between 502.1 km and 545 km broke up at once. This is likely due to the larger ice roughness for the ice cover upstream of the slope break (545km), which led to large  $\bar{w}_i$  on the left-hand side of equation [1-3]. The same  $\Phi_{B0}$  value was used to simulate the partial release event. The modeled front propagation had a similar trend as the one following the complete release event but was not in good agreement with the field observations.

When it comes to the 2018 breakup,  $\Phi_{B0}$  was calibrated to be 70 kPa. Again, the breaking front moved instantly from 510 km to 545 km, indicating this segment of the ice cover breaking all at once according to the boundary constraint criterion. The modeled breaking front in general follows along the observed trajectory until 702 km. It showed several temporary stoppages near  $\sim 580$  km

and 650 km, but the field observations were not frequent enough to verify this. The modeled front then stopped at 740 km, and the field observation of the breaking front at 702 km and 757 km also indicate a possible stoppage or at least a significant slow-down had occurred nearby. The modeled breaking front resumed movement at 821 km downstream at 2:02 on April 27 and finally came to a stop at 846 km, while the actual breaking front was observed for the last time to be at 757 km.

It is interesting to note that the simulation of each event all produced a long stall at 740 km despite of the different flow conditions. The javes appeared to attenuate to the scale here that they could not continue breaking up ice. Interestingly, the record in 2018 also shows that the breaking front got arrested and formed a large ice jam at ~723 km. Furthermore, this location is within the ~170 km subreach where channels are approximated with all rectangular cross sections. The model results emphasize the importance of having real channel geometry when applying physics-based criterion to predict ice breakup. It can be observed from satellite images that many of the channels within the subreaches with rectangular cross sections contain large bars and islands. Substituting  $W - W_i$  with an empirical value would not have captured these real channel characteristics.

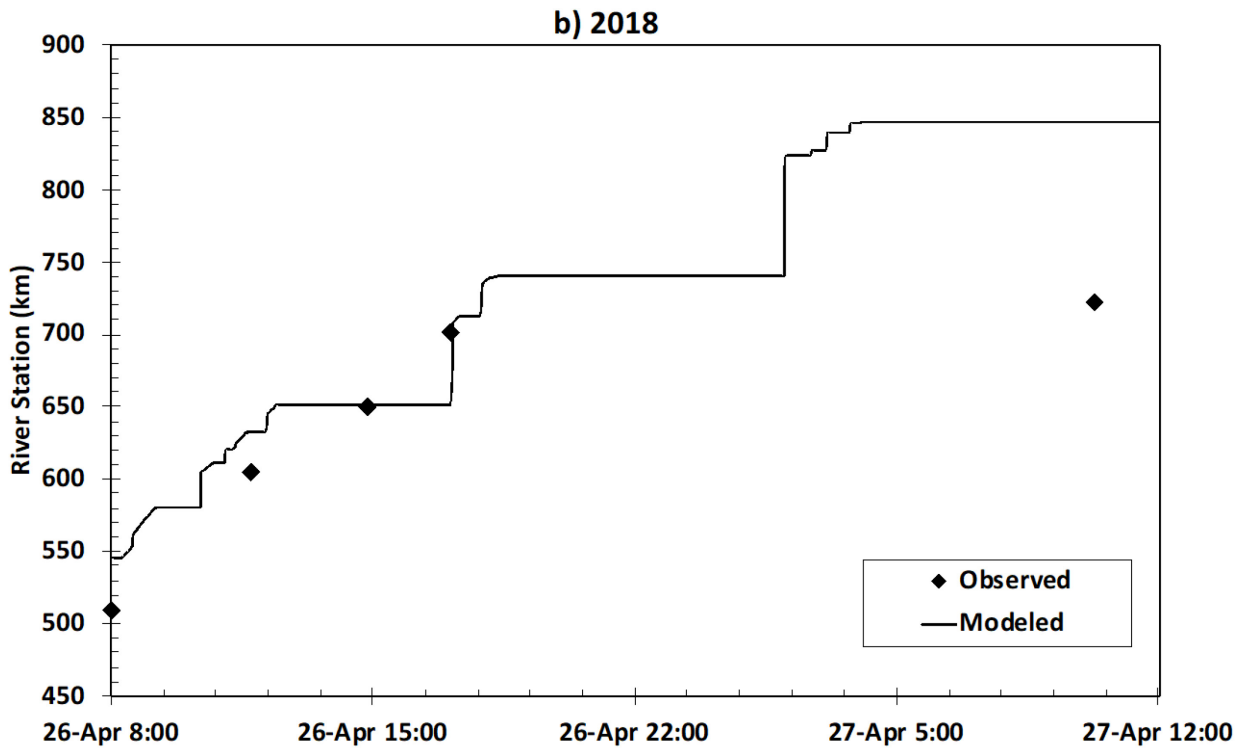
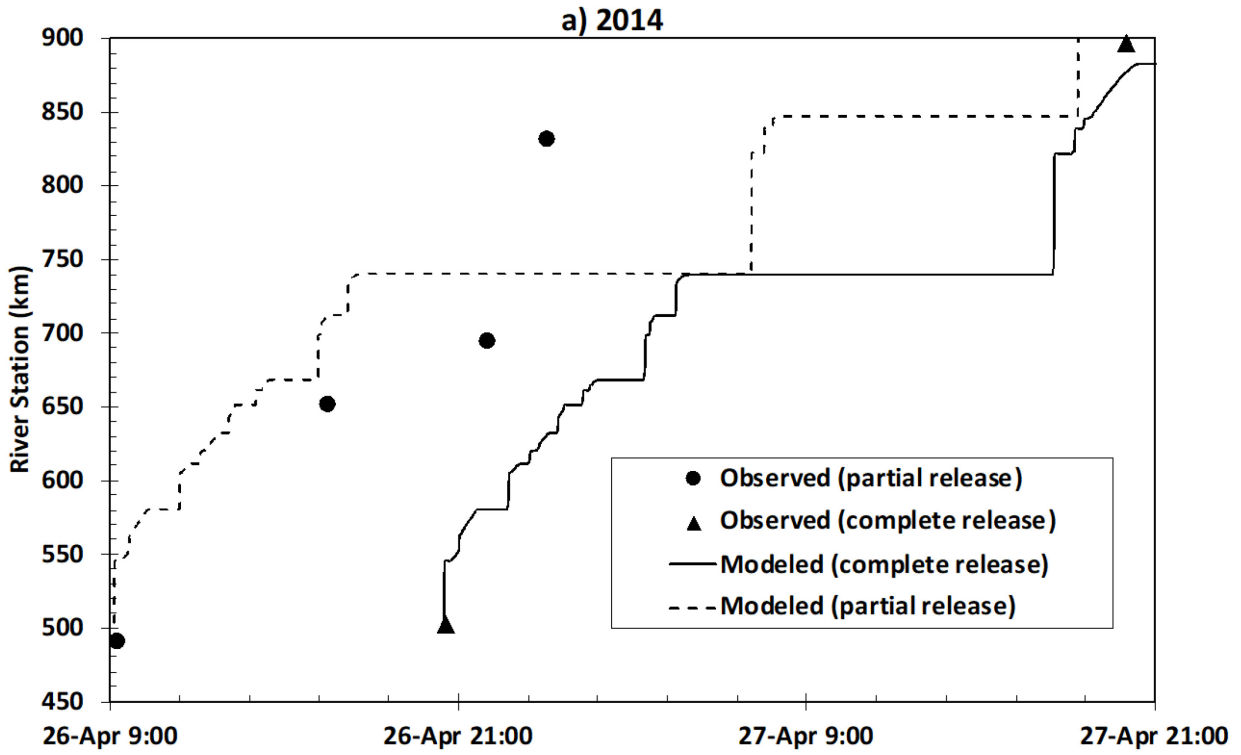
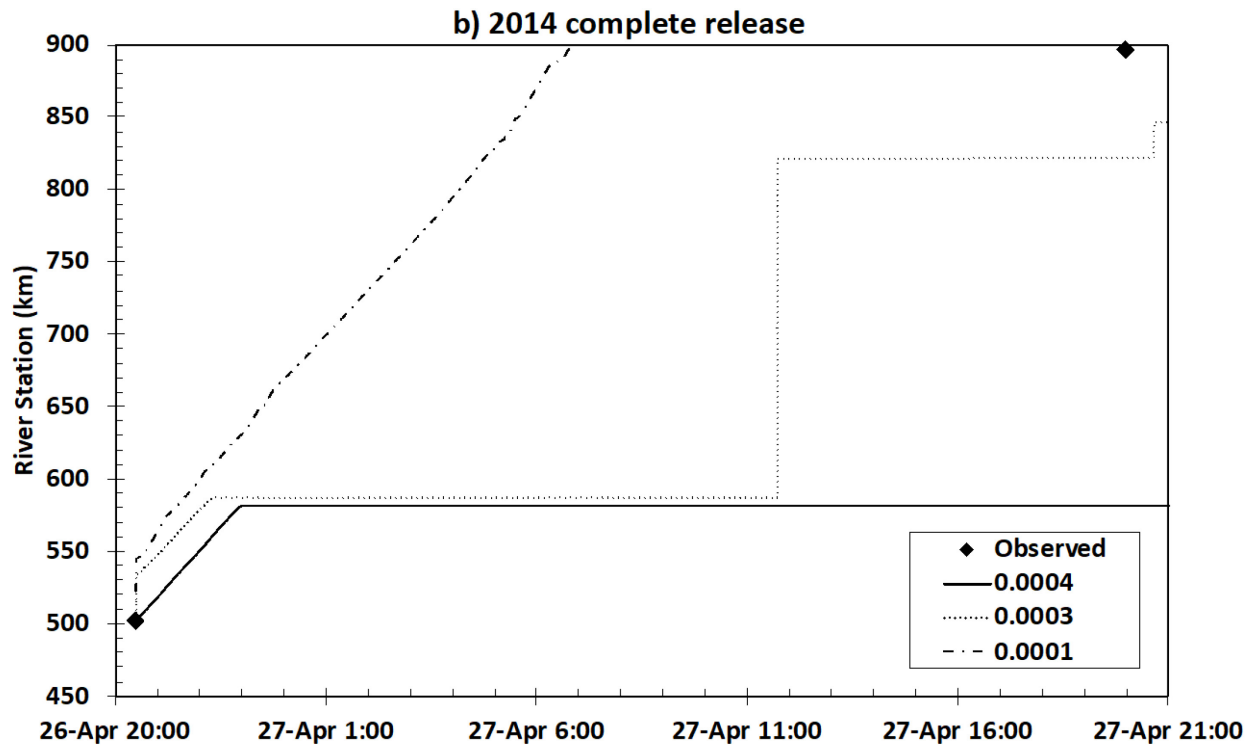
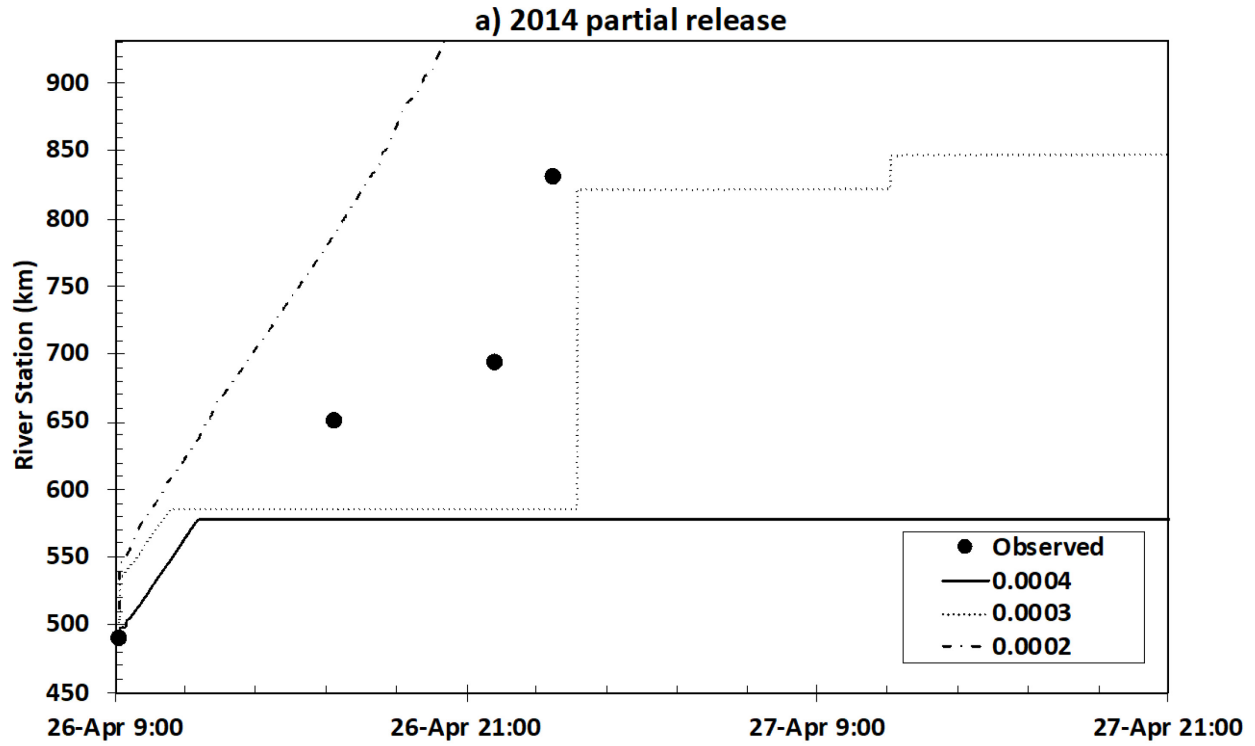


Figure 4-21. Comparison of observed and modeled breaking front location in 2014 and 2018 on the Peace River (boundary constraint criterion).

#### **4.5.1.6 Flexural and buckling criterion**

As shown in previous chapters, the application of the flexural and buckling criterion was simplified to a water surface slope criterion for jave-induced breakups. Previous studies suggested that waves with water surface slope of 0.005 or more are able to break ice cover (Billfalk 1982, Beltaos 1985, Nzokou et al. 2009). For the Peace River events, the computed water surface slopes of the two events in 2014 only outnumbered 0.0005 for less than 5 minutes and that of the 2018 event were always under  $\sim 0.0005$ . The water surface slopes of these two events mostly ranged from 0.0001 – 0.0004. Therefore, a number of threshold values in the range of 0.0001 – 0.0004 were tested and the results are shown in Figure 4-22. It can be seen that the water surface slope criterion was not able to reproduce the observed trajectory of the breaking front, regardless the threshold value. The modeled breaking front trajectories of all events share a similar pattern. For the breakup initiating water surface slope of 0.0004, the modeled breaking front stopped completely shortly after the ice jam release. For the case with the lowest threshold value of 0.0001, the jave quickly broke up the ice cover in the whole reach. These results are consistent with those of the 2007 Athabasca River water intake ice jam release event. It again proved that using water surface slope as a single threshold may not be adequate to capture a jave-induced breakup.



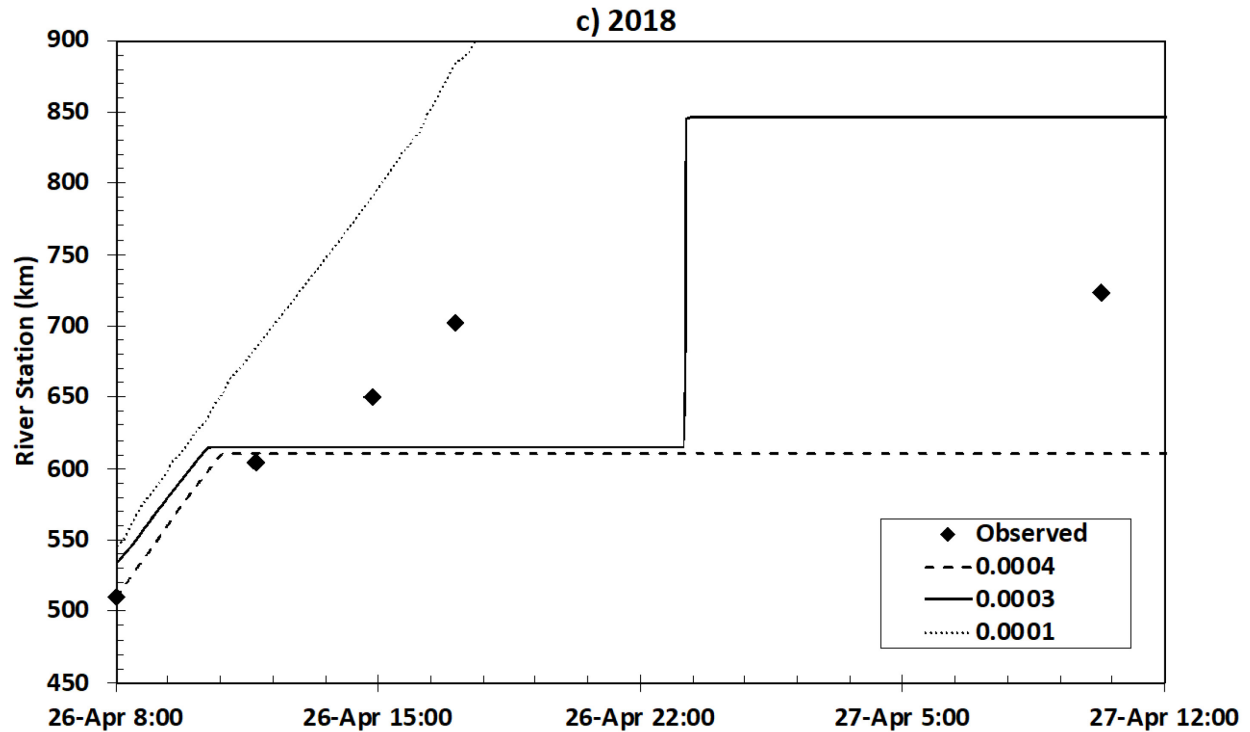


Figure 4-22. Comparison of observed and modeled breaking front location in 2014 and 2018 on the Peace River (flexural and buckling or water surface slope criterion criterion).

#### 4.5.1.7 Summary and Discussion

Among the empirical criteria, the discharge criterion appears to best reproduce the breaking front progression for the 2014 complete ice jam event, in which the long stall has also coincided with the ice jam formation near Fort Vermillion. The water level criterion also captured the two observed data points very well, but no stoppage happened near where the ice jam formed. None of the criteria was able to completely capture the 2018 breaking front propagation, but the water level criterion, discharge, and boundary constraint criteria were able to reproduce the earlier phase of the front propagation (up to ~700 km). In addition, the parameters and/or threshold values of these criteria varied largely between 2014 and 2018. Even in the same year (2014), a set of common parameter values cannot capture the breaking front propagation following both the complete and

partial ice jam release. These simulation results suggest that the empirical criteria are highly site and situation specific. The side resistance criterion did not work well when simulating the 2018 event but produced acceptable results of the 2014 complete release event. The results also showed some potential of applying same threshold values of side resistance to the same river site, but its highly site specific nature may require more calibrations to get threshold values for smaller river segments. Among all the tested criteria, the boundary constraint criterion appeared to produce reasonable results in all three events although with some discrepancies when compared to the observed breaking front trajectory. These results also showed the importance of real channel geometry when using such criterion. It was again shown that the flexural and buckling criterion reduces to water surface slope criterion was too simplified to produce the promising breaking front propagation induced by major ice jam release events.

#### **4.5.2 Stage hydrographs**

The stage hydrographs for the 2014 complete ice jam release event were produced with the discharge criterion since it best captured the documented breaking front propagation (Figure 4-23). The modeled water level hydrograph matches well with the recorded at the South Gauge of TPR but was consistently lower by ~0.3 m during the event. The sharp rise and fluctuation of the water level at Fort Vermillion at around 0:00 on April 27<sup>th</sup> were the results of the arrival of the breaking front (Jasek 2019a). This was the last observation of the breaking front that was believed to be linked to the partial jam release. This breaking front was not simulated due to lack of information, and thus the model could not capture this trend and stayed flat during this period. The large increase of the modeled water level after 8:30 of April 27<sup>th</sup> indicated that the jave arrived and the local ice breakup was initiated. This is consistent with the gauge record also showing a second wave associated with the arrival of the breaking front. The comparisons of the water level hydrographs

at Berreth Flats and Sunny Valley were just shown to compare the stage change due to the lack of datum elevations. The recorded data at Berreth Flats was moved 101.637 m up to match the first datapoint of the computed hydrograph, while the measured water level at Sunny Valley was moved 94.975 m down. It can be seen that the model successfully captured the wave at Berreth Flats and the water level decrease at Sunny Valley caused by the release of the ice jam. The water level hydrographs of the partial release event were not compared because its breaking front propagation was not well captured by any of the criteria.

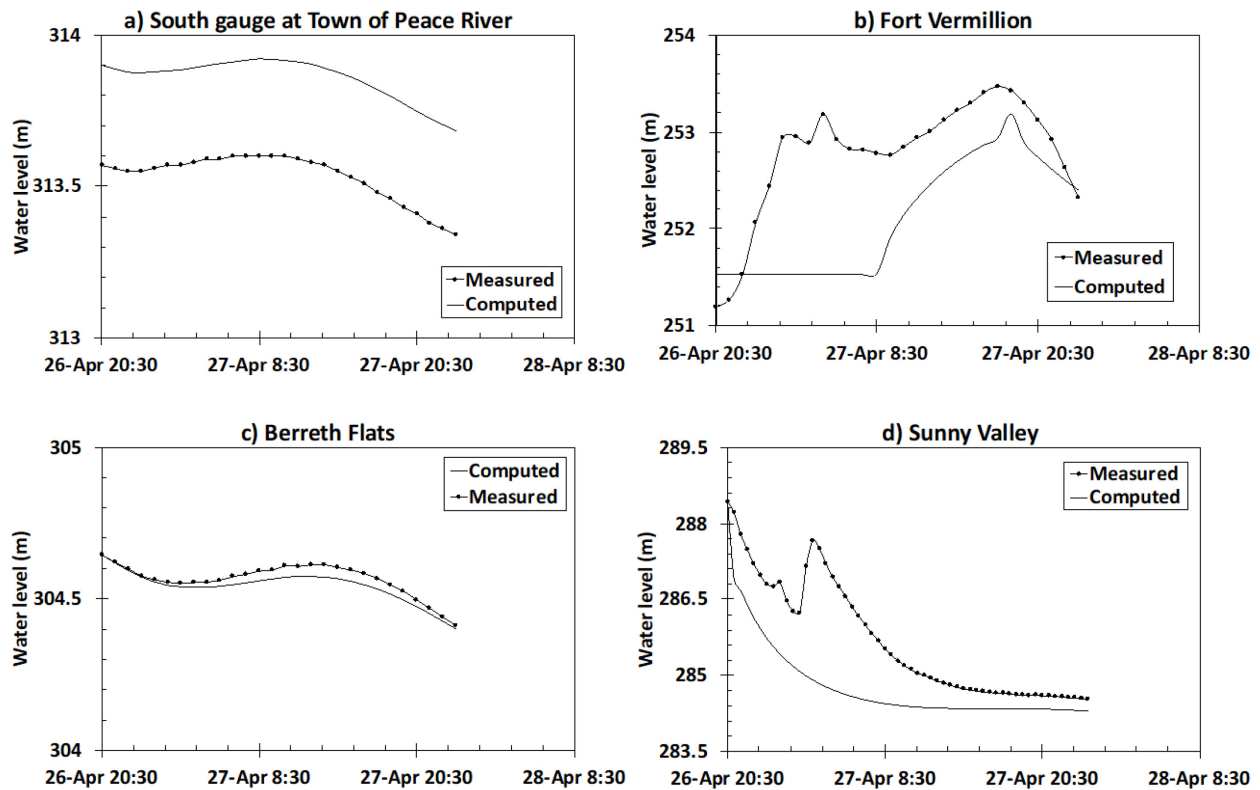


Figure 4-23. Comparison of modeled and measured water level hydrographs at various stations on the Peace River during the 2014 breakup event.

For the 2018 ice jam release event, the discharge, water level and boundary constraint criteria better captured the observed breaking front propagations than other criteria, and it was found that

the water level hydrographs produced with these three criteria were almost identical. Therefore, the results of the water level criterion are shown here as an example (Figure 4-24). Only three stations, TPR, Berreth Flats, and Sunny Valley, successfully recorded water levels during this event. The large difference between the modeled and measured water levels at TPR may be due to the malfunction of the gauge station (Jasek 2019a). The modeled water levels at Berreth Flats and Sunny Valley both matched well with the measured water levels. The recorded water level at Sunny Valley was also moved 94.975 m down to allow a direct comparison between the measured and modeled. Berreth Flats water levels did not need to be shifted.

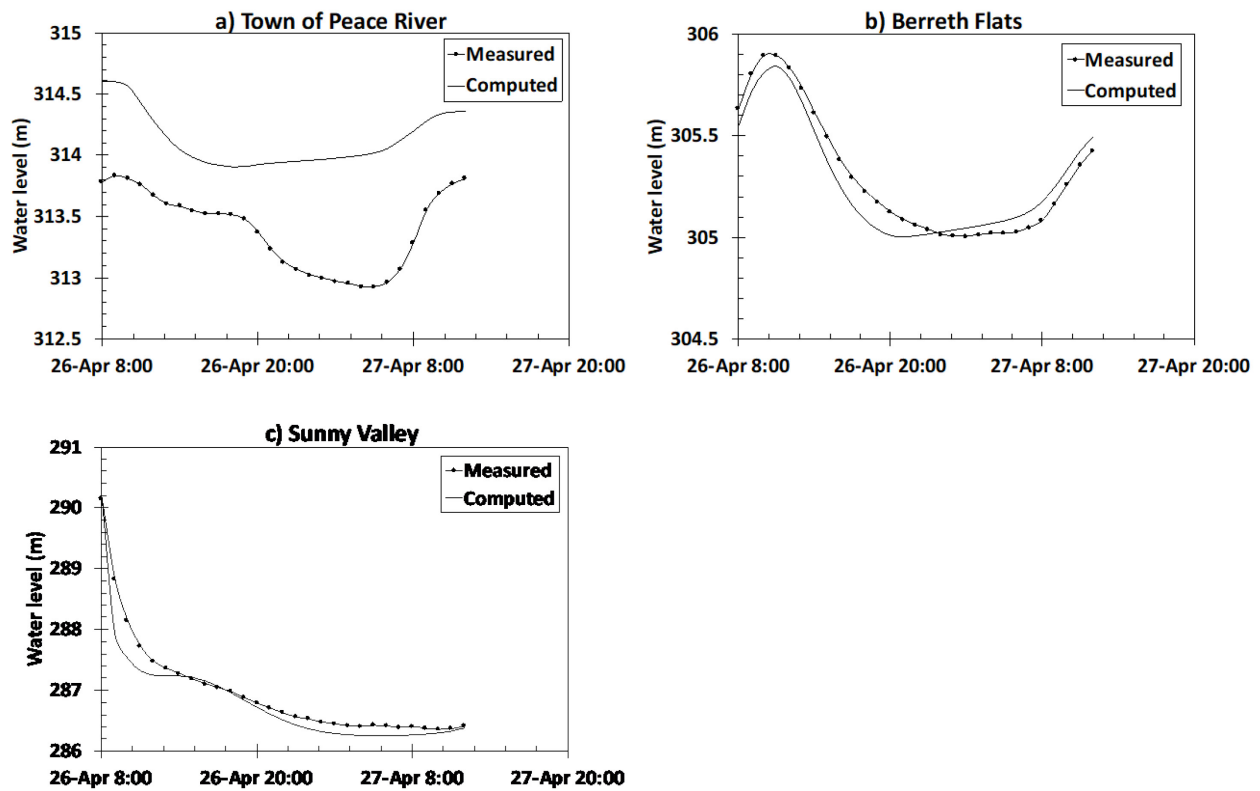


Figure 4-24. Comparison of modeled and measured water level hydrographs at various stations on the Peace River during the 2018 breakup event.

### 4.5.3 Self-sustaining wave (SSW)

The discharge domain snapshots were included in the output to facilitate the visualization of the SSW under natural river conditions. Likewise, the criterion which produced the best predictions when modeling the breaking front location was used to output the results here, i.e. discharge criterion for the 2014 complete jam release event (Figures 4-25), discharge, water level and boundary constraint criteria for the 2018 event (Figure 4-26, Figure 4-27 and Figure 4-28 respectively). The 2014 partial release event was not taken into consideration here since no criterion was able to capture the subsequent breaking front. For each breakup case, a parallel no-breakup case was modeled by simulating the same ice jam release event without allowing the breakup of the intact ice cover. The discharge variation in the study reach for the breakup case and the parallel no-breakup case are shown in the same figure for a clear illustration of the formation and evolution of the SSW. The triangle symbol indicates the breaking front location for the breakup case.

Figure 4-25 shows the discharge profile at different time during the 2014 complete ice jam release event. It can be seen that for the no-breakup case, the wave gradually attenuated as it travelled downstream. While for the breakup case, the wave got amplified due to the water released from storage as the wave broke the ice cover. 10 min after the wave released, the waveforms were quite similar between the two but the wave of the breakup case was a little ahead. This is very similar to what has been observed in the SSW model results of 2007 Athabasca River jam release event, during which the breaking front was only tracked and modeled over a short distance downstream of the toe of released ice jam. The peak of the wave of the breakup case reached maximum and then decreased a little to approach a self-sustaining value of  $\sim 9000 \text{ m}^3/\text{s}$  at around 4 hours after the ice jam release. The wave started to develop a shape with a steep front and a flat crest, the typical

shape of an SSW developed in prismatic rectangular channel (numerically shown by Jasek et al. 2005). This is likely due to the longer distance the breaking front had traveled, as compared to in the Athabasca River 2007 event, which allowed more time for the SSW to develop. The large number of rectangular cross sections in the Peace River geometry may be another explanation. The SSW kept traveling downstream and part of the SSW was traveling under the solid ice cover. The SSW kept causing ice breakup as it moved downstream until the breaking front stopped 12 hours after the jam release and the wave transformed into a more typical wave form. At 21 hours, the breakup was initiated again and the wave started to gain water released from the broken ice, as indicated by the small peak on the top of the wave. The discharge at the breaking front was computed as  $6558 \text{ m}^3/\text{s}$ . This number is only slightly larger than the breakup initiating discharge ( $Q_{\text{br}} = 6500 \text{ m}^3/\text{s}$ ).

The results produced with the discharge criterion in 2018 are shown in Figure 4-26. Similar to the 2014 complete ice jam release event, the wave was amplified and then abated before it reached a self-sustaining status, but the SSW did not attain a wide flat top. The self-sustaining discharge was  $\sim 11300 \text{ m}^3/\text{s}$ . At 13 hours, the simulated breaking front stopped at 817 km and did not resume movement afterwards. The discharge at the breaking front ( $10075 \text{ m}^3/\text{s}$ ) was also found to be slightly larger than the breakup initiating discharge ( $Q_{\text{br}} = 9800 \text{ m}^3/\text{s}$ ).

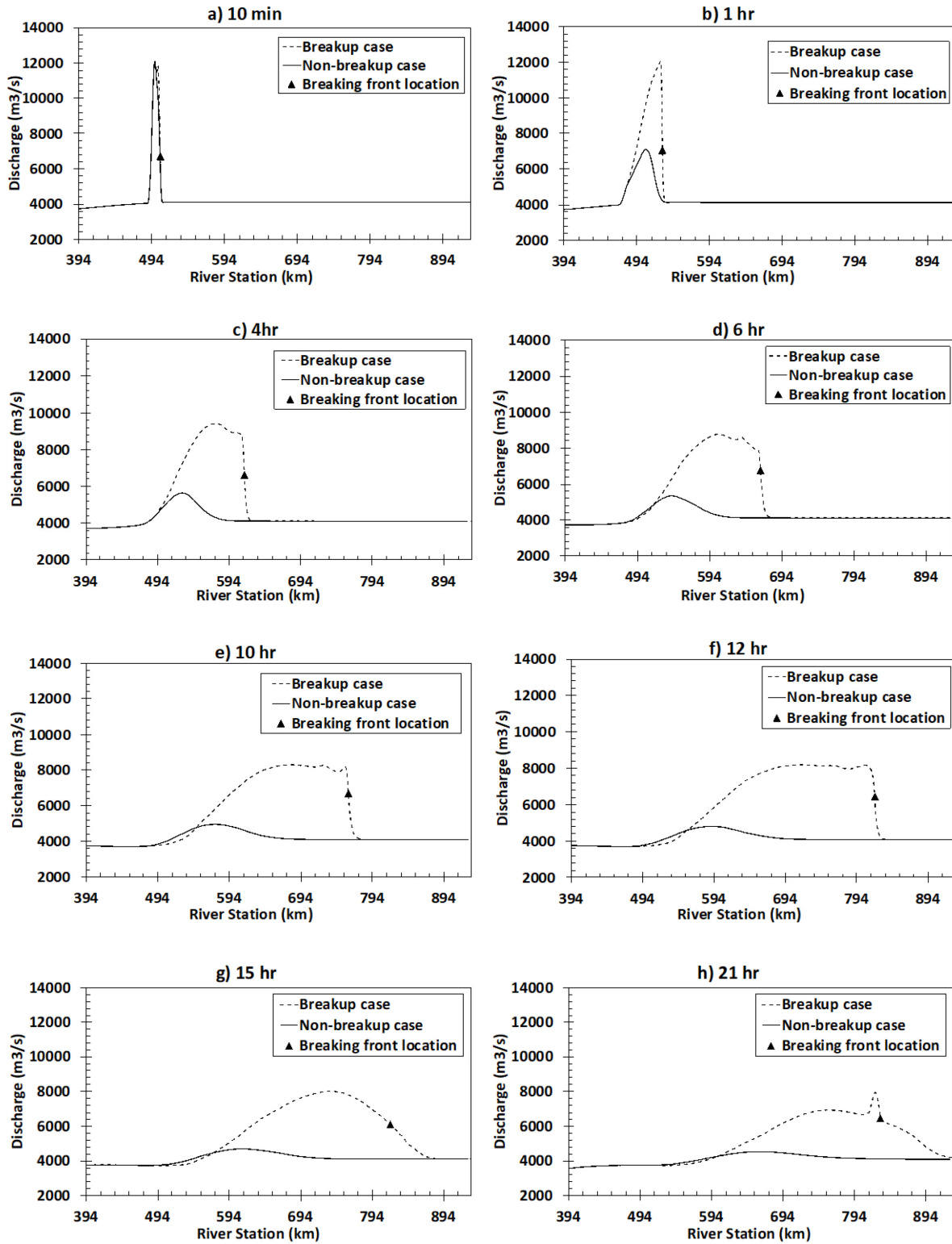


Figure 4-25. Comparison of discharge in the study reach between breakup and no-breakup cases at various times after the 2014 complete ice jam release on the Peace River (discharge criterion).

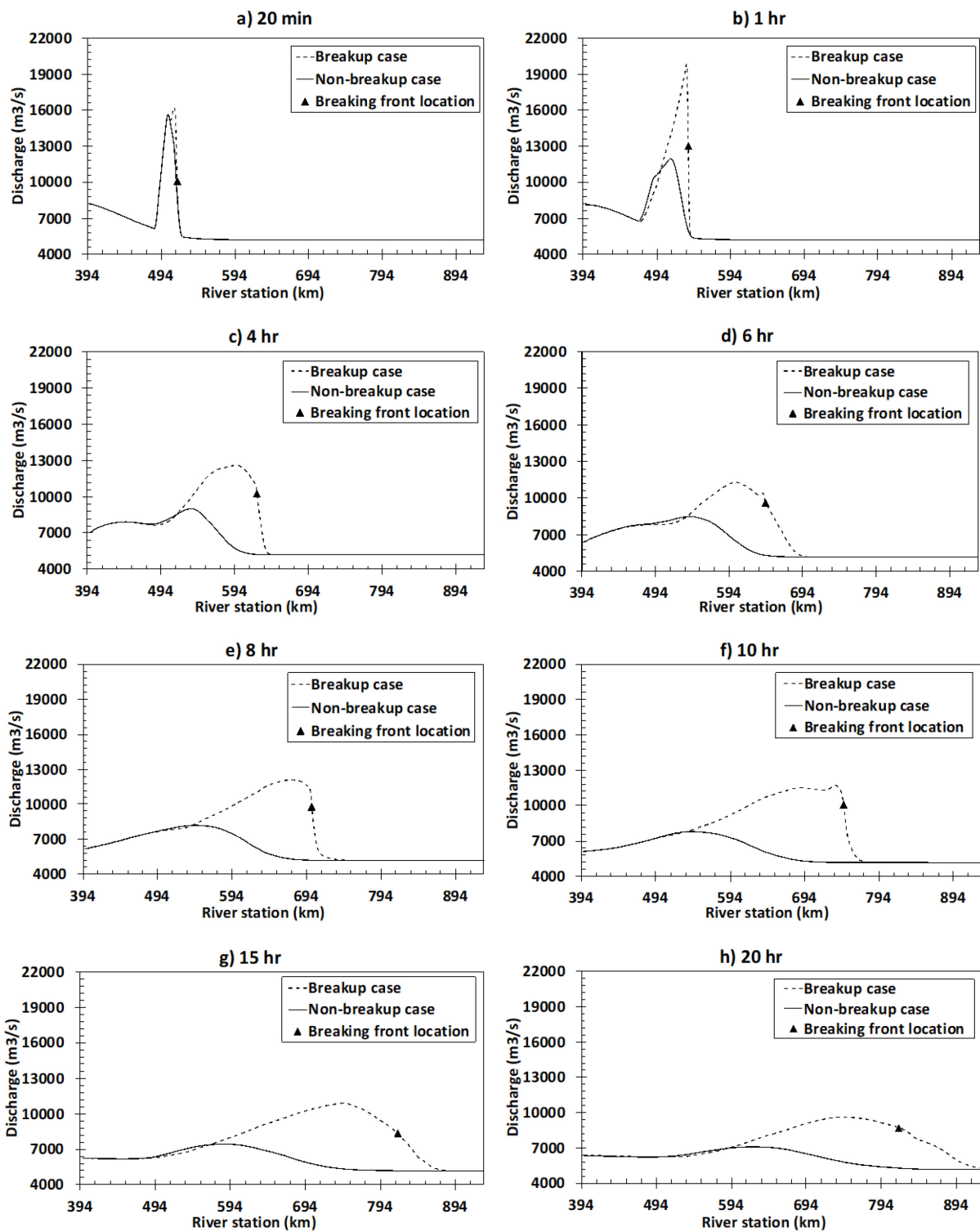


Figure 4-26. Comparison of discharge in the study reach between breakup and no-breakup cases at various times after the 2018 ice jam release on the Peace River (discharge criterion).

Figure 4-27 presented the results produced by using the boundary constraint criterion. The typical SSW shape was again not observed, but the behaviour of the modeled SSW was quite different from the one generated through the discharge criterion. At 20 minutes, the waveforms between the breakup and no-breakup cases showed a large difference. This is because of when using the boundary constraint criterion, the ice cover over a long stretch broke up instantly after the jam release. The modeled breaking front temporarily stopped at 4 hours after the jam release and the sharp rise was gradually flattened from 4-8 hours. At around 10 hours, the breakup was reinitiated in the model and the SSW got amplified again. The flatter wave at 15 hours is associated with the stall of the modeled breaking front near 740 km and the amplified wave at 20 hours is corresponding to restart of the breaking front in the model. These results show that the breaking front progression can considerably affect the SSW characteristics. Different breakup rates, which is in response of various resistance to ice breaking, can produce different amounts of water released from the storage and thus different SSW.

The results above revealed that the shape of the SSW depends on both the breaking distance and the breakup rate. The modeled breaking front of 2014 complete release traveled over ~300 km for 12 hours before it stopped, and the breakup rate was 7.3 m/s within this period of time. These numbers are similar to those modeled with the discharge criterion for the 2018 jam release, the breaking front traveled for ~300 km within 12.5 hours, and the breakup rate was computed as 6.8 m/s. While for the other two simulations in 2018, the breaking front of boundary constraint criterion experienced many starts and stops and the traveling distance between each stall was always under 140 km. Hence, a SSW couldn't form even the breakup rate was about 8 m/s. The breaking front of water level criterion in 2018 didn't stop, but the breakup rate was only around 4 m/s. It appeared that a slow breakup rate and breaking stoppages will both lead to reduced storage

release. Thus, the amount of water being released from the broken ice cover cannot sustain the formation of a typical SSW shape.

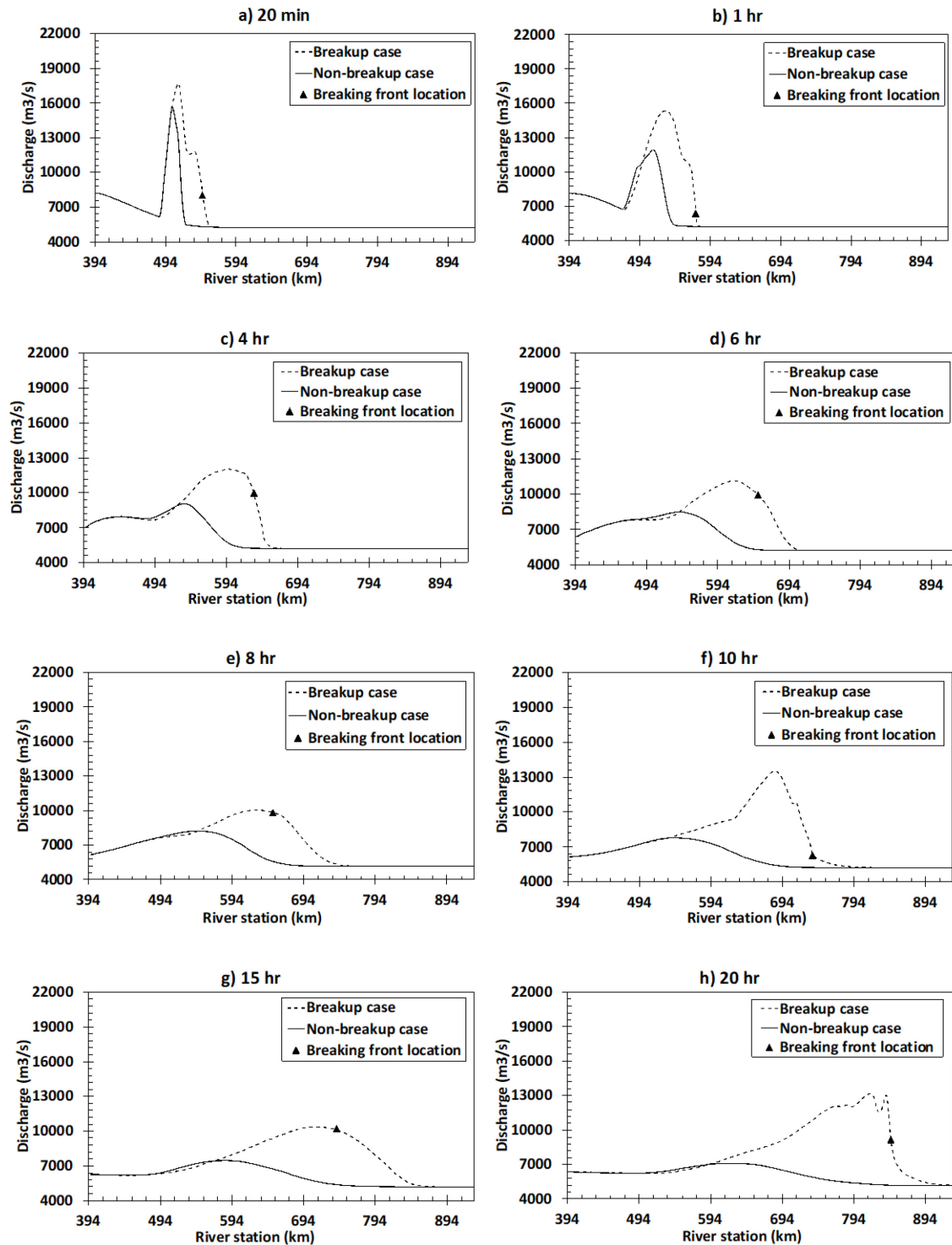


Figure 4-27. Comparison of discharge in the study reach between the breakup and no-breakup cases at various times after the ice jam release in 2018 on the Peace River (boundary constraint criterion).

Figure 4-28 reintroduced the results obtained from the test cases of Jasek et al. (2005) shown in Chapter 2, in which excess discharge ratios are used to present the characteristics of SSW formed during different wave-induced ice cover breakup events. Three extra data points from jave-induced events were added here. Two are from this study, the 2014 complete ice jam release event and the 2018 ice jam release event on the Peace River, and the third one is from Beltaos (2017a). Beltaos (2017a) numerically showed that jave-induced ice cover breakup can also lead to the formation of SSW in prismatic channel. Although the simulated channel has different geometric and hydraulic conditions, and shear stress breakup criterion rather than discharge threshold was used, the data point roughly follows the extended linear fit for the steeper channel. With an excess breakup ratio of 1.2, the sustained discharge is over 2 times higher than the base discharge. The two data points from the Peace River events also fall on the linear trendline for the mild-slope channel. For the 2014 complete release, the base discharge ( $Q_o$ ) was 4100 m<sup>3</sup>/s, and the breakup initiating discharge ( $Q_{br}$ ) was 6500 m<sup>3</sup>/s. The excess breakup ratio ( $Q_{br}/Q_o - 1$ ) was calculated as 0.59, and the sustained discharge nearly doubled the base discharge ( $Q_{sustained}/Q_o = 1.99$ ). For the 2018 event, . The excess breakup ratio ( $Q_{br}/Q_o - 1$ ) was calculated as 0.88 with  $Q_o = 5200$  m<sup>3</sup>/s and  $Q_{br} = 9800$  m<sup>3</sup>/s, and  $Q_{sustained}/Q_o = 2.17$ . These results suggest that the properties of an SSW are not impacted by whether it is triggered by a jave or a less dynamic wave like those in Jasek et al. (2005), but greatly depending on the threshold discharge. This revealed the potential to apply such empirical relationships to estimate the sustaining discharge based on the base discharge and the breakup initiating discharge as these can be measured in the field. Different than the incoming waves tested by Jasek et al. (2005), a jave is not amplified by storage release and the  $Q_{sustained}$  is lower than the peak discharge of the jave.

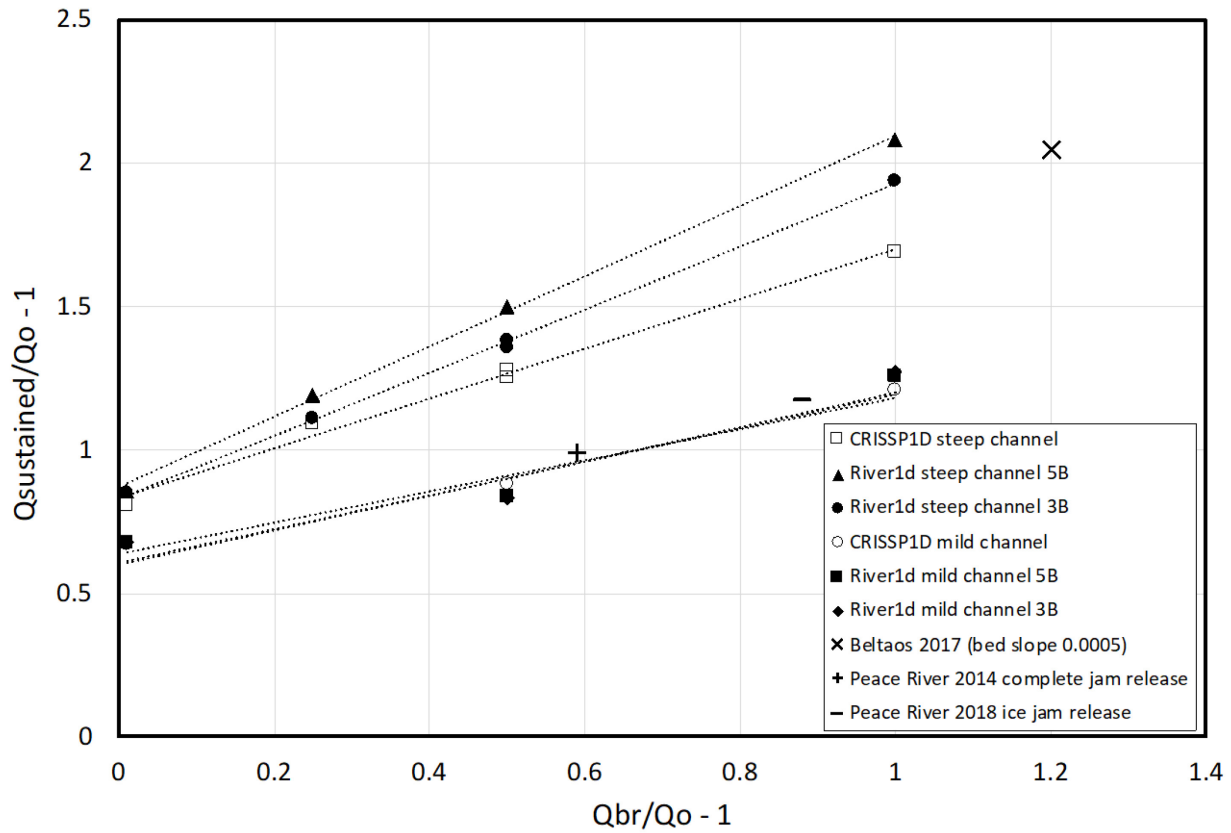


Figure 4-28. The variation of sustaining wave discharge and breakup initiating discharge. Both excess ratios were normalized with base discharge and subtracted by 1 to show the storage release amount. The data of the 2014 complete release and 2018 event of the Peace River are added (adapted from Beltaos 2017a).

## Chapter 5 Conclusions and Recommendations

River ice breakups are often associated with ice jams and high water levels. The ‘jave’ produced by sudden ice jam release can break up long stretches of ice cover downstream, resulting in an ice run. The ice run accelerates and decelerates when it travels down the river as the resistance to ice breakup varies. A new ice jam can reform if the ice run is arrested, causing the water level to rise again. Where and when this may happen are highly uncertain, thus increasing the unpredictability of floods related to river breakup. A number of studies have focused on predicting the initiation of breakup as it is a prerequisite for forecasting flood risk associated with river ice breakup. Several breakup initiation criteria, both empirical- and physics-based, exist in the literature. However, these criteria have not been systematically compared and none of the existing numerical models include the physics-based breakup criteria. The objectives of this thesis research were to expand our understanding of how ice cover breakup is initiated and sustained, as well as to enhance our capability of breakup forecasting. The key contributions of this study are:

1. Physics-based breakup criteria have been implemented into a river ice model.
2. A systematic test and comparison of the existing breakup criteria in the context of a river ice model using field data has been conducted. Recommendations have been made based on applicability and transferability of the criteria.
3. The existence and characteristics of the self-sustaining wave (SSW) have been numerically explored under natural channel conditions.

The breakup criteria were compared utilizing three field observed jave-induced breakup events. The Athabasca River 2007 event was relatively small-scale, with the breaking front observed within a 3 km reach during 30 minutes after the ice jam release. The 2014 and 2018 events on the Peace River involved ~400 km breaking front travel distance. The two single-variable empirical

breakup criteria based on water level and discharge performed well in capturing the propagation of the sheet breaking front of the 2007 breakup on the Athabasca River. The modeled breaking front locations of the 2014 complete jam release on the Peace River also matched the observations very well, but the discharge criterion appeared to work better with possibly simulating the formation of the new ice jam downstream. The two criteria also successfully captured the breaking front propagation of the earlier phase of the 2018 breakup but failed to match the later observations. Generally speaking, these empirical criteria are simple and practical to use and can be calibrated to produce good results for both small and large scale events, but the calibrated threshold values appear to be site and situation specific. The coefficient  $K$  in the water level criterion was calibrated as 3, 1.2 and 2, and the breakup initiating discharge was calibrated as 4000  $\text{m}^3/\text{s}$ , 6500  $\text{m}^3/\text{s}$ , and 9800  $\text{m}^3/\text{s}$  for the 2007 Athabasca River breakup, the 2014 complete release and 2018 breakup on the Peace River, respectively. The results showed that these calibrated parameters could even vary from section to section for each specific event. Improvements can be made with subdividing the study reach and calibrating parameters for each subreach. These two calibrated parameters were different for the two events on the Peace River, revealing that their transferability is possibly low.

The other empirical criterion based on discharge rate also provided a reasonable result for the 2007 breakup of the Athabasca River, but again the calibrated parameters were not transferrable to the events on the Peace River. This may be due to the different scales of the events happened on the two rivers. The discharge rate criterion also requires the determination of two threshold discharge rate values as well as a cumulated time value, rendering it less practical than the other single-variable criteria in the empirical category.

The physics-based side resistance criterion did not work well for all modeled events. Some of the calibrated threshold values were also outside of the typical range found in the literature. The side resistance at the onset of breakup is not readily quantifiable, rendering it site and situation specific. It is worth noticing that the two threshold values of the side resistance were calibrated to be the same for two events on the Peace River, which may be an indication of possible reuse of the side resistance threshold within the same river reach from year to year. The other physics-based criterion (i.e. the boundary constraint criterion) appeared to produce reasonable results in all events even though the results did not completely agree with the observations. It was also the only criterion that was able to simulate the breaking front caused by the 2014 Peace River partial ice jam release event. The calibrated composite parameter in this criterion appeared to be relatively consistent among the events, being 70 kPa for the 2007 Athabasca River breakup and the 2018 Peace River breakup, and 55 kPa for the 2014 Peace River breakup. The results also highlighted the importance of having real channel geometry and possibly accounting for the 2D geometric effects when applying the boundary constraint criterion. Improvements can be possibly made with more surveyed cross sections available. Furthermore, the criterion can be potentially promising for predicting the stall of ice runs and subsequent formation of ice jams since it simulated the accelerations and decelerations of the breaking fronts as the resistance to break up along the river changes. The flexural and buckling criterion reduced to water surface slope criterion for long wavelength associated with javes and was shown to be too simplified to capture the breaking front propagation induced by major ice jam release events.

The self-sustaining wave (SSW) under natural river conditions was observed through either water depths hydrographs or discharge domain snapshots. The results suggest that SSW can be developed through gaining water from the storage release as jave initiated ice breakup. SSW under

natural river conditions may or may not take on a constant shape with a sharp rising wave front and a flat crest as those shown in the previous numerical studies with rectangular channels. It was observed that the ice breaking distance and speed affect whether a typical shape of the SSW developed or not, and have significant impact on the SSW characteristics. Various breakup rates represent different resistance to ice breakup, and the front traveling distance determined the quantity of the ice being broken, which both affect the amount of water being released from the hydraulic storage. Part of the SSW under natural channel conditions travels under the solid ice cover, which was different than the SSW in numerical simulations with rectangular geometry. When the breaking front is arrested in places where the resistance is high, the SSW will attenuate while traveling downstream under the ice cover. This can sometimes lead to ice jam formation. The SSW under natural river conditions should be explored with more numerical simulations, and more surveyed geometry data and field observations will help facilitate studies on this topic.

## References

- Andres, D.D. and Doyle, P.F., 1984. Analysis of breakup and ice jams on the Athabasca River at Fort McMurray, Alberta. *Canadian Journal of Civil Engineering*, 1984, 11:444-458.
- Andres, D., 1996. Ice formation and Break-up at the Town of Peace River – A study of regulated conditions, 1969-1994. A report prepared for The Town of Peace River, BC Hydro and Alberta Environmental Protection by Trillium Engineering and Hydrographics Inc., Northwest Hydraulics Consultants Ltd. and Thurber Engineering Ltd.
- Andrishak, R. and Hicks, F., 2008. Simulating the effects of climate change on the ice regime of the Peace River. *Canadian Journal of Civil Engineering*, 2008, 35:461-472.
- Ashton, G.D., 1986. *River and Lake Ice Engineering*, Water Resources Publications, Littleton, CO, 485 pp.
- Beltaos, S., 1985. Initial Fracture Patterns of River Ice Cover. National Water Resource Institute Contribution No. 85-139. National Water Research Institute, Burlington, ON, Canada.
- Beltaos, S., 1990a. Fracture and breakup of river ice cover. *Canadian Journal of Civil Engineering*, 17(2), 173-183.
- Beltaos, S., 1995b. Chapter 4: Theory. In: *River Ice Jams*. Water Resources Publications, Highlands Ranch, Colorado, USA.
- Beltaos, S., 1996a. Chapter 4: Breakup, Ice Jams and Related Flooding, In: *A Primer on the Hydraulics of Ice Covered Rivers*. Edited by Kersi S. Davar, Spyros Beltaos and Bruce Pratte, CGU-HS Committee on River Ice Processes and the Environment, Edmonton, Canada.

- Beltaos, S., 1997a. Onset of river ice breakup. *Cold Regions Science and Technology*, Volume 25, Issue 3, Pages 183-196.
- Beltaos, S., 2003. Threshold between mechanical and thermal breakup of river ice cover. *Cold Regions Science and Technology*, Volume 37, Issue 1, Pages 1–13.
- Beltaos, S., 2008. Progress in the study and management of river ice jams. *Cold Regions Science and Technology*, Volume 51, Issue 1, 2008, Pages 2-19.
- Beltaos, S., 2013a. Hydrodynamic and climatic drivers of ice breakup in the lower Mackenzie River. *Cold Regions Science and Technology*, Volume 95, 2013, Pages 39–52
- Beltaos, S., 2013b. Hydrodynamic characteristics and effects of river waves caused by ice jam releases. *Cold Regions Science and Technology*, Volume 85, 2013, Pages 42-55
- Beltaos, S., 2016. Extreme sediment pulses during ice breakup, Saint John River, Canada. *Cold Regions Science and Technology*, Volume 128, 2016, Pages 38-46
- Beltaos, S., 2017a. Hydrodynamics of storage release during river ice breakup. *Cold Regions Science and Technology*, Volume 139, 2017, Pages 36-50.
- Beltaos, S., 2018a. Erosion potential of dynamic ice breakup in Lower Athabasca River. Part II: field data analysis and interpretation. *Cold Regions Science and Technology*.
- Beltaos, S., Burrell, B.C., 1999. Transport of metals on sediment during the spring breakup of river ice. In *Ice in Surface Waters*, Shen HT (ed.). Proceedings, 14th International Symposium on Ice, held at Potsdam, NY, 27–31 July 1998, IAHR, A.A.Balkema: Rotterdam, Vol. 2, 793–800.

- Beltaos, S., Burrell, B.C., 2000. Suspended sediment concentrations in the Saint John River during ice breakup. Proceedings, 2000 Annual Conference of the Canadian Society for Civil Engineering, London, Ontario; 235–242.
- Beltaos, S., Carter, T., 2009. Field studies of ice breakup and jamming in lower Peace River, Canada. Cold Regions Science and Technology, Volume 56, Issues 2–3, 2009, Pages 102-114.
- Beltaos, S. and Tang, P., 2013. Applying HEC-RAS to simulate river ice jams: snags and practical hints. Proceedings of 17th Workshop on the Hydraulics of Ice Covered Rivers, Edmonton, Alberta, Canada, July 21-24, 2013, CGU-HS Committee on River Ice Processes and the Environment, Edmonton, Canada.
- Billfalk, L., 1982. Breakup of solid ice covers due to rapid water level variations, CRREL Rep.82–3, Cold Reg. Res. and Eng. Lab., Hanover, N. H.
- Blackburn, J. and She, Y., 2019. A comprehensive public-domain ice process model for complex natural river system. Journal of Cold Regions Science and Technology. 163: 44-58.
- Blackburn, J. and Hicks, F., 2002. Combined Flood Routing and Flood Level Forecasting. Canadian Journal of Civil Engineering, 2002, 29(1): 64–75.
- CRISSPID Programmer's Manual, CEATI Report No. T012700-0401, Department of Civil and Environmental Engineering, Clarkson University, October 2005.
- Daly, F. 1993. Wave propagation in ice-cover channels. Journal of Hydraulic Engineering, ASCE, 119(8), 895-910.
- Daly, F. 1995. Fracture of river ice covers by river waves. Journal of Cold Regions Engineering, 9(1): 41-52.

- Ferrick, M. and Mulherin, N.D. 1989. Framework for control of the dynamic ice breakup by river regulation. US Army CRREL Rpt. 89-12, Hanover, N.H., USA.
- Fread, D. L.: NWS FLDWAV model: Theoretical description, National Weather Service, USA, 1998.
- Friesenhan, E., 2004. Modeling of historic ice jams on the Athabasca River at Fort McMurray. Report prepared in partial fulfillment of the requirements for the degree Master of Engineering (supervisor F. Hicks), Dept. of Civil and Environmental Engineering, University of Alberta, 64 pp.
- Friesenhan, E., Mahabir, C., Trevor, B., Cline, A., and Granson, W., 2008. Innovations in River Ice Monitoring and Management in Alberta, Canada. Proceedings of the 19th IAHR International Symposium on Ice, Vancouver, Canada, 311-326.
- Gerard, R., Kent, T.D., Janowicz, R., Lyons, R.O. 1984. Ice regime reconnaissance, Yukon River, Yukon. Proceedings of the 3rd International Specialty Conference on Cold Regions Engineering, 4–6 April 1984, Edmonton, Alta. Compiled and edited by D.W. Smith. Canadian Society for Civil Engineering, Montréal, Quebec, pp. 1059–1073.
- HEC-RAS Hydraulic Reference Manual, version 5.0. U.S. Army Corps of Engineers Hydrologic Engineering Center (HEC)., Davis, CA, USA, 2016.
- Hicks, F.E. 1996. Hydraulic flow routing with minimal channel data: Peace River, Canada, Canadian Journal of Civil Engineering, 1996, 23, 524–535.
- Hicks, F.E. and Steffler, P.M., 1990. Finite Element Modeling of Open Channel Flow Water Resources Engineering Report No. 90-6, Department of Civil Engineering, University of Alberta, Edmonton, Alberta, 383 pp.

- Hicks, F.E. and Steffler, P.M., 1992. A Characteristic-Dissipative-Galerkin Scheme for Open Channel Flow, *ASCE Journal of Hydraulic Eng.*, 118(2): 337-352.
- Hicks, F.E. and Steffler, P., 1995. Comparison of Finite Element Methods for the St. Venant Equations, *Int. Journal for Numerical Methods in Fluids*, 20: 99-113.
- Jasek, M., 2003. Ice jam release surges, ice runs, and breaking fronts: field measurements, physical descriptions, and research needs. *Canadian Journal of Civil Engineering*, 2003, 30:113-127.
- Jasek, M., Ashton, G., Shen, H.T., Chen, F. 2005. In: Numerical modeling of storage release during dynamic river ice break-up. Proceedings of 13th Workshop on the Hydraulics of Ice Covered Rivers, Hanover, NH, September 15–16, 2005, CGU-HS Committee on River Ice Processes and the Environment, Edmonton, Canada. pp. 421–439.
- Jasek, M., 2017b. Peace River 2014 Break-up and Ice Jam at Peace-Athabasca Delta: Field Investigations and Analysis. BC Hydro report. BC Hydro.
- Jasek, M., 2019a. An Emerging Picture of Peace River Break-up Types that Influence Ice Jam Flooding of the Peace-Athabasca Delta Part 2: Insights from the comparison of the 2014 and 2018 Break-ups. Proceedings of 20th Workshop on the Hydraulics of Ice Covered Rivers, Ottawa, Ontario, Canada, May 14-16, 2019, CGU-HS Committee on River Ice Processes and the Environment, Edmonton, Canada.
- Jasek, M., 2019a. An Emerging Picture of Peace River Break-up Types that Influence Ice Jam Flooding of the Peace-Athabasca Delta Part 1: The 2018 Peace River Break-up. Proceedings of 20th Workshop on the Hydraulics of Ice Covered Rivers, Ottawa, Ontario, Canada, May 14-16, 2019, CGU-HS Committee on River Ice Processes and the Environment, Edmonton, Canada.

- Kellerhals, R., Neill, C.R., and Bray, D.I., 1972. Hydraulic and geomorphic characteristics of rivers in Alberta. Alberta Research Council, Edmonton, Alta., River Engineering and Surface Hydrology Report 72-1.
- Kowalczyk, T. and Hicks, F., 2003. Observations of ice jam release waves on the Athabasca River near Fort McMurray. *Alberta Canadian Journal of Civil Engineering*, 2007, 34:473-484.
- Mao, Z., Zhao, X., Wang, A., Liu, Y., Hu, Y., 2009. Boundary constraint criterion for onset of mechanical ice-cover breakup (in Chinese). *Advances in Science and Technology of Water Resources*, 2009.
- Marr, J. and Parker, Gary and Wilcock, Peter., 2005. Stream Restoration Toolbox of the National Center for Earth-surface Dynamics. AGU Spring Meeting Abstracts.
- Michel, B., 1971. 'Winter regime of rivers and lakes', US Army Cold Regions Research and Engineering Laboratory, Hanover, NH, Monograph III-B1a.
- Nzokou, F., Morse, B., and Quach-Thanh, T. 2009. River ice cover flexure by an incoming wave. *Cold Regions Science and Technology*, 55(2): 230-237.
- Nafziger, J., She, Y., Hicks, F., 2016. Celerities of waves and ice runs from ice jam releases. *Cold Regions Science and Technology*, Volume 123, 2016, Pages 71-80.
- Prowse, T., Culp, J., 2003. Ice breakup: a neglected factor in river ecology. *Canadian Journal of Civil Engineering*, 2003, 30:128-144.
- She, Y. and Hicks, F., 2006a. Modeling ice jam release wave with consideration for ice effects. *Journal of Cold Region Science and Technology*, 45: 137-147.

- She, Y. and Hicks, F., 2006b. Ice jam release wave modeling: considering the effects of ice in a receiving channel. Proc. 18th International Symposium on Ice. 28 Aug.–1 Sept. 2006, Sapporo, Japan, pp. 125-132.
- She, Y., Andrishak, R., Hicks, F., Morse, B., Stander, E., Krath, C., Keller, D., Abarca, N., Nolin, S., Tanekou, F., and Mahabir, C., 2009. Athabasca River ice jam formation and release events in 2006 and 2007. *Journal of Cold Regions Science and Technology*, Special Issue on River Ice, 55:249-261.
- Shulyakovskii, L.G. (editor)., 1966. Manual of forecasting ice-formation for rivers and inland lakes. Translated from Russian. Jerusalem Israel Program for Scientific Translations.
- Taggart, J., 1995. The Peace River natural flow and regulated flow scenarios - daily flow data report. Surface Water Assessment Branch, Alberta Environmental Protection, Edmonton, Alta.
- Xia, X. and Shen, H.T., 2002. Nonlinear interaction of ice cover with shallow water waves in channels. *Journal of Fluid Mechanics*, 467:259-268.